FINITE DENSITY SIMULATIONS IN LATTICE QUANTUM CHROMODYNAMICS

Thesis by

MUHAMMAD RAFIQ

for the degree of

DOCTOR OF PHILOSOPHY

Department of Physics and Astronomy,

The University, Glasgow G12 8QQ

June 1987

To

My father Hafiz Noor Muhammad

and my mother.

ACKNOWLEDGEMENTS

First of all I would like to thank my supervisor Dr.I.M. Barbour for his great help, encouragement and kindness during my stay at Glasgow. In fact, this research work was not possible without his continuous guidance and co-operation. Iwould like to acknowledge the efforts made by Prof.R.G. Moorhouse for my studies during the first year of my studies at Glasgow. His continuous encouragement afterwards helped me keeping my morale up during the entire period of my Ph.d. Dr.R.L. Crawford is responsible for settling me down not only in this department but also in Glasgow, as he helped me throughout my studies and it is due to him that I always felt at home. I am also grateful to him for correcting the English of my thesis. N.E. Behilil was responsible for introducing me to Lattice gauge theory and my supervisor. P.E. Gibbs helped me a lot in understanding the computer programmes. I am thankful to both of them for more than one reasons. My thanks also go to Dr. David Sutherland, Dr.Andrew Davies and Dr.Froggatt for their help and for making this department a suitable and peaceful place for working. I am also thankful to Dr. C.J. Burden, Dr.Brian Dolan, and Dr.T. Vladikas for their patience in helping me during my research work. I would like to acknowledge the discussions made with S.Psycharis . During the days of depression my wife, Abida, was a source of great encouragement for me.I am also grateful to my brother Dr.Akram for moral help during my studies at Glasgow. In the end, I thank the Federal Ministry of Education, Govt. of Pakistan, for their financial help for this research work.

DECLARATION

Chapter1 is a review of the part of the existing knowledge on Lattice gauge theory especially related to my project. Chapter 2 and 3 are a mixture of original and existing work on Lanczos algorithm. Chapter 4 is purely original work done in collaboration with Ian Barbour, Philip Gibbs,Clive Bailie and K.C. Bowler. Chapter 5 describes studies performed in collaboration with Ian Barbour, T.Vladikas, Philip Gibbs and Clive Baillie.

CONTENTS

ABSTRACT

Quantum Chromodynamics(Q.C.D) is considered as a very strong candidate as a theory describing the strong interaction. However, it has to give answers about the phenomena believed to occur in nuclear matter such as the status of the bound states of the quarks in the nucleus and the absence of free quarks from the final states of the reactions. The possible deconfinement of the quarks(quark or quark-gluon plasma) at high temperature or density or both, is also a very important question which Q.C.D. faces and which involves the study of thermodynamic aspects of Q.C.D. The production of very hot and dense matter(quark-gluon plasma) in the laboratory may help us understand the phenomena occuring in the Supernovae, neutron stars and the early universe. The planned attempts to produce such an environment on a mini-scale at CERN in the near future has made this study even more important. Theoretical physicists are using different models and methods to predict the events in the quark-gluon plasma. One of the most promising method being used is Lattice gauge theory. The finite temperature lattice Q.C.D. gives a strong signal of the phase transition from ordinary hadron matter to quark-gluon plasma at a critical temperature $T_c \cong 180$ Mev which is unexpectedly very high and finite density lattice Q.C.D.(quark number >0) can be considered as a possibility for correcting this . This method requires the determination of eigenvalues of a big sparse non-hermitian matrix and its inversion.

The Lanczos algorithm has been found exact for obtaining the eigenvalues of the large sparse matrices and for inverting them. We develop the block Lanczos algorithm which gives an optimization in computer time when inverting these matrices. The existing algorithm employs only even-even and even-odd field interactions on a lattice. An additional algorithm is given, using which, with the above mentioned interactions, we can simultaneously use odd-odd and odd-even interactions, which again gives a further optimization in computer time, at least for small lattices. The application of block inversion to the fermion matrix is discussed; the convergence at small mass is comparable or better than the other existing methods. Taking advantage of the block form of the Lanczos algorithm, other numerical methods are brought together to update the blocks of the lattice efficiently which makes larger lattices possible. Most of the previous work at finite density has been done using the quenched approximation (which means neglecting fermion internal loops in the theory) . By the above mentioned techniques, we can calculate the part of the fermion determinant necessary to include the internal fermion

loops. Having included the fermion loops, we calculate the chiral condensate,$<\bar{\psi}\psi>$, (which is an order parameter for signalling the chiral phase) to explore Q.C.D at finite density, using the SU(2) and SU(3) gauge groups on a 4^4 lattice. For SU(2) we use an analogy between the expression for $<\bar{\psi}\psi>$ in terms of the small eigenvalues on an infinite lattice and an electrostatic field. We also calculate explicit values of the chiral condensate for two representations. With all the parameters of the theory fixed, the critical chemical potential for restoring chiral symmetry goes to zero as quark mass goes to zero. As the critical chemical potential is expected to be propotional to the two quark hadron mass in SU(2), this signifies a zero mass baryonic state and this result is similar to the one obtained in the quenched approximation. It is argued, that, in the case of SU(2), this is not surprising. However, it would be a disaster if the corresponding result(the three quark hadron mass) held for SU(3). For SU(3) finite density calculations with internal fermion loops, the chiral condensate is more difficult to calculate since it involves a complex determinant. The resulting problems are described. We use m_q=0.1 and β=1.5, for our analysis .The chiral condensate appears to be in a zero divided by zero indeterminant form in our region of interest. By means of two independent methods for interpreting the chiral condensate, we show that there could be a phase transition at $\mu \cong 0.5$. However, chiral symmetry seems to be restored at μ=1.0.

CHAPTER ONE

INTRODUCTION

1.1)- HISTORICAL INTRODUCTION:

Quantum chromodynamics (Q.C.D.) and the G-W-S electro- weak model, are the successful quantum theories of the strong and electro-weak interaction. In all attempts at further advancement in these theories, a significant part of the dynamics is beyond the reach of perturbation theory. For example, in the strong coupling regime of Q.C.D., where the quarks are believed to be confined, the convergence of the perturbation theory is too slow to be of much use if indeed convergence exists. Only at very high momentum scales where the running coupling constant becomes small (and perturbation theory is applicable) can some predictions be made. For the strong coupling of Q.C.D., the associated phenomena, such as confinement and chiral symmetry breaking, it is necessary to have a non-perturbative method. Coventional analytic techniques expand around some classical solution and remain always essentially perturbative. Some phenomenological models show a partial success in solving certain non-perturbative aspects but there is a growing need for a quantitative understanding of these theories from basic principles.

In June, 1974, K.G.Wilson{1} introduced a lattice regularization of field theories and with the advent of new, powerful computers it has become an efficient method for non-perturbative studies.

1.2)- PATH INTEGRALS IN LATTICE FORMALISM:

Path integrals were first introduced by Feynmann{2}. The expectation value of an observable is given by its average over all the classical field configurations weighted by the factor exp{iS/h} where S is the action.

As an example of the use of the path integral in quantum field theory, let us take a simple scalar field $\phi(x)$ with a ϕ^4 interaction given by,

$$S[\phi(x)] = \int [(\partial\phi)^2 - \frac{1}{2} m^2 \phi^2 - \frac{1}{2} g^2 \phi^4] \, d\phi \qquad (1.1)$$

The two point Green's function is given by,

$$<\phi(x)\,\phi(y)> = \frac{1}{Z}\int D\phi\;\phi(x)\,\phi(y)\,e^{i\,S[\phi]/\hbar} \qquad (1.2)$$

where Z is the partition function of the corresponding field theory given by ,

$$Z = \int D\phi\; e^{i\,\beta\,S[\phi]};\ \beta = \frac{1}{\hbar} \qquad (1.3)$$

The integrals can be thought of as sums over all possible configurations in the space-time of the field variables $\phi(x)$.It is possible to calculate the free case (g=0) and then by means of perturbation in powers of g to calculate the non-free case. The individual terms involve divergent integrals and even after all renormalization and regularization, the series diverges but gives accurate answers for small g provided the high order terms are ignored.

For large g , perturbation theory fails and we have to think about some non-perturbative method. As mentioned earlier, the lattice regularization introduced by Wilson provides an efficient tool for non-perturbative calculations.

The expression eq.1.3, resembles the corresponding formula in classical statistical physics for the partition function, apart from the fact that the measure in it is complex. Moreover, the function involved is very oscillatory and is very difficult to handle in a numerical computation. Statistical physics already uses computer simulations and it would be very helpful to use its techniques. The Wick rotation is already familiar in field theory. It is the process of replacing ix_0 by x_0 in eq.1.2 and 1.3. It moves the Minkowsky space to Euclidean and as a consequence we will be working with imaginary time. In principle we should be able to return to Minkowsky space by analytic continuation. The Wick rotation transforms eq.1.3 into,

$$Z_E = \int D\phi\; e^{-\beta\,S_E} \qquad (1.4)$$

where Z_E and S_E are respectively the path integral and the action in

Eclidean space. Note that in Euclidean space all the directions are on the same footings. Eclidean quantum field theory can be treated as a classical statistical system and this has opened the door for the thermodynamical studies of Q.C.D.

1.2a)-PATH INTEGRALS AND LATTICE REGULARISATION:

In a quantum field theory, the dynamical variable (fields) are labelled by the points of the four dimensional Euclidean space, so it is very natural to approximate a volume of space-time by a four dimensional hypercubic lattice of points x separated by a distance a called the lattice spacing to obtain a discrete set of variables. The lattice introduced in this way, not only defines the path integral representation of the vacuum functional but gives an ultraviolet regularization as well. We shall denote n_σ as the number of points of the lattice in each space direction while n_β in the time direction.

The scalar fields and spinors sit on the sites of the lattice while the vector fields go to the *links* joining the sites. A 3^2x4 lattice is shown in fig.1.1. The derivatives in the action are to be approximated to a finite difference. For example,

$$\partial_\mu \phi[x] \cong \frac{1}{a} \Delta_\mu \phi_i = \frac{1}{a} [\, \phi(x_i + \mu) - \phi(x_i) \,] \qquad (1.5)$$

where $\mu = a\hat{\mu}$ and $\hat{\mu}$ is the unit vector in the μ direction.

By defining the scalar fields on a lattice of finite number of sites x_i , they and their degrees of freedom have been reduced to a finite number.We write any scalar field $\phi(x_i)$ on a site x_i as ϕ_i . The path integral is transformed into a product of ordinary integrals on each of the lattice sites,

$$Z_E = \int (\pi_n \, d\phi_n) \; e^{-\beta S[\phi]} \qquad (1.6)$$

The two point Green's function can be given as,

$$\langle \phi_i \, \phi_j \rangle = \frac{\int (\pi_n \, d\phi_n) \, \phi_i \phi_j \, e^{-\beta S[\phi]}}{\int (\pi_n d\phi_n) \, e^{-\beta S[\phi]}} \qquad (1.7)$$

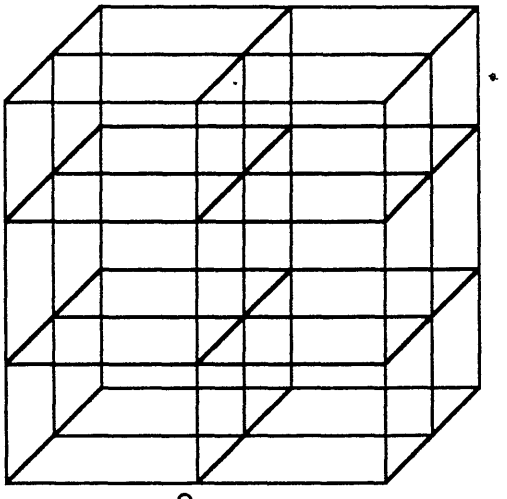

Fig.1.1 a 3^2x4 lattice.

with the action,

$$S_E = \frac{1}{2} a^2 \sum_{i,\mu} (\Delta_\mu \phi_i^2) + \frac{1}{2} a^4 \sum_i [m^2 \phi_i^2 + g^2 \phi_i^4] \qquad (1.8)$$

It is necessary to be able to return to the continuum theory by taking the classical limit n_σ ----> ∞, n_β ----> ∞, a---->0 with X =a n_σ, T=a n_β fixed. We also should be able to renormalize m and the coupling constant by choosing functions of a such that the resulting observables [the Green's functions, for example] converge to finite quantities. It is by no means a trivial matter to prove that this renormalization can be done consistently or that the resulting continuum theory will have Lorentz invariance.

1.3)- THE WILSON ACTION:

In formulating Q.C.D. on the lattice, where the gauge group is $SU(3)_{col.}$, we want to keep as many symmetries as possible of the continuum theory. For the Wilson action, which is a lattice version of the pure Y-M continuum action, we would it like to be locally gauge invariant. The fermion part of the continuum lagrangian can be written in a naive discrete form which, by requiring local gauge invariance shows how the gauge fields should be written.

The fermion part of the continuum lagrangian dendity can be written as,

$$L = i \bar{\Psi}(x) \gamma_\mu \partial_\mu \Psi(x) \qquad (1.9)$$

where $\Psi(x)$ is a fermion field variable while γ_μ are the well-know γ-matrices due to Dirac. . This lagrangian is invariant under the global transformation,

$$\Psi(x) \text{ -----> } V \Psi(x)$$
$$\bar{\Psi}(x) \text{ -----> } \bar{\Psi}(x) V^{-1} \qquad (1.10)$$

where V is some SU(N) matrix acting on quark field. Writing the

derivative in eq.1.9 in a discrete form, the fermion and antifermion fields do not refer to one point and local gauge invariance is lost,

$$L = i\bar{\Psi}(x)\gamma_0\{\frac{\Psi(x+\epsilon n_\beta) - \Psi(x-\epsilon n_\beta)}{2\epsilon}\} + \sum_{n_\sigma=1}^{4} i\Psi(x)\frac{(\gamma.n_\sigma)\Psi(x+\epsilon n_\sigma)}{2\epsilon} \qquad (1.11)$$

In order to regain local gauge invariance, we place a *connection* U(x,y) between $\Psi(x)$ and $\Psi(y)$, where y is a position infinitesimally close to x. $\Psi(x)$ U(x,y) $\Psi(y)$ is invariant under the local transformation V(x) if the connection variable transforms as,

$$U(x,y) \text{ -----}> V(x)\ U(x,y)\ V(y)^{-1} \qquad (1.12)$$

For some infinitesimally small path dl, U can be written as,

$$U(x,x+dl) = 1 + i\,g\,A.dl = e^{ig\,A.dl} \qquad (1.13)$$

where g is a bare coupling constant and A is given by the relation

$$A = A_\mu^i\ T^i \qquad (1.14)$$

where $A_\mu{}^i$ are gauge fields while T^i are the generators of the gauge group. Under the transformation law of U, A must transforms as,

$$A_\mu \text{ ----}> V(x)\ A_\mu(x)\ V^{-1}(x) + (1/ig)\ V(x)\ \partial_\mu\ V^{-1}(x) \qquad (1.15)$$

to give gauge invariance of $\Psi(x)$ U(x,y) $\Psi(y)$.

On the lattice, the fermion fields are defined on the sites so that the connection becomes the gauge variable which sits on the link between the sites.

With this understanding we write a lattice approximation of the pure Y-M continuum action and hope to be able to restore it in the limit a----->0.

Different shapes of lattices can be used for different problems (or for the same problem with the condition of universality that they should not lead to different continuous field theories). For simplicity we use a hypercubic lattice with only nearest neighbour interactions, the building blocks of which are the link or gauge variable.

The simplest action for Wilson's SU(N) pure lattice gauge

theory is the product of the link variables around a plaquette, which is analogous to Wegner's plaquette variable in the Ising model.

$$S = -\beta \sum_{n,\hat{\mu},\hat{\nu}} tr \{ U_\mu(n)\, U_\nu(n+\mu)\, U_\mu^\dagger(n+\nu)\, U_\nu^\dagger(n) + C.C. \} \qquad (1.16)$$

where μ and ν are unit vectors in the direction of μ and ν respectively. β is some constant to be determined. We have also used,

$$U_{-\mu}(n+\mu) = U_\mu^\dagger(n) = U_\mu^{-1}(n) \qquad (1.17)$$

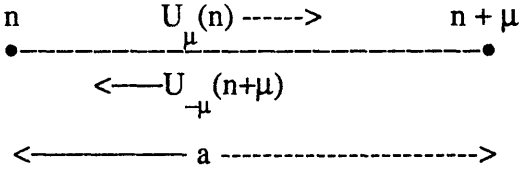

we write the plaquette action as,

$$S = \beta \sum_{\square} \sum_{n,\hat{\mu},\hat{\nu}} tr \left[\square + \square \right] \qquad (1.18)$$

In SU(N) lattice gauge theory, the link variable are elements of SU(N) group defined as,

$$U_\mu(n) = \exp\{ iagA \} \qquad (1.19)$$

where g is the bare coupling constant. The plaquette action eq.1.15 is invariant under the *discrete* kind of local transformation, (see eq.1.12)

$$U_\mu(n) \text{ ----> } G(n)\, U_\mu(n)\, G^{-1}(n+\mu) \qquad (1.20)$$

where G(n) is an SU(N) rotation at site n. The total gauge action for the whole lattice can be written as,

$$S_G = \frac{\beta}{N} \{ \sum_{\square\, n,\hat{\mu},\hat{\nu}} \mathrm{tr} [\square + \square^{\dagger}] \qquad (1.21)$$

$$\hat{\mu} < \hat{\nu} \qquad (1.22)$$

Starting from this action, expanding U in powers of A, and taking the continuum limit a---->0, it is possible to show {6}, that,

$$S_G \text{-----} > \frac{1}{4} \frac{\beta}{N} \int \mathrm{tr}\, F_{\mu\nu} F_{\mu\nu}\, d^4x \qquad (1.23)$$

where,

$$F_{\mu\nu} = \partial_\nu A_\mu - \partial_\mu A_\nu + [A_\mu, A_\nu] \qquad (1.24)$$

and it is continuum action if we identify ,

$$\beta = 2N/g^2 \qquad (1.25)$$

Two things should be noted; we have restored the O(4) invariance of the continuum action and the local invariance included at the start ensures that we recover the standard covariant $F_{\mu\nu}$ of Y-M theory.

1.3b)- STRONG COUPLING EXPANSION AND CONFINEMENT:

Eq.1.15 represents the simplest form of the Wilson loop {1}, which, in its most general form, is the trace of a directed product of the gauge link variables round an arbitrary closed loop and is a gauge invariant construction. It is used as an order parameter in lattice gauge theory ; that a parameter concerned with the phase structure of the theory. Elitzur's theorem {3} forbids the possibility of any local order parameter in lattice gauge theory but we can use gauge invariant order parameters.

The strong coupling limit is very natural and simple in the Lattice gauge theory. But it is very difficult to treat in the perturbation theory. In this limit, the inverse coupling constant β of eq.1.21 become very small and we can expand the Boltzmann factor in

terms of β as explained below.Wilson proved in his original paper {1} that, in this limit, confinement holds for Lattice quenched QCD. Quenched QCD or the quenched approximation is described later in this chapter but here it is sufficient to know that it involves ignoring the dynamical fermions part of the action.

In this approximation, the Wilson loop is given as,

$$\langle W(U) \rangle = \frac{1}{Z} \int dU \, W(U) \, e^{-S_G} \qquad (1.26)$$

Expanding the Boltzmann factor in terms of β we get the terms of the series containing products of gauge elements multiplied by the Wilson loop(which also consists of the gauge elements). From the integrals,

$$\int dU \, U = 0 \qquad (1.27)$$

$$\int dU \, 1 = 1 \qquad (1.28)$$

$$\int dU \, U_{ij} \, U^{\dagger}_{kl} = (\frac{1}{n}) \, \delta_{il} \, \delta_{jk} \qquad (1.29)$$

eq.1.26 for a Wilson loop of size (RxT) comes out to be,{5,6},

$$\langle W(R,T) \rangle \propto e^{-(R \times T)} \qquad (1.30)$$

and we can note an area law dependence.

Also the potential V, required to seperate a fermion and an antifermion, R distance apart for a period of time T is related to the Wilson loop by the relation{4},

$$\langle W(R,T) \rangle \propto e^{-V(R) \times T} \qquad (1.31)$$

so that,

$$V(R) \propto R \qquad (1.32)$$

and we have a linearly confining potential.

$$V(R) = \sigma R \qquad (1.33)$$

where the constant σ is called the *string tenston*.

1.4)- THE CONTINUUM LIMIT:

Putting a theory on a lattice is a regularization of the theory. But this regularization has a temporary role since, at the end, it should be removed and, in a renormalizable theory, final results should not carry any trace of the regularization used.

In the case of lattice regularization, this is the process of taking the continuum limit a---->0, but it is not a very simple process.

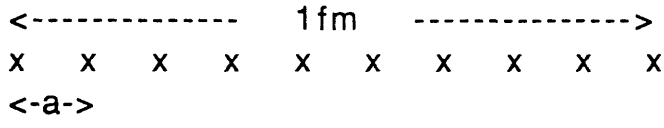

After regularization, the elementry interactions extend over a distance of order of a . In strong interactions, events are correlated over about 1fm. As a becomes small, 1fm corresponds to a large number of lattice units which goes to infinity as a goes to zero.

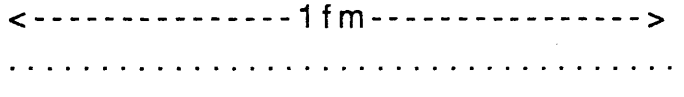

The final solution of the theory should have a non-zero correlation over many lattice units. The main difficulty of the theory lies in achieving a collective behaviour over this distance.

For simplicity, let us consider a theory without dimensionful parameters. The only dimensional parameter available is the lattice spacing a. Mass in this regularization can be written as,

$$m = \frac{1}{a} f(g_1, g_2, g_3, ...) \qquad (1.34)$$

where g_1, g_2, g_3, ..., are the dimensionless couplings of the theory. In the limit a ----> 0, these go to the limit g_1----$>g_1^*$,g_2----$>g_2^*$,....., so that $f(g_1^*, g_2^*, ...)$ ----$>$0, to get a finite mass prediction. The correlation length measured in terms of lattice units,

$$\xi \sim (am)^{-1}. \qquad (1.35)$$

So the tuning procedure will be,

$$\begin{aligned} &a \text{ ----> } 0 \\ &g_1 \text{----->} g_1^* \\ &g_2 \text{----->} g_2^* \\ &\text{.....} \\ &\text{....etc.....} \end{aligned} \qquad (1.36)$$

where g_1^*, g_2^*, etc, are the critical points of the corresponding statistical system. Near these critical points, there will be large scale fluctuations which could break the underlying lattice structure in a Euclidean rotational symmetric continuum theory.

1.5)- SCALING:

A pure Y-M theory has a single dimensionless coupling constant g and we know that g = g(a). In the continuum limit when a ----->0, and g ----->g_c(some critical g), we have to choose g_c so that all the physical predictions become independent of the lattice spacing. Renormalization also requires that this critical point should have scaling properties, i.e, all physical quantities should tend to finite values in this limit. It means we are looking for the critical g_c of a second order transition.

On the lattice, the only dimensionful parameter is the lattice spacing a. All the observables on the lattice are measured as dimensionless numbers. We can write the masses of two mesons as,

$$m_\pi = m/a \qquad (1.37)$$

$$m_\rho = n/a \qquad (1.38)$$

where m and n are masses of the π and ρ mesons in lattice units respectively.

In the scaling region we should have,

$$\frac{m}{n} = \frac{m_\pi}{m_\rho} = \text{constant.} \qquad (1.39)$$

For asymptotically free theories as g ---->0 the critical point is β_c----> ∞. The inverse of the coupling constant ,β, and a can be combined to give a dimensionful lattice parameter, $\Lambda_{lattice}$, by which most physical quantities can be described.

The relation between $\Lambda_{lattice}$ and Λ_{MS}, (MS stands for minimal subtraction scheme of the continuum theory) permits us to write the lattice predictions in the physical units.

For example,

$$\frac{\Lambda_{lattice}}{\Lambda_{MS}} = 29 \qquad \text{for SU(3)}$$
$$\Lambda_{MS} = 100 \sim 200 \text{ Mev} \qquad \{11\} \qquad (1.40)$$

so that $\Lambda_{lattice}$ ~ 5Mev.

$\Lambda_{lattice}$ is a physical quantity so that,

$$a\frac{d\Lambda_{lattice}}{da} = 0 \qquad (1.41)$$

If we write,

$$\Lambda_{lattice} = (1/a)\,\lambda$$

then,

$$-\frac{1}{a}\lambda + \tilde{\beta}(g)\frac{d}{dg}(\lambda/a) = 0 \qquad (1.42)$$

where $\beta(g)$ is the beta function of the renormalization group equation.

From the continuum theory,

$$\lambda = \exp\left[-\frac{1}{\beta_0 g^2}\right]\left(\beta_0 g^2\right)^{\beta_1/2\beta_0^2} \qquad (1.43)$$

Remember that $\beta = 2N_c/g^2$. All the masses should behave similarly as a function of β as eq.1.38 can be written as,

$$m_\pi = C_1 \Lambda_{lattice} \quad \text{or} \quad m = C_1\lambda \; ; \; m = f(\beta)$$
$$m_\rho = C_2 \Lambda_{lattice} \quad \text{or} \quad n = C_2\lambda \; ; \; n = f(\beta) \qquad (1.44)$$

If we are close to the continuum limit, where g(a)---->0 we expect that masses will vary with β in the perturbative way eq.1.42. This is called *asymptotic scaling*.

1.6)- MONTE CARLO SIMULATION:

The expectation value of any observable can be given as,

$$\langle O \rangle = \frac{\int (\Pi\, dU)\, O\, e^{-S_G}}{\int (\Pi\, dU)\, e^{-S_G}} \qquad (1.45)$$

which involves a very high dimensional integral. If we evaluate this integral directly, much effort is wasted on configurations with a large action which do not contribute significantly. The idea of the Monte Carlo (M.C.) method is to replace the computation of the expectation value of O by an average over the gauge configuration U. Here a configuration means a set of U matrices on all the links of the lattice,

$$\langle O \rangle = \frac{\sum_i O\{U\}}{\sum_i 1} \qquad (1.46)$$

and we want only those configurations which are distributed according to a Boltzmann distribution $\exp(-S_G)$.

This replacement of eq.1.45 by 1.46 involves the technique *importance sampling* from statistical physics. It is a method which

avoids the configurations with large actions, which do not contribute to $< O >$. Thus, the centre of the problem is shifted towards the techniques of generating configurations which are distributed according to the Boltzmann weight.

Two algorithms using M.C. techniques are believed to be the most important; namely (1) Metropolis and (2) Heat bath algorithms. The Metropolis algorithm is more popular due to its simplicity of application and we have used a modified form in our calculations.

In both these algorithms one begins with a random configuration U_i. Then, a single variable is varied and a new configuration $U_i^{'}$ is generated. If this new configuration obeys the rules of the algorithm it is *accepted* and replaces the old one otherwise it is *rejected*. One *sweep* through the lattice involves the sampling of all variables. The aim of both the procedures is to generate a gauge configuration U which is closer to an equilibrium Boltzmann distribution. $O(U_i^{'})$ is calculated for $U_i^{'}$ and its contribution towards eq.1.46 is recorded. Next, the algorithm is applied to this configuration $U_i^{'}$ and a new statistically independent configuration $U_i^{''}$ at thermal equilibrium is generated and its contribution towards eq.1.46 is again recorded. This procedure is repeated many times and $< O >$ is calculated by virtue of eq.1.46.

Passage from one configuration U to $U^{'}$ is controlled by the transition matrix,

$$\text{with} \qquad \sum_{U^{'}} P(U \text{ ----> } U^{'}) \; (U \text{ ----> } U^{'}) = 1 \qquad (1.47)$$

One condition on $P(U \text{ ----> } U^{'})$ is that it leaves an equilibrium emsemble in equilibrium, i.e, the Boltzmann weight is its eigenvector, so that,

$$\sum_{U^{'}} P(U \text{ ----> } U^{'}) \; \exp\{-S(U^{'})\} = \sum_{U} P(U^{'} \text{ ----> } U) \; \exp\{-S(U)\} = \exp\{-S(U^{'})\} \qquad (1.48)$$

As already mentioned, this stochastic change is produced by changing one link variable and we get a new configuration. The acceptance or rejection of this change depends upon the algorithm being applied. Once a change is accepted or rejected, a next link variable is selected for the change. The selection could be *random* but

it is convient computationally to move through the lattice in an orderly fashion. The Markovian chain can still be given as,

$$P_{tot.}(U \text{ ----> } U') = P(U \text{ ----> } U')_1 \times P(U \text{ ----> } U')_2 \times \ldots\ldots$$

Our aim is to define a stochastic sequence with the property that after the statistical equilibrium is reached the probability of finding any configuration is weighted by Boltzmann distribution exp{-S(U)}.

A sufficient but not necessary condition on each step of algorithm is,

$$\exp\{-S(U)\} \times P(U \text{ ----> } U') = \exp\{-S(U')\} \times P(U' \text{----> } U) \quad (1.49)$$

It can be proved that each step of a M.C. algorithm makes the emsemble more closer to equilibrium {25}.

1.6a)-THE METROPOLIS ALGORITHM;{7}

We can begin with a *cold* or *hot* start. In the lattice gauge theory, a hot start means a start with some random configuration of the gauge group.

We start with some configuration U and make a new U' by changing a link variable.We accept this change as a *trial change* U^t with a temporary (arbitrary) transition probability $P(U \text{ ----> } U^t)$. The change produced in the action, ΔS, is computed. If, $\Delta S < 0$, it is accepted, as this configuration is more inclined towards the equilibrium. If $\Delta S > 0$, a random number R, between 0 and 1 is generated and if $\exp\{-\Delta S\} \geq R$ it is accepted with probability R, otherwise rejected. The *detailed balanced condition* eq.1.49 is satisfied.

$$\frac{P(U \text{ ----> } U')}{P(U' \text{ ----> } U)} = \frac{P_t(U \text{ ----> } U^t)}{P_t(U^t \text{----> } U)} \times \frac{\exp\{-\Delta S\}}{1} = \frac{\exp\{-\Delta S\}}{1}$$

$$= \frac{\exp\{-S(U)\}}{\exp\{-S(U)\}} \quad (1.50)$$

1.7)- FERMIONS ON THE LATTICE;

Putting fermions on the lattice requires the lattice equivalent of the Dirac operator. A theorem exists which shows that it is impossible to write a lattice Dirac operator which exhibits all the

properties of its continuum counterpart. However, although it is difficult to put fermion fields on the lattice, there are some schemes around which are partially successful. We shall describe the most important ones briefly.

1.7a)- THE NAIVE FERMIONS:

The complete action for the fermion fields coupled with gauge fields can be written as,

$$S_F = -\int \{ \bar{\psi}(\gamma_\mu(\partial_\mu + A_\mu)) \psi + m \bar{\psi} \psi \} d^4x \qquad (1.51)$$

At zero mass , this action shows partial invariance under the substitution,

$$\begin{aligned} \psi &\longrightarrow \gamma_5 \psi \\ \bar{\psi} &\longrightarrow -\bar{\psi}\gamma_5 \\ \bar{\psi}\psi &\longrightarrow -\bar{\psi}\psi \end{aligned} \qquad (1.52)$$

This is chiral symmetry and it is broken by the mass term in the action.

On a lattice, the fermion fields are defined at sites by

$\bar{\psi}(n)$ and $\psi(n)$

Under a local transformation analogous to eq.1.10,

$$\begin{aligned} \psi(n) &\text{------}> G(n)\,\psi(n) \\ \bar{\psi}(n) &\text{------}> \bar{\psi}(n)\,G^{-1}(n) \end{aligned} \qquad (1.53)$$

the object $\bar{\psi}(n)\psi(n+\mu)$ is not gauge invariant, as discussed already. To make it invariant, we introduce a gauge field U on the links between the sites which tranforms (see eqs.1.11 and 1.12) as,

$$U(n) \text{-----}> G(n)\,U(n)\,G^{-1}(n+\mu)$$

The fermion fields interact through these gauge fields or gluons. The lattice action is,

$$S = a^4 \sum_n \{ \sum_{\hat{\mu}}^4 \frac{1}{2a} [\bar{\psi}(n)\, \gamma_{\hat{\mu}}\, U(n)\psi(n+\mu) - \bar{\psi}(n)\, \gamma_{\hat{\mu}}\, U(n-\mu)\, \psi(n-\mu)\,] + m\, \bar{\psi}(n)\psi(n)$$

(1.54)

Rescaling by $\psi \longrightarrow 2^{1/2}\, a^{3/2}\psi$, we get,

$$S_{NF} = \sum_n \{ \sum_{\hat{\mu}}^4 [\, \bar{\psi}(n)\, \gamma_{\hat{\mu}}\, U(n)\, \psi(n+\mu) - \bar{\psi}(n)\, \gamma_{\hat{\mu}}\, U(n-\mu)\, \psi(n-\mu)\,] + 2ma\, \bar{\psi}(n)\psi(n)\}$$

(1.55)

All we have done is a result of a replacement of the differential by a symmetric difference.

$$\partial_{\hat{\mu}}\, \psi \longrightarrow \frac{\psi(n+\mu) - \psi(n-\mu)}{2a} \qquad (1.56)$$

This is the *naive fermion scheme.*

Using a matrix notation, the action can be written as

$$S = -\bar{\psi}(\, M + 2ma)\, \psi \qquad (1.57)$$

where M is the naive fermion matrix. It is anti-hermitian.

We choose a boundary condition for gauge fields to preserve a discrete kind of translational symmetry. We shall use anti-periodic boundary conditions for fermion fields to avoid zero modes.

Another thing notable is the effect of chiral symmetry on the eigenvalues of M which come in the conjugate pairs.

$$M\, \psi = i\, \lambda\, \psi$$

$$\Rightarrow \quad M\, \gamma_5 \psi = -\gamma_5 M\, \psi = -i\, \lambda\, \gamma_5\, \psi \qquad (1.57a)$$

1.7b)- SPECIES DOUBLING:

The free continuum Dirac Green's function satisfies,

$$(\gamma_\mu \partial_\mu + m)\, G_F(x - y) = \delta(x - y) \qquad (1.58)$$

From eq.1.56 the corresponding lattice propagator, in our notation, will become,

$$\sum_{\hat{\mu}} \gamma_{\hat{\mu}} \{ G(n + \mu, 0) - G(n - \mu, 0)\} + 2ma\, G(n,0) = \delta_{n,0} \qquad (1.59)$$

Putting the propagator equation on a hypercube of length L and defining a Fourier transform by,

$$G(n,0) = \sum_{\{q\}} \exp(iq.n)\, \tilde{G}(q) \qquad (1.60)$$

with q = 2πi/L; i = 0,1, ...L-1.This gives the propagator eq.,

$$\frac{1}{2}\sum_{\hat{\mu}} \gamma_{\hat{\mu}} \sum_{\{q\}} [\exp\{iq.(n+\mu\} - \exp\{-iq.(n-\mu)\}]\tilde{G}(q) + 2ma\, \tilde{G}(q) \sum_{\{q\}} \exp(iq.n) = \frac{1}{L^4}\sum_{\{q\}} \exp(iq.n) \qquad (1.61)$$

which gives,

$$\tilde{G}(q) = \frac{1}{L^4\{\sum_{\hat{\mu}} i\gamma_{\hat{\mu}} \sin q_{\hat{\mu}} + 2ma\}} = \frac{2ma - \sum_{\hat{\mu}} i\gamma_{\hat{\mu}} \sin q_{\hat{\mu}}}{L^4\{(2ma)^2 + \sum_{\hat{\mu}} \sin^2 q_{\hat{\mu}}\}} \qquad (1.62)$$

Consider the case m = 0.

$$\tilde{G}(q) = \frac{-\sum_{\hat{\mu}} i\gamma_{\hat{\mu}} \sin q_{\hat{\mu}}}{L^4 \sum_{\hat{\mu}} \sin q_{\hat{\mu}}} \qquad (1.63)$$

G(q) has a pole at $\Sigma_\mu \sin q_\mu = 0$.

This happens not just when q_μ = (0,0,0,0,) but also when any component of $q_\mu = \pi$. Thus there are 2^d or 16 poles in 4 dimensions. It seems to be describing 16 degenerate fermions per lattice site. This is the *doubling problem.*

1.7c)- REMEDIES;

The lattice eq.1.55 preserves the chiral symmetry at the mass m = 0 limit. The doubling problem is a characteristic of chiral symmetry {16}, so we have two chioces,

1)- Either a non-chiral symmetric lattice regularization is defined

or,

2)- Doubling is expected { 8 }.

The procedure suggested by Wilson belongs to first category while Kogut-Susskind (staggered) fermion scheme belongs to the second. The Wilson fermion scheme gives an effective mass of order 1/a to the 15 unwanted flavours. The mass of the 16th can be adjusted by varying a parameter in front of the action called the *hopping parameter*.In this scheme, calculations become very complicated and chirality is lost.

1.7d)- KOGUT-SUSSKIND FERMION SCHEME;

Consider a unitary transformation on a site n,

$$\psi(n) = T(n)\,\chi(n)$$
$$\bar{\psi}(n) = \bar{\chi}(n)\,T(n) \qquad (1.64)$$

where $T(n) = \prod_{\hat{\mu}} \gamma_{\hat{\mu}}^{n_{\hat{\mu}}}$ and $T\,T^{\dagger} = 1$.

Any site can be given as n = (n_1, n_2, n_3, n_4) where n_i are the co-ordinates of site n.

For the naive action with U = 1,

$$S = \sum_{n,\hat{\mu}} \{\, \bar{\psi}(n)\,\gamma_{\hat{\mu}}\,[\,\psi(n+\mu) - \psi(n-\mu)\,] + 2ma\;\bar{\psi}\psi\,\}, \qquad (1.65)$$

under the above transformation,

$$\bar{\psi}(n)\,\psi(n) \text{ ------> } \bar{\chi}(n)\,\chi(n) \qquad (1.66)$$

and eq.1.65 becomes,

$$S^{KS} = \sum_{n,\hat{\mu}} \eta_{\hat{\mu}}(n)\,\bar{\chi}(n)\,\{\,\chi(n+\mu) - \chi(n-\mu)\,\} + 2ma\,\bar{\chi}(n)\,\chi(n) \qquad (1.67)$$

where η_μ are the *fermion signs* which can be given as,

$$\begin{aligned} \eta_{\hat{\mu}}(n) &= 1, && \hat{\mu} = 1 \\ &= (-1)^{n_1} && \hat{\mu} = 2 \\ &= (-1)^{n_1 + n_2} && \hat{\mu} = 3 \\ &= (-1)^{n_1 + n_2 + n_3} && \hat{\mu} = 4 \end{aligned} \qquad (1.68)$$

This action eq.1.67 is now diagonal in the Dirac indices. One might attempt to consider only one and drop the other three. So it becomes a one-component spinor field and four component quark fields are constructed from it at different corners of the lattice. By this trick, the number of quark fields is reduced to four which might be interpreted as describing four different flavours {8}.

Considering the transformation eq.1.64 in the matrix notation and considering eq.1.57,

$$\bar{\chi}(n)\,T^{\dagger}(n)\,M\,T(n)\,\chi(n) = \bar{\chi}(n)\,M_D\,\chi(n) \qquad (1.69)$$

where M_D has four block matrices along its diagonal only. Its explicit representation will be,

$$= \overbrace{\chi_1\,\chi_2\,\chi_3\,\chi_4} \begin{pmatrix} M_{KS} & & & \\ & M_{KS} & & \\ & & M_{KS} & \\ & & & M_{KS} \end{pmatrix} \begin{pmatrix} \chi_1 \\ \chi_2 \\ \chi_3 \\ \chi_4 \end{pmatrix} \qquad (1.70)$$

so that action for each component becomes,

$$\overset{KS}{S} = -\bar{\chi}(M_{KS} + 2ma)\chi \qquad (1.71)$$

In the staggered fermion scheme flavour symmetry is explicitly broken and it is hoped that it will be recovered in the continuum limit. However chiral symmetry is recovered at m = 0.

1.7e)- THE EFFECTIVE ACTION:

The Monte Carlo method devised for the bosonic fields cannot be used for fermionic fields, because fermionic fields are anti-commuting objects of a Grassmann algebra. The properties of fermionic fields ψ's are,

$$\begin{aligned} &\{ \psi_i, \bar{\psi}_j \} = \mathbb{O}, \\ &\{ \psi_i, \psi_j \} = \{ \bar{\psi}_i, \bar{\psi}_j \} = 0 \\ &(\psi_i)^2 = (\bar{\psi}_j)^2 = 0 \\ &\int d\psi\, \psi = 1 \,, \int d\psi = 0 \end{aligned} \qquad (1.72)$$

By the use of these properties and by using the quadratic form of Q.C.D. fermion action , eq.1.71 becomes,

$$S = -\sum_{i=1}^{N_f/4} \bar{\chi}_i (M_{KS} + 2ma)\chi_i \qquad (1.73)$$

We can calculate the *partition function* of Q.C.D.,

$$Z = \int d\bar{\chi}\, d\chi\, dU\, e^{S^{KS} + S_G}$$

Integrating over the fermion fields using eqs.1.72, this becomes,

$$Z = \int dU\, e^{S_G} [\, \det (M_{KS} + 2ma)]^{\frac{N_f}{4}} \qquad (1.74)$$

where N_f are number of flavours and it is clear that we can use the *effective action*,

$$S_{eff.} = S_G + \frac{1}{4} N_f \log [\det (M_{KS} + 2ma] \qquad (1.75)$$

The two point Green's function satisfies the equation,

$$[(M_{KS} + 2ma)\, G]_{ij} = \delta_{ij} \qquad (1.76)$$

so that,

$$< \bar{\chi}_i \chi_j > = \int d\bar{\chi}\, d\chi\, dU\, \bar{\chi}_i \chi_j\, e^{S_G + S^{KS}}$$

Integrating over fermion fields again, this becomes,

$$= \int dU \frac{1}{4} N_f (M_{KS} + 2ma)^{-1}_{ij}\, e^{S_{eff}} \qquad (1.77)$$

In particular,{ 9 },

$$< \bar{\chi}\, \chi > = \frac{1}{n_\sigma^3 n_\beta} \frac{N_f}{4} < tr\, (M_{KS} + 2ma)^{-1} > \qquad (1.78)$$

1.8)- FINITE DENSITY:

There is a straight forward way of introducing a finite temperature in lattice gauge theory calculations{10}.The value of the critical temperture,T_c, for deconfinement is believed to be 180Mev and is too high for current laboratory experiments. The decisive element in the deconfinement of the quarks is the increase of colour charge density, which is here achieved by an increase of temperature resulting in particle production. Matter at high density can, however, also be formed by compressing a system of many nucleons at low temperature; this leads to a high density of baryons and hence also of quarks.

The complete phase diagram of strongly interacting matter must thus describe the phase structure as a function of the temperature T and the baryonic number density n_B or the corresponding baryonic *chemical* potential μ. A schematic view of a possible phase diagram from hadron matter to a quark gluon plasma in Q.C.D. , as function of T and μ is shown in fig.1.5. The dotted area between these two phases represents a sub-nuclear phase due to

some phenomenon analogous to Cooper pair production in superconducting material.

The introduction of a finite density has a problem associated with defining the chemical potential on the lattice in a satisfactory way. At $\mu = 0$,

$$Z = \text{tr } \{\exp(-\beta H)\} \qquad (1.79)$$

where β is the inverse temperature and H is the Hamiltonian of some statistical system. With the introduction of the chemical potential, it becomes,

$$Z = \text{tr } \{\exp[-\beta(H - \mu N_B)]\} \qquad (1.80)$$

with N_B denoting the operator for the overall baryon number.

For Q.C.D. at finite density we must introduce an extra term in the time direction of the fermion part of the action in eq.1.51, which has the form,

$$\bar{\psi}(\partial_4 + A_4)\psi + \mu\bar{\psi}\gamma_4\psi \qquad (1.81)$$

The energy density is defined as,

$$E = -V^{-1}\frac{\partial(\ln Z)}{\partial\beta} \qquad (1.82)$$

where V is the spatial volume (of the lattice), while,

$$Z = \int d\bar{\chi}\, d\chi\, e^{-\beta S_F^{KS}} \qquad (1.83)$$

where S_F^{KS} is the fermion action, which is modified by the introduction of chemical potential but can still be given by eq.1.81.

The energy density E, calculated by using the naive application of eqs.1.81, 1.82 and 1.83 is quadratically divergent in the continuum limit and the appropriate form of the Kogut-Susskind fermion action at finite density suggested {12} is,

$$S_F^{KS} = -\{\sum_n \bar{\chi}(n) \sum_{\hat{\mu}}^{3} \eta_{\hat{\mu}}(n) [U_{\hat{\mu}}(n)\chi(n+\mu) - U_{\hat{\mu}}^{\dagger}(n-\mu)\chi(n-\mu)] \qquad (1.84)$$

$$+ \sum_n \bar{\chi}(n) \eta_{\hat{4}}(n) [e^{\mu a} U_{\hat{4}}(n)\chi(n+4) - e^{-\mu a} U_{\hat{4}}^{\dagger}(n-4)\chi(n-4) + 2ma \sum_n \bar{\chi}(n)\chi(n)\}$$

and we have used this form in our calculations.

We can write the action eq.1.84 in a matrix notation as before,

$$S_F^{KS} = -\bar{\chi}(M_c + 2ma)\chi \qquad (1.85)$$

For a zero mass quark, this becomes,

$$S_F^{KS} = -\bar{\chi} M_c \chi \qquad (1.86)$$

where M_c is the fermion matrix with the chemical potential . It is an $(N_c x n_\sigma x n_\beta)$ x $(N_c x n_\sigma x n_\beta)$ matrix where N_c is the number of colour degrees of freedom. The chiral condensate can still be given by eq.1.78.

The thermal average of an arbitrary operator O can be written as,

$$< O > = \frac{1}{Z} \int dU\, d\bar{\chi}\, d\chi\, O(U,\bar{\chi},\chi)\, e^{S_G + \bar{\chi} M_C \chi} \qquad (1.87)$$

After integrating over the fermion variables χ and $\bar{\chi}$, we get,

$$= \frac{1}{z} \int dU\, \bar{O}(U)\, (\det M_c)\, e^{S_G}$$

$$= \frac{\int dU\, \bar{O}\, (\det M_c)\, e^{S_G}}{\int dU\, (\det M_c)\, e^{S_G}} \qquad (1.88)$$

The calculation of $(\det M_c)$ requires an enormous amount of computation. In the *quenched approximation* $(\det M_c)$ is set constant , so that,

$$< O >_{\text{quenched}} = \frac{\int dU\, \bar{O}(U)\, e^{S_G}}{\int dU\, e^{S_G}} \qquad (1.89)$$

This approximation leaves out the internal quark loops.

1.9)- SOME PREVIOUS RESULTS AND SPECULATIONS:

It might be chance, but in the quenched approximation, at least, convincing evidence has been found to show that the critical temperatures for deconfinement and chiral symmetry restoration are coincident. Most of the calculations so far have been done in the quenched approximation as this theory is easy to simulate on a computer but there is a problem since with a zero quark mass, the chiral symmetry is restored at an arbitrary critical chemical potential, μ_c, which is consistent with $\mu_c=(1/2)m_\pi$, where m_π is the pion mass, and is inconsistent with contemporary physic which favours $\mu_c=(1/3)m_P$, where m_P is the proton mass. Therefore, it is necessary to examine the theory, including dynamical fermions, via the fermion determinant, $\det M_c$. We call this the *full or unquenched theory* and it is expected that this will smooth out the pseudo-transition at half the pion mass.{21}

As indicated above, the expression for the chiral condensate $<\chi\chi>$ eq.1.78 at finite density in the full theory, demands the calculation of the determinant and the inverse of the fermion matrix and with the introduction of the chemical potential, the fermion matrix M_c, becomes a non-hermitian matrix.

1.10)- OVERVIEW OF THE THESIS:

In chapter 2, we modify the Lanczos algorithm for hermitian matrice, to include non-hermitian matrices. We apply it to calculate the eigenvalues of the large sparse matrices and their inverses. The block Lanczos technique is developed to invert the blocks of the big sparse general matrices with an optimization.

Chapter 3 contains the application of the block Lanczos(non-hermitian) method to the fermion matrix M_c. A computer method is described for the discrete derivative part of the fermion action. A modified Metropolis algorithm is given and applied for fast updating. This chapter also contains an algorithm for M_c^{-2} and an additional algorithm to the block Lanczos algorithm to save computer time.

The above mentioned techniques enable us to explore QCD at finite density and for this, we have presented our results , using SU(2) and SU(3) gauge groups, in chapter 4 and 5 respectively.

At the end of the thesis, we describe the conclusion drawn from our research work.

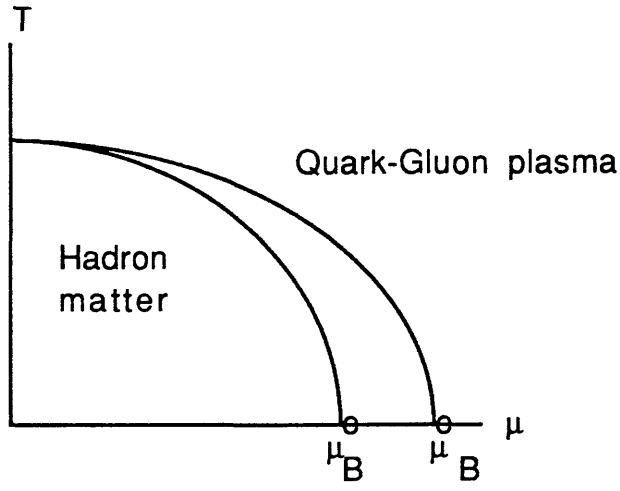

Fig.1.5

CHAPTER 2

THE NON-HERMITIAN LANCZOS ALGORITHM

2.1)- NEED FOR NON-HERMITIAN LANCZOS METHOD:

As indicated earlier, the introduction of the chemical potential causes the fermion matrix, for gauge groups SU(2) and SU(3) to become non-hermitian. The fermion matrix for nearest neighbour interactions only, is shown in fig.2.1 for a 4^2 lattice shown in fig.2.1a. We have taken anti-periodic boundary conditions for the fermion field on this lattice in (1 + 1) directions. A method, for dealing with the non-hermitian matrices, is needed for the finite density calculations. The hermitian Lanczos method{13} is modified to include non-hermitian matrices and this method can be used to diagonalise and invert a big sparse general matrix like the fermion matrix.

2.2)- TRIDIAGONALIZATION OF AN ARBITRARY COMPLEX MATRIX:{13}

The inclusion of non-hermitian matrices in Lanczos method requires a similarity transformation, to produce a tridiagonal symmetric matrix T from a general non-hermitian matrix H.

$$X^{-1} H X = T \qquad (2.1)$$

with,

$$T = \begin{pmatrix} \alpha_1 & \beta_1 & 0 & 0 & 0 & . & . & . & . \\ \beta_1 & \alpha_2 & \beta_2 & 0 & 0 & . & . & . & . \\ 0 & \beta_2 & \alpha_3 & \beta_3 & 0 & . & . & . & . \\ . & . & . & . & . & . & . & . & . \\ . & . & . & . & . & . & . & . & . \end{pmatrix} \qquad (2.2)$$

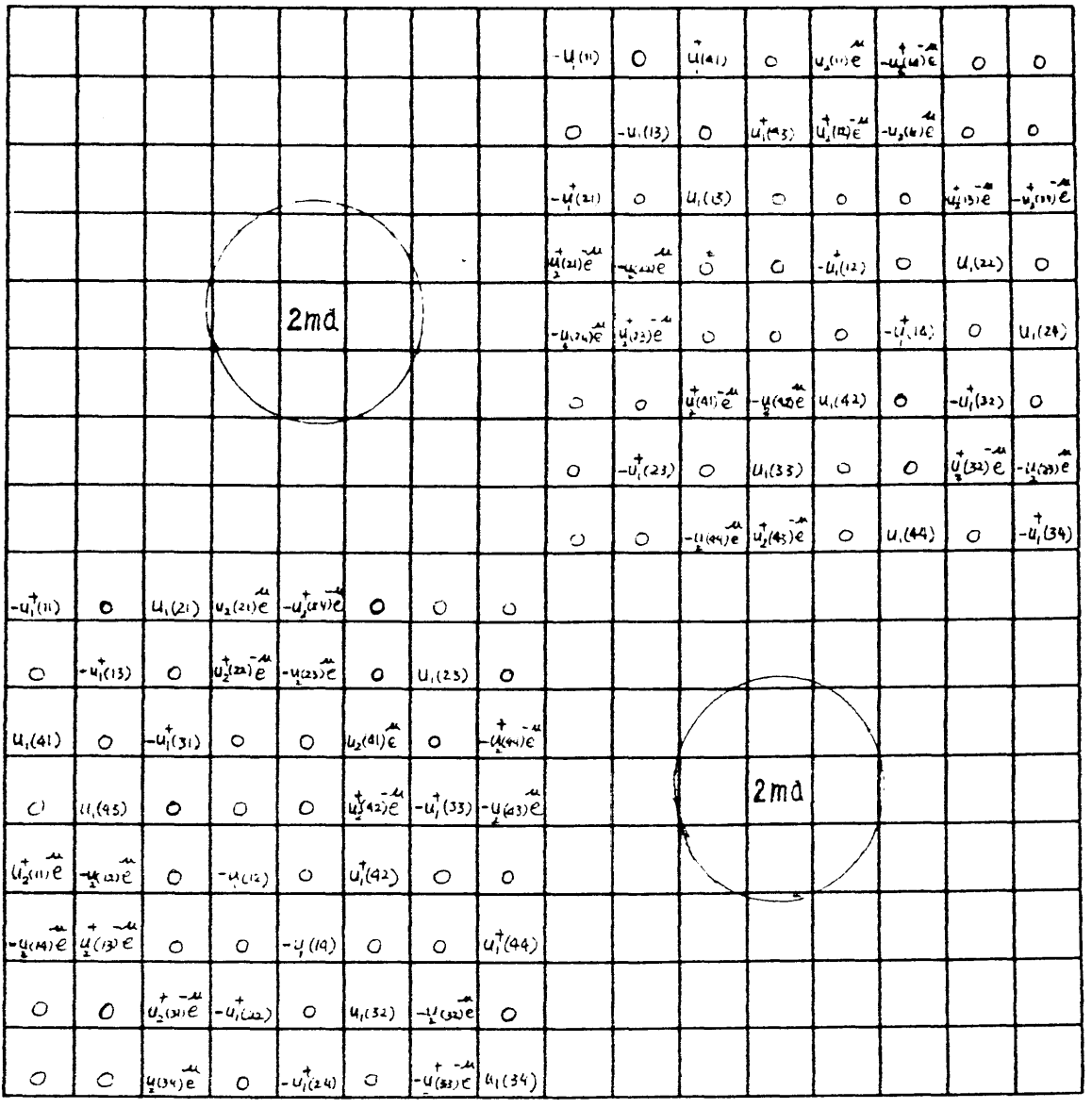

Fig.2.1. Finite density fermion matrix(H/i), with anti-periodic boundary conditions for ferimion fields. The matrix becomes anti-hermitian at $\mu=0$

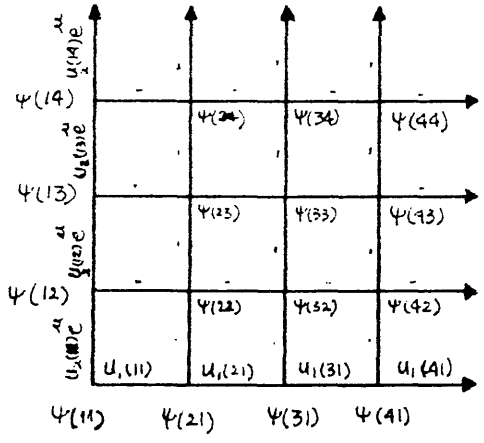

Fig.2.1a. Chemical potential on a 4^2 lattice.

Write X as a series of column vectors,

$$X = (x_1, x_2, x_3, \ldots\ldots\ldots\ldots\ldots) \qquad (2.3)$$

H being a general matrix, may have eigenvalues which are complex and the α's and β's can also be complex. We have the same Lanczos equations as in the hermitian case,

$$Hx_1 = \alpha_1 x_1 + \beta_1 x_2 \qquad (2.4)$$

$$H\, x_i = \beta_{i-1} x_{i-1} + \alpha_i x_i + \beta_i x_{i+1} \qquad (2.5)$$

We also need the matrix Y given by,

$$Y = (X^{-1})^{\dagger}\ ,\ H^{\dagger} Y = Y T^{\dagger},\ Y^{\dagger} X = 1 \qquad (2.6)$$

Y can also be written as a series of the column vectors,

$$Y = (y_1, y_2, y_3, \ldots\ldots\ldots\ldots\ldots\ldots) \qquad (2.7)$$

The columns of Y can be calculated with the additional Lanczos equations,

$$H^{\dagger} y_1 = \alpha_1^{*} y_1 + \beta_1^{*} y_2 \qquad (2.8)$$

$$H^{\dagger} y_i = \beta_{i-1}^{*} y_{i-1} + \alpha_i^{*} y_i + \beta_i^{*} y_{i+1} \qquad (2.9)$$

$$y_i^{\dagger} x_j = \delta_{ij} \qquad (2.10)$$

These are the Lanczos equations for the non-hermitian matrices, which can be used recursively to calculate all the α's, β's, x's, and y's starting by, choosing the x_1 and y_1 to be unit vectors and using the bi-orthogonality relation eq.2.10, we get the α's,

$$\alpha_i = y_i^{\dagger} H x_i \qquad (2.11)$$

The β's come from ,

$$\beta_i x_{i+1} = Hx_i - \alpha_i x_i - \beta_{i-1}x_{i-1} = X_i \qquad (2.12)$$

$$\beta_i^* y_{i+1} = H^\dagger y_i - \alpha_i^* y_i - \beta_{i-1}y_{i-1} = Y_i \qquad (2.13)$$

so that,

$$\beta_i^2 = Y_i^\dagger X_i \qquad (2.14)$$

eqs.2.12 and 2.13 give recursion relations for x_{i+1} and y_{i+1},

$$x_{i+1} = \frac{X_i}{\beta_i} \ , \ y_{i+1} = \frac{Y_i}{\beta_i^*} \qquad (2.15)$$

This completes the definition of the method. Last equation is automatically satisfied because we show that,

$$\begin{aligned} U &= Hx_N - \beta_{N-1} x_{N-1} - \alpha_N \ x_N \\ V &= H^\dagger y_N - \beta_{N-1}^* y_{N-1} - \alpha_N y_N \end{aligned} \qquad (2.16)$$

are orthogonal to all the vectors and so must therefore be individually equal to zero, so that,

$$\beta_N^2 = V^\dagger U = 0$$

The tridiagonal matrix T can, now, be diagonalised by some standard method.

Another cause of the failure of the algorithm other than rounding errors is that some β might be zero. This gives a division by zero. Two things can cause this problem.

1)- If the first Lanczos vector $x_1(y_1)$ is chosen to be orthogonal to some eigenvector of H,

2)- If H has degenerate eigenvalues, a division by zero enters into the calculations again.

The only solution is to choose the next $x_i(y_i)$ to be any unit vector orthogonal to all previous ones and continue the calculation. This requires a reference to previous vectors which would create a

storage problem but as we never encountered such a situation we ignore it.

One of the advantages of the Lanczos method over other methods, is that it does not need to store the huge matrix H, even if it has large number of zero elements. We require only 6 Lanczos vectors at every step of the algorithm and require an equivalent space for their storage. We also require a subroutine to multiply a vector by H. All but the last four Lanczos vectors can be discarded after each iteration.

2.3)- REORTHOGONALISATION:

When we apply the Lanczos method to large matrices, we find $\beta_N \neq 0$, due to rounding errors. This is due to a loss of biorthogonality between the first few Lanczos vectors and the last one. We cannot ignore the errors becaues they build up exponentially and, no matter what precision is used, we find this loss of biorthogonality between the first Lanczos vectors $x_1(y_1)$ and the one after the last iteration $x_i(y_i)$. The most straightforward way to overcome this problem is reorthogonalisation. The newly calculated Lanczos vectors $x_i(y_i)$ can be reorthogonalized against the previous vectors $x_j(y_j)$ by the projection,

$$\begin{aligned} x_i &\text{ -------> } x_i - x_j(y_j^\dagger x_i) \\ y_i &\text{ -------> } y_i - y_j(x_j^\dagger y_i) \\ &(j = 1 \text{ to } i\text{-}1) \end{aligned} \qquad (2.17)$$

on each step. Then provided we have not lost too much orthogonality, the rounding errors will be reduced to a reasonable level. Usually this does not need to be done after each iteration unless there are many close eigenvalues. Unfortunately orthogonalisation slows down the calculations and requires a large space for storing all the Lanczos vectors and it is impractical to reorthogonalize for N > 1000.

2.4)- WITHOUT REORTHOGONALISATION:

Fortunately it is possible to use the Lanczos method without reorthogonalisation and, consequently, we can deal with much larger matrices. We allow the Lanczos algorithm to proceed beyond the Nth iteration calculating new Lanczos vectors and α's and β's until we

have done $\widetilde{N}$ iterations. The α's and β's now form a $\widetilde{N}$ x$\widetilde{N}$ tridiagonal matrix $\widetilde{T}$ with $\widetilde{N}$ eigenvalues $\widetilde{\lambda}_r$ from which we can sort out the eigenvalues λ_i of H. It has been found empirically{13}, that if $\widetilde{N}$ is sufficiently large, then all the eigenvalues of H will converge as eigenvalues of $\widetilde{T}$. But $\widetilde{T}$ will also have spurious eigenvalues, which are not the eigenvalues of H. For large $\widetilde{N}$, the fastly converging eigenvalues (ghosts) of H will appear many times as eigenvalues of $\widetilde{T}$. These ghosts can be recognised as H is assumed to be non-degenerate. The spurious eigenvalues of $\widetilde{T}$ can be recognised by comparing with the eigenvalues of the tridiagonal matrix $\hat{\mathbf{T}}$ formed from the first $(\widetilde{N}-1)$ iterations. The real eigenvalues of H will be the eigenvalues of both $\widetilde{T}$ and $\hat{\mathbf{T}}$ but $\hat{\mathbf{T}}$ will have different spurious eigenvalues.

2.5)- MATRIX INVERSION:{13}

The Lanczos method can be used to invert a matrix column by column and can be applied to both hermitian and non-hermitian matrices. Considering eq.2.4 and using the Lanczos equations iteratively, we can calculate $H^{-1}x_1$ as a series,

$$H^{-1}x_1 = c_1x_1 + c_2x_2 + \ldots\ldots\ldots\ldots \qquad (2.18)$$

After K iterations of the algorithm, we get K terms in the series for $H^{-1}x_1$ with a remainder involving $H^{-1}x_K$ and $H^{-1}x_{K+1}$,

$$H^{-1}x_1 = V_K + a_K H^{-1}x_K + b_K H^{-1} x_{K+1} \qquad (2.19)$$

$$\text{where} \quad V_K = \sum_{i=1}^{K} c_i x_i$$

The next Lanczos eq.2.5 can be used to eliminate $H^{-1}x_K$, giving,

$$H^{-1}x_K = \frac{1}{\beta_K} x_K \frac{\alpha_{K+1}}{\beta_K} H^{-1}x_{K+1} - \frac{\beta_{K+1}}{\beta_K} H^{-1}x_{K+2}$$

which gives,

$$H^{-1}x_1 = V_K + \frac{a_K}{\beta_K}\, x_{K+1} + (b_K - \frac{\alpha_{K+1}}{\beta_K}\, a_K)\, H^{-1}x_{K+1} - \frac{\beta_{K+1}}{\beta_K}\, a_K\, H^{-1}x_{K+2} \qquad (2.20)$$

This gives the following recursion relations,

$$V_{K+1} = V_K + \frac{a_K}{\beta_K}\, x_{K+1} \qquad (2.21)$$

and the remainder coefficients,

$$\begin{bmatrix} a_{K+1} \\ b_{K+1} \end{bmatrix} = \begin{bmatrix} -\frac{\alpha_{K+1}}{\beta_K} & 1 \\ -\frac{\beta_{K+1}}{\beta_K} & 0 \end{bmatrix} \begin{bmatrix} a_K \\ b_K \end{bmatrix} \qquad (2.22)$$

From eq.2.4 we get, as the first step of the procedure,

$$H^{-1}\, x_1 = \frac{1}{\alpha_1}\, x_1 - \frac{\beta_1}{\alpha_1}\, H^{-1}\, x_2 \qquad (2.23)$$

but this starting point is not unique, since it is equally possible to start from the identity,

$$H^{-1}\, x_1 = H^{-1}\, x_1 \qquad (2.24)$$

combining s times eq.2.23 and r times eq.2.24 gives,

$$(r - \frac{\alpha_1}{\beta_1}\, s)\, H^{-1}\, x_1 = -\frac{s}{\beta_1}\, x_1 + r\, H^{-1}x_1 + s\, H^{-1}\, x_2 \qquad (2.25)$$

so that we get the starting point,

$$V_1 = - \frac{s}{r - \frac{\alpha_1}{\beta_1} s} \frac{x_1}{\beta_1} \qquad (2.26)$$

and,

$$\begin{bmatrix} a_1 \\ b_1 \end{bmatrix} = \frac{1}{r - \frac{\alpha_1}{\beta_1} s} \begin{bmatrix} r \\ s \end{bmatrix} \qquad (2.27)$$

The coefficient r and s are to be determined at the end of the calculations where they can be chosen in such a way that the final remainder is very small. The coefficients a_k and b_k are given by,

$$\begin{bmatrix} a_K \\ b_K \end{bmatrix} = \frac{1}{r - \frac{\alpha_1}{\beta_1} s} \Pi_K \begin{bmatrix} r \\ s \end{bmatrix} \qquad (2.28)$$

where Π_K is the (2x2) matrix given by,

$$\Pi_1 = \begin{bmatrix} 1 & 0 \\ 0 & 1 \end{bmatrix} \qquad (2.29)$$

and the recursion relation from eq.2.22,

$$\Pi_{K+1} = \begin{bmatrix} \frac{-\alpha_{K+1}}{\beta_K} & 1 \\ \frac{-\beta_{K+1}}{\beta_K} & 0 \end{bmatrix} \Pi_K \qquad (2.30)$$

For the convergence we want,

$$\begin{bmatrix} a_K \\ \\ b_K \end{bmatrix} \text{----------} > 0 \qquad (2.31)$$

but this can only happen if Π_K ----> 0, but,

$$\det \Pi_K = \prod_{i=1}^{K-1} \det \begin{bmatrix} \frac{-\alpha_{i+1}}{\beta_i} & 1 \\ \\ \frac{-\beta_{i+1}}{\beta_i} & 0 \end{bmatrix} = \prod_{i=1}^{K-1} \frac{\beta_{i+1}}{\beta_i} = \frac{\beta_K}{\beta_1} \qquad (2.32)$$

Therefore unless we have a β_K equal to zero, we cannot have Π_K--->0. However, if one eigenvalue of Π_K is zero, we can take $\begin{bmatrix} r \\ \\ s \end{bmatrix}$ to be the corresponding eigenvector and this will be sufficient to make the remainder term small. Since we will not know r and s until the end, we must compute V_K as a linear combination of r and s,

$$V_K = \frac{1}{r - \frac{\alpha_1}{\beta_1} s} \sigma_K \begin{bmatrix} r \\ \\ s \end{bmatrix} \qquad (2.33)$$

σ_K is a 2 component vector which is generated from following relations,

$$\sigma_1 = (0, \frac{-x_1}{\beta_1}) \qquad (2.34)$$

$$\sigma_{K+1} = \sigma_K + (\frac{x_{K+1}}{\beta_K}, 0)\Pi_K$$

Now if we proceed to calculate Π_K and σ_K from eqs.2.29,2.30 and

2.34, we have the problem of rounding errors because one eigenvalue of Π_K converges to zero while the other grows large since the determinant fluctuates around a constant value. This means that the components of Π_K and σ_K will grow large and the convergent part will be lost in rounding errors since it is a difference of large values.These errors can be avoided if we choose an unconventional representation of Π_K and σ_K which separates the convergent and divergent parts. Let

$$\Pi_K = \begin{bmatrix} A_K & Y_K A_K \\ B_K & Y_K B_K + t_K \end{bmatrix} \qquad (2.35)$$

$$\sigma_K = (0, 1)\, v_K + (1, Y_K)\, U_K \qquad (2.36)$$

As one eigenvalue of Π_K converges to zero we will have t_K--->0, while A_K, B_K, U_K --->∞. If we then choose,

$$\begin{bmatrix} r \\ s \end{bmatrix} = \begin{bmatrix} y_K \\ -1 \end{bmatrix} \qquad (2.37)$$

we will have,

$$\begin{bmatrix} a_K \\ b_K \end{bmatrix} = \frac{1}{y_K + \frac{\alpha_1}{\beta_1}} \begin{bmatrix} 0 \\ -t_K \end{bmatrix} \rightarrow 0 \qquad (2.38)$$

and

$$V_K = \frac{-1}{y_K + \frac{\alpha_1}{\beta_1}} \; v_K \rightarrow H^{-1} x_1 \qquad (2.39)$$

The recurrence relations for Π_K, σ_K translate into the following relations for y_K, t_K ,A_K ,B_K ,V_K ,U_K

$$\begin{aligned} U_1 &= 0 \\ Y_1 &= 0 \\ t_1 &= 1 \\ A_1 &= 1 \\ B_1 &= 0 \\ V_1 &= \frac{x_1}{\beta_1} \end{aligned} \qquad (2.40)$$

$$\begin{pmatrix} A_{K+1} \\ B_{K+1} \end{pmatrix} = \begin{pmatrix} \frac{-\alpha_{K+1}}{\beta_K} & 1 \\ \frac{-\beta_{K+1}}{\beta_K} & 0 \end{pmatrix} \begin{pmatrix} A_K \\ B_K \end{pmatrix} \qquad (2.41)$$

$$y_{K+1} = y_K + \frac{t_K}{A_{K+1}} \qquad (2.42)$$

$$t_{K+1} = \frac{-B_{K+1}}{A_{K+1}} t_K \qquad (2.43)$$

$$U_{K+1} = U_K + \frac{A_K}{B_K} x_{K+1} \qquad (2.44)$$

$$V_{K+1} = V_K - \frac{t_K}{A_{K+1}} U_{K+1} \qquad (2.45)$$

2.6)- NON-HERMITIAN BLOCK LANCZOS: {14}

A further improvement in the lattice fermion calculations can be obtained by generalising the above inversion method for the non-hermitian matrices to *block lanczos* in which the α's and β's are replaced by small matrices. If we take the α's and β's as LxL small

matrices, H is transformed into a band matrix of width (2L+1) while the Lanczos vectors become NxL arrays(L < N). The α's are hermitian and the β's are chosen to be triangular. With this method, any number of rows can be inverted simultaneously with no increase in the number of matrix by vector multiplications.

Consider the transformation,

$$H X = X T \tag{2.46}$$

and write the general triadiagonal form as,

$$T = \begin{bmatrix} \alpha_1 & \gamma_1^\dagger & 0 & 0 & 0 & \cdots \\ \beta_1 & \alpha_2 & \gamma_2^\dagger & 0 & 0 & \cdots \\ 0 & \beta_2 & \alpha_3 & \gamma_3^\dagger & 0 & \cdots \\ \cdot & & & & & \end{bmatrix}$$

As mentioned above, for the general case, we generate the inverse of X so that,

$$H^\dagger y = y T^\dagger \tag{2.47}$$

The first two Lanczos equations can be written as,

$$Hx_1 = x_1\alpha_1 + x_2\beta_1 \tag{2.48}$$

$$Hx_i = x_{i-1}\gamma_{i-1}^\dagger + x_i\alpha_i + x_{i+1}\beta_i \tag{2.49}$$

with the identity,

$$y_i^\dagger x_j = \delta_{ij} \tag{2.50}$$

Using the eq.2.47 and demanding that the α's to be hermitian, the coupled equations analogous to eqs.2.8 and 2.9 are written as,

$$H^\dagger y_1 = y_1\alpha_1 + y_2\gamma_1 \tag{2.51}$$

$$H^\dagger y_2 = y_{i-1}\beta_{i-1}^\dagger + y_i\alpha_i + y_{i+1}\gamma_i \tag{2.52}$$

And if we choose(for example,taking L = 3),

$$\beta = \begin{bmatrix} \beta_{11} & \beta_{12} & \beta_{13} \\ 0 & \beta_{22} & \beta_{23} \\ 0 & 0 & \beta_{33} \end{bmatrix} \qquad (2.53)$$

$$\gamma = \begin{bmatrix} \gamma_{11} & \gamma_{12} & \gamma_{13} \\ 0 & \gamma_{22} & \gamma_{23} \\ 0 & 0 & \gamma_{33} \end{bmatrix} \qquad (2.54)$$

with the condition,

$$\gamma_{ii} = \beta_{ii}^{*} \qquad (2.55)$$

we can calculate the elements of the β's and γ's from the matrix C,where C via eqs.2.48, 2.49,2.51 and 2.52, is,

$$C = (y_{i+1}\gamma_i)^{\dagger}(x_{i+1}\beta_i) \qquad (2.56)$$

2.6a)- HERMITIAN BLOCK LANCZOS:

In case of a hermitian H, we require only one set of the Lanczos equations with,

$$\beta_i = \gamma_i,$$

and of course,

$$x_i^{\dagger} x_j = \delta_{ij} \times \mathbf{1} \qquad (2.57)$$

where **1** is a unit matrix.

2.6b)- MATRIX INVERSION: (NON-HERMITIAN BLOCK LANCZOS):{14}

There is no advantage in using the block Lanczos algorithm if the problem is to calculate the eigenvalues of H. However, as mentioned earlier, there is an advantage in calculating L rows of the inverse at the same time and, provided L is not too large, the amount of computation required is significantly less as compared to that required to invert L rows one at a time.

We start with the Lanczos eqs.2.48 and 2.49. The algorithm proceeds in a way analogous to the L = 1 case {13}given above, except that, we are dealing with the matrices, their ordering is very important.Due to this,the representation of Π_K and σ_K of eq.2.35 and 2.36 is slightly different,

$$\Pi_K = \begin{bmatrix} A_K & A_K\, y_K \\ B_K & B_K\, y_K + t_K \end{bmatrix} \qquad (2.58)$$

$$\sigma_K = V_K(0,1) + (1, y_K)\, U_K \qquad (2.59)$$

As a result,we get following modified recursion relations;

$$\begin{aligned} A_1 &= \mathbf{1} \\ B_1 &= 0 \\ y_1 &= 0 \\ t_1 &= \mathbf{1} \\ V_1 &= -\, x_1 \cdot \beta_1^{-1} \\ U_1 &= 0 \end{aligned} \qquad (2.60)$$

$$A_{K+1} = B_K - \alpha_{K+1} (\gamma_K^{\dagger})^{-1} A_K \qquad (2.61)$$

$$B_{K+1} = -\beta_{K+1} (\gamma_K^{\dagger})^{-1} A_K \qquad (2.62)$$

$$y_{K+1} = y_K + t_K A_{K+1}^{-1} \qquad (2.63)$$

$$U_{K+1} = U_K + x_{K+1} (\gamma_K^{\dagger})^{-1} A_K \qquad (2.64)$$

$$V_{K+1} = V_K - U_{K+1} t_K x_{K+1}^{-1} \qquad (2.65)$$

and,

$$V_{K+1} (y_{K+1} + \alpha_1 \beta_1^{-1})^{-1} \rightarrow H^{-1} x_1 \qquad (2.66)$$

It should be noted that the coefficients A,B,Y and t are LxL matrices while U and V are NxL arrays. The condition on the convergence is similar i.e, all the elements of t_K should be zero at this point.

CHAPTER 3

BLOCK LANCZOS ALGORITHM AND THE FERMION MATRIX

3.1)- APPLICATION:

We have already discussed how efficient the Lanczos method is for

i)- calculating eigenvalues which come from off-diagonal elements of the triadiagonal matrix T and

ii)- inverting a general matrix such as,

$$H = i\,M$$

where M is a non-hermitian matrix. Now we shall explore how best we can apply the Lanczos algorithm to this matrix for the eigenvalue problem and for its inversion.

First we shall consider the eigenvalue problem of a non-hermitian matrix and apply it to the fermion matrix M_c of eq.1.85. For this we have to calculate the β's and γ's of the Lanczos eqs.2.4,2.5,2.8 and 2.9. We can introduce a simplication into the calculation if we note the odd-even structure of M_c.

In the zero mass quark limit, we can write, (as in fig.2.1)

$$M_c = \begin{pmatrix} 0 & \hat{M} \\ \hat{N} & 0 \end{pmatrix} \qquad (3.1)$$

Now if we choose the initial Lanczos vectors to be non-zero only on even sites,

$$x_1 = \begin{pmatrix} \hat{x}_1 \\ \\ 0 \end{pmatrix} \qquad (3.2)$$

then, by virtue of eq.2.4,

$$\alpha_1 = (\hat{x}_1^{\dagger}, 0) \begin{bmatrix} 0 & \hat{M} \\ \hat{N} & 0 \end{bmatrix} \begin{bmatrix} \hat{x}_1 \\ 0 \end{bmatrix} = 0 \qquad (3.3)$$

so that all α's become zero. Also, from eq.2.5,

$$x_2\beta_1 = Hx_1 = \begin{bmatrix} 0 & \hat{M} \\ \hat{N} & 0 \end{bmatrix} \begin{bmatrix} \hat{x}_1 \\ 0 \end{bmatrix} = \begin{bmatrix} 0 \\ \hat{N}\hat{x}_1 \end{bmatrix} \qquad (3.4)$$

and half of each Lanczos vector becomes zero.

$$x_{2K-1} = \begin{bmatrix} \hat{x}_{2K-1} \\ 0 \end{bmatrix}, \qquad x_{2K} = \begin{bmatrix} 0 \\ \hat{x}_{2K} \end{bmatrix} \qquad (3.5)$$

We can write Lanczos equations representing the even-odd structure as,

$$\hat{N}\hat{x}_1 = \hat{x}_2\beta_1 \qquad (3.6)$$

$$\hat{M}\hat{x}_{2K} = \hat{x}_{2K-1}\gamma_{2K-1}^{\dagger} + \hat{x}_{2K+1}\beta_{2K} \qquad (3.7)$$

$$\hat{N}\hat{x}_{2K+1} = \hat{x}_{2K}\gamma_{2K}^{\dagger} + \hat{x}_{2K+2}\beta_{2K+1} \qquad (3.8)$$

and

$$\hat{M}^{\dagger}\hat{y}_1 = \hat{y}_2\gamma_1 \qquad (3.9)$$

$$\hat{N}^{\dagger}\hat{y}_{2K} = \hat{y}_{2K-1}\beta^{\dagger}_{2k-1} + \hat{y}_{2K+1}\gamma_{2K} \qquad (3.10)$$

$$\hat{M}^{\dagger}\hat{y}_{2K+1} = \hat{y}_{2K}\beta^{\dagger}_{2K} + \hat{y}_{2K+2}\gamma_{2K+1} \qquad (3.11)$$

By this trick we avoid the calculation of α's and half of the Lanczos vectors and this reduces the time of the computation by a half.

We can rewrite the above equations by denoting the even and odd half x-vectors by B and W respectively while the even and odd half y-vectors are R and G respectively.

$$x_{2i-1} = \begin{Bmatrix} B_i \\ \\ 0 \end{Bmatrix} \qquad y_{2i-1} = \begin{Bmatrix} R_i \\ \\ 0 \end{Bmatrix}$$

$$x_{2i} = \begin{Bmatrix} 0 \\ \\ W_i \end{Bmatrix} \qquad y_{2i} = \begin{Bmatrix} 0 \\ \\ G_i \end{Bmatrix}$$

The Lanczos equations become,

$$\hat{N}\,B_1 = W_1\,\beta_1 \qquad (3.12)$$

$$\hat{M}\,W_i = B_i\,\gamma^{\dagger}_{2i-1} + B_{i+1}\,\beta_{2i} \qquad (3.13)$$

$$\hat{N}\,B_{i+1} = W_i\,\gamma^{\dagger}_{2i} + W_{i+1}\,\beta_{2i+1} \qquad (3.14)$$

and

$$\hat{M}^{\dagger}R_1 = G_1\,\gamma_1 \qquad (3.15)$$

$$\hat{N}^{\dagger}G_i = R_i\,\beta^{\dagger}_{2i-1} + R_{i+1}\gamma_{2i} \qquad (3.16)$$

$$\hat{M}^{\dagger}R_{i+1} = G_i\beta^{\dagger}_{2i} + G_{i+1}\gamma_{2i+1} \qquad (3.17)$$

It is necessary to store only the two even Lanczos vectors B and R and the two odd Lanczos vectors W and G between iterations. The Lanczos method with or without blocking takes the same time for calculating

the eigenvalues of the fermion matrix but an optimization is obtained while inverting it by block Lanczos. The flow chart for the computer simulation of the algorithm using above equations for calculating β's and γ's is shown in fig.3.1.

3.2)- PARALLEL COMPUTATION:

The inversion of big sparse matrices and the calculation of their eigenvalues requires a large amount of computation and any optimization in computer time and storage is very important. In this section using the odd-even structure of the fermion matrix , we describe a method for the parallel computation of the derivative part of the fermion matrix M_c. This method was initially described by Gibbs{15} for the hermitian matrices.

i)- B,W,R and G are conveniently stored as two arrays,

$$f=\begin{bmatrix} B \\ W \end{bmatrix} \qquad h=\begin{bmatrix} R \\ G \end{bmatrix} \qquad (3.18)$$

f and h being 5 dimensional arrays in general; 4 for space - time position and one for colour, representing a field on the sites of the lattice. The multiplication of NB_i and MW_i is similar in structure to $M^{\dagger}R_i$ and $N^{\dagger}G_i$ so we shall take only the former case.

ii)- The gauge field is generally stored as a 7 dimensional array; 4 for space-time position , 2 for the colour indices and 1 for direction. The gauge link variables point in the positive space-time direction and are stored, in the array, at the site at the negative end of the link.

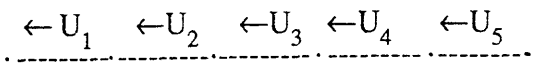

To change a gauge field into a fermion matrix element we multiply with appropriate fermion sign and reverse the direction on even sites by taking the hermitian conjugate so that all matrix elements go from odd to even sites.

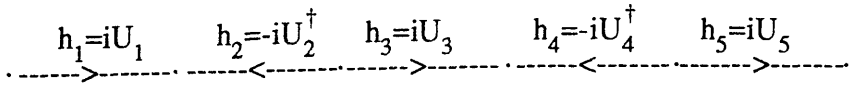

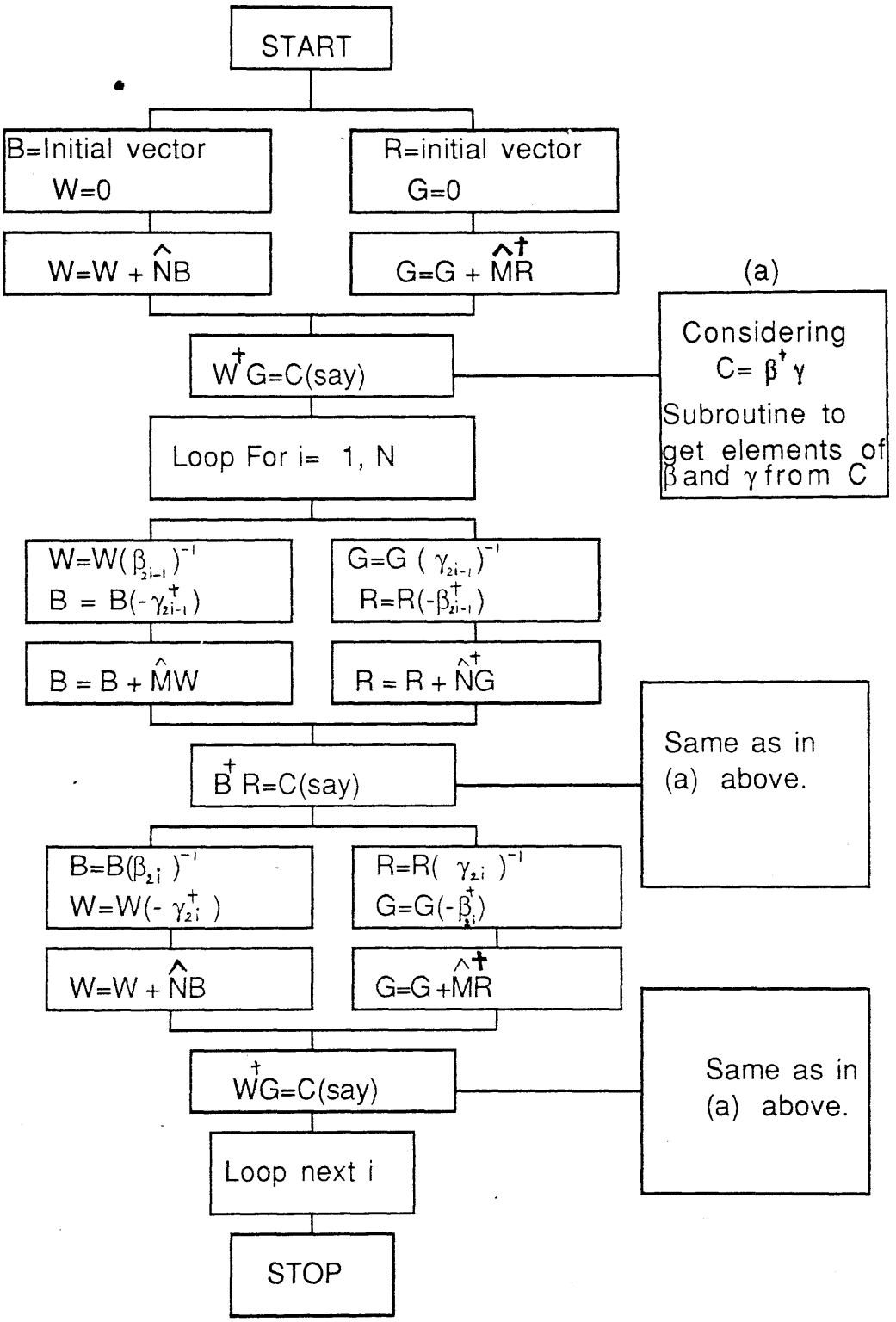
START
B=Initial vector
W=0
R=initial vector
G=0
W=W + $\hat{N}$B
G=G + $\hat{M}^{\dagger}$R
(a)
$W^{\dagger}G=C$(say)
Considering
$C=\beta^{\dagger}\gamma$
Subroutine to get elements of β and γ from C
Loop For i= 1, N
$W=W(\beta_{2i-1})^{-1}$
$B = B(-\gamma^{\dagger}_{2i-1})$
$G=G(\gamma_{2i-1})^{-1}$
$R=R(-\beta^{\dagger}_{2i-1})$
B = B + $\hat{M}$W
R = R + $\hat{N}^{\dagger}$G
$B^{\dagger}R=C$(say)
Same as in (a) above.
$B=B(\beta_{2i})^{-1}$
$W=W(-\gamma^{\dagger}_{2i})$
$R=R(\gamma_{2i})^{-1}$
$G=G(-\beta^{\dagger}_{2i})$
W=W + $\hat{N}$B
G=G +$\hat{M}^{\dagger}$R
$W^{\dagger}G=C$(say)
Same as in (a) above.
Loop next i
STOP

Fig.3.1

This is the best representation for doing multiplication and should be set up before starting the algorithm.

iii)- As shown flow chart fig.3.1, the operation of normalising the odd vector and multiplying the even vector by $(-\beta)$ on a vector or array processor is best combined into one operation by multiplying f by and array with (β^{-1}) on the odd sites and $(-\beta)$ on the even sites.

iv)- The matrix multiplication is a very complicated part of the optimisation. It can best be viewed as operating on the field f with the discrete form of the covariant Dirac operator,i.e., we numerically differentiate the field. Each of the four space-time direction is taken in turn, the odd part is differentiated and the result is added to the even part. In order to do the multiplication simultaneously at each site,we combine the multiplication for the forward and backward part into one operation. A temporary field t with W on the odd sites is constructed by moving w back from the even to the odd lattice sites as shown in fig.3.2.

f	w_1	b_1	w_2	b_2	w_3	b_3
t	w_1	w_2	w_2	w_3	w_3	w_1

fig.3.2

Then, t is multiplied by $h^{\dagger}$ as shown in fig.3.3.

$-iU_1^{\dagger}w_1$	iU_2w_2	$-iU_3^{\dagger}w_2$	iU_4w_3	$-iU_5^{\dagger}w_3$	iU_1w_1

fig.3.3

This vector is added to the vector obtained by moving it forward by one lattice space, which gives,

$-iU_1^{\dagger}w_1+iU_1w_1$	$iU_2w_2-iU_1^{\dagger}w_1$	$iU_2w_2-iU_3^{\dagger}w_2$	$iU_4w_3-iU_3^{\dagger}w_2$	$iU_4w_3-iU_5^{\dagger}w_3$	$iU_1w_1-iU_5^{\dagger}w_3$

The result on the odd sites is ignored,

$iU_2w_2-iU_1^{\dagger}w_1$	$iU_4w_3-iU_3^{\dagger}w_2$	$iU_1w_1-iU_5^{\dagger}w_3$

The result can be added to the even vector b before proceeding to the next direction.

For a finite density, we have to find a method to introduce the chemical potential in the formalism. Considering the time direction, we multiply the w vector on the odd sites by exp(-μ) and the shifted vector w by exp(μ). The whole process of the differentiation is performed as before. The result is,

$$iU_2w_2e^{\mu}\text{-}iU_1^{\dagger}w_1e^{-\mu} \quad iU_4w_3e^{\mu}\text{-}iU_3^{\dagger}w_2e^{-\mu} \quad iU_1w_1e^{\mu}\text{-}iU_5^{\dagger}w_3e^{-\mu}$$

Thus, we have constructed the derivative of the odd part in a way which is most convenient for the array processing.

3.3)- APPLICATION OF THE BLOCK LANCZOS TO THE THEORY WITH MASS:

3.3a)- EIGENVALUE PROBLEM:

With 2ma=0 and considering only nearest neighbour interactions, the finite density fermion matrix takes the form,

$$H = \begin{bmatrix} 0 & \hat{M} \\ \hat{N} & 0 \end{bmatrix} \qquad (3.19)$$

The characteristic equation gives,

$$\det(H-\lambda I) = \begin{bmatrix} -\lambda & \hat{M} \\ \hat{N} & -\lambda \end{bmatrix} = |\lambda^2 - \hat{M}\hat{N}| = 0 \quad (3.20)$$

Therefore it is possible to apply the Lanczos algorithm to $\hat{M}\hat{N}$ to get the squares of the eigenvalues of H. In the previous chapters we calculated the β's and γ's which translate into eigenvalues of the fermion matrix. As mentioned earlier, that the eigenvalues of the fermion matrix come in conjugate pairs which is a characteristic of the chiral symmetry (see eq.1.57a). Now it can be confirmed by the

even-odd block structure of the fermion matrix as below,

$$\text{if} \quad \begin{bmatrix} 0 & \hat{M} \\ \hat{N} & 0 \end{bmatrix} \begin{bmatrix} U \\ V \end{bmatrix} = \lambda \begin{bmatrix} U \\ V \end{bmatrix} \quad \text{then} \quad \begin{bmatrix} 0 & \hat{M} \\ \hat{N} & 0 \end{bmatrix} \begin{bmatrix} U \\ -V \end{bmatrix} = -\lambda \begin{bmatrix} U \\ -V \end{bmatrix} \tag{3.21}$$

Now consider the fermion matrix with mass,

$$H = \begin{bmatrix} 2ma & \hat{M} \\ \hat{N} & 2ma \end{bmatrix} \tag{3.22}$$

The characteristic equation becomes,

$$\det \begin{bmatrix} 2ma - \lambda & \hat{M} \\ \hat{N} & 2ma - \lambda \end{bmatrix} = 0 \tag{3.34}$$

It means the theory is unchanged except that the eigenvalues will be shifted by an amount 2ma. Therefore, we can apply the Lanczos method to calculate the eigenvalues at several mass limits. As we shall see α of eqs.2.48,2.49,2.51 and 2.52 can be used as a mass term.

3.3b)- INVERSION OF THE FERMION MATRIX WITH MASS:

We can prove that the β's(γ's) and the Lanczos vectors x(y) are independent of mass {14}. At zero mass, in the even-odd block structure of the fermion matrix, all the α's of the block Lanczos eqs.2.4,2.5,2.8 and 2.9 via eq.3.3 become zero, consequently T of eq.2.2 is a tridiagonal matrix with zeros along its diagonal. Considering the fermion matrix, eq.3.22,

and

$$X^{-1} H X = T' \tag{3.35}$$

where T' is T of eq.2.2, with 2mai terms along its diagonal. It is to be noted that the α's are the diagonal elements of T when we do not use the even-odd block structure. With this change, the block Lanczos equations become,

$$Hx_1 = x_1 2mai + x_2\beta_1 \qquad (3.36)$$

$$Hx_i = x_{i-1}\gamma_{i-1}^{\dagger} + x_i\, 2mai + x_{i+1}\beta_i \qquad (3.37)$$

$$H^{\dagger}y_1 = y_1(2mai)^{\dagger} + y_2\gamma_1 \qquad (3.38)$$

$$H^{\dagger}y_i = y_{i-1}\beta_{i-1}^{\dagger} + y_i(2mai)^{\dagger} + y_{i+1}\gamma_i \qquad (3.39)$$

INVERSION:

The algorithm described in section 2.6 can be immediately applied to the fermion matrix,

$$H = i\,(M_c + 2ma)$$

but a term involving a division by mass gives a singularity at zero mass in eq.2.63. In order to avoid this, and remembering that we are utilizing the even-odd block structure, we use a slightly different representation of Π_K and σ_K from that of eqs.2.58 and 2.59,

$$\Pi_{2K-1} = \begin{pmatrix} t_{2K-1} - (2ma)^2 B_{2K-1} y_{2K-1} & 2mai\, B_{2K-1} \\ 2mai\, A_{2K-1} y_{2K-1} & A_{2K-1} \end{pmatrix} \qquad (3.40)$$

$$\Pi_{2K} = \begin{pmatrix} 2mai\, A_{2K}\, y_{2K} & A_{2K} \\ t_{2K} - (2ma)^2\, B_{2K}\, Y_{2K} & 2mai\, B_{2K} \end{pmatrix} \qquad (3.41)$$

and

$$\sigma_K = V_K(2mai\ ,\ 0) + U_K\ (2mai\ Y_K\ ,\ 1) \qquad (3.42)$$

If we take the β's and γ's as small LxL matrices then the coefficients A,B,Y and t are LxL matrices while U and V NxL arrays.

The method is carried out in a similar fashion to that of section 2.5 and 2.6. With these representations the factor 2mai divides out explicitly. The extra advantage is that the coefficients A,B,Y and t are real. The recurrence relations are as follows;

$$A_1 = 1 \qquad (3.43)$$

$$y_1 = 0 \qquad (3.44)$$

$$B_1 = 0 \qquad (3.45)$$

$$t_1 = 1 \qquad (3.46)$$

$$V_1 = 0 \qquad (3.47)$$

$$U_1 = -x_1 . \beta_1^{-1} \qquad (3.48)$$

$$A_{2K} = A_{2K-1} + (2ma)^2 (\gamma_{2K-1}^{-1})^{\dagger} \beta_{2K-1}$$

$$B_{2K} = -\beta_{2K} (\gamma_{2K-1}^{-1})^{\dagger} t_{2K-1}$$

$$y_{2K} = y_{2K-1} - A_{2K}^{-1} (\gamma_{2K-1}^{-1})^{\dagger} t_{2K-1}$$

$$t_{2K} = \beta_{2K} A_{2K-1} A_{2K}^{-1} (\gamma_{2K-1}^{-1})^{\dagger} t_{2K-1}$$

$$U_{2K} = U_{2K-1} + x_{2K} (\gamma_{2K-1}^{-1})^{\dagger} 2mai\ B_{2K-1}$$

$$V_{2K} = V_{2K-1} + x_{2K} \beta_{2K-1}^{-1} t_{2K-1} + 2mai\ U_{2K} A_{2K}^{-1} \beta_{2K-1}^{-1} t_{2K-1} \qquad (3.49)$$

and

$$A_{2K+1} = -\beta_{2K} (\gamma_{2K}^{-1})^{\dagger} A_{2K}$$

$$B_{2K+1} = B_{2K} - (\gamma_{2K}^{-1})^{\dagger} A_{2K}$$

$$y_{2K+1} = y_{2K}$$

$$t_{2K+1} = t_{2K}$$

$$V_{2K+1} = V_{2K}$$

$$U_{2K+1} = U_{2K} + x_{2K+1} (\gamma_{2K}^{-1})^{\dagger} A_{2K} \qquad (3.50)$$

so that

$$(1 + (2ma)^2 y_{2K+1}\, \beta_1^{-1})^{-1}\, V_{2K+1} \rightarrow H^{-1}x_1 \qquad (3.50a)$$

The condition on the convergence of the series is similar to that for the algorithm described in section 2.6b,i.e., it will converge to $H^{-1}x_1$ when all the elements of t_{2K+1} are equal to zero.

3.4)- LANCZOS UPDATING WITH FERMIONS: SU(2) CASE.

Simulating the theory with dynamical fermions is a quite hard task. For this, we have to calculate the ratio of the determinants for the configurations created by Metropolis algorithm and differing at one link at each update. This requires much computation as compared to the pure gauge field case where we need only the ratio of the statistical weight. Therefore it is very important to optimize the calculations as much as possible.

We want,

$$R = \frac{\det(H + \delta H)}{\det H} \qquad (3.51)$$

$$= \det(1 + H^{-1}\delta H) \qquad (3.52)$$

When one link is altered, this change corresponds to a 4x4 block. If we denote the corresponding 4x4 block H^{-1} as $\bar{H}^{-1}$ and 4x4 changed block by $\bar{\delta H}$, then,

$$R = \det(1 + \bar{H}^{-1}\,\bar{\delta H}) \qquad (3.53)$$

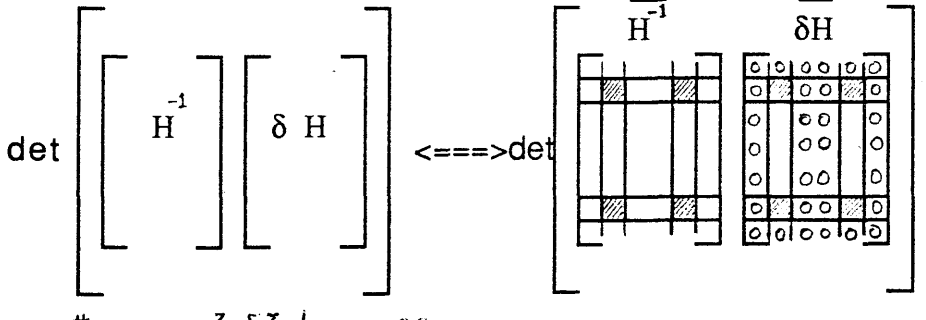

then eq.3.53 becomes,

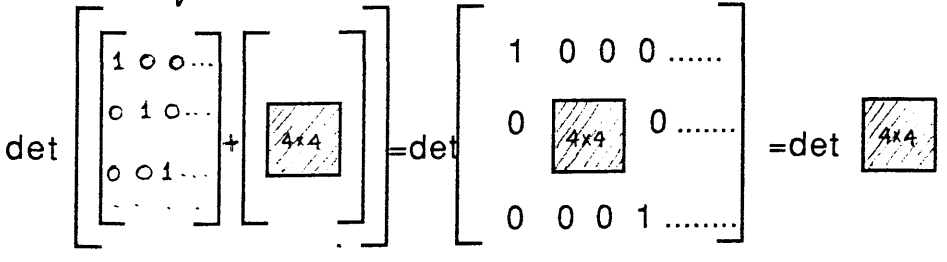

Fig.3.4

and as explained by fig.3.4 updating one link requires 4 rows ofthe H^{-1} and then a small 4x4 determinant.

In practice, we update the same link many times before moving to a new link. This has the advantage that we do not need to calculate fresh H^{-1} for every update because,

$$\frac{\det(H+\delta H_1)}{\det(H+\delta H_2)} = \frac{\det(1+\bar{H}^{-1}\delta\bar{H}_1)}{\det(1+\bar{H}^{-1}\delta\bar{H}_2)} \qquad (3.54)$$

Of course, the probability of the system to reach the equilibrium state is also increased. We shall call this as Modified Metropolis algorithm and updating a link , as a *hit*. It is like a *mini heat bath*. If the number of hits are increased to infinity, it becomes the Heat bath algorithm{20}.

3.5)- LANCZOS ALGORITHM FOR UPDATING BY RANK ANNIHILATION; THE SU(2) CASE:

The updating idea can be extended for a number of links at a time. Consider 32 links of a hypercube. To calculate the ratio of the determinants for any change to these links, we need a 32x32 block corresponding to the 16 sites of the hypercube. By doing one hypercube at a time we get a factor of four as compared to doing it link by link. It is worthwhile to go to each for about five times (*laps*) *hitting* each link about ten times per lap so that each link is brought near to equilibrium before moving to the next hypercube. It is suitable to take the β's and γ's as 16x16 matrices because we first invert for the 8 odd(even) sites of the hypercube and then take up the even(odd) sites. All these improvements make larger lattices possible. The Lanczos algorithm provides a technique for obtaining a 32x32 block of the inverse corresponding to a hypercube.

Rank annihilation {14} can then be applied. Let H be the block of the inverse of the fermion matrix corresponding to a hypercube. Changing one link of the hypercube makes a change ΔH in the fermion matrix with 8 non-zero elements, which we separate into 8 consecutive changes, one to each element,

$$\Delta H = \Delta H_1 + \Delta H_2 + \ldots\ldots\ldots + \Delta H_8 \qquad (3.55)$$

Write each change in the form,

$$\Delta H_i = U\, a\, V^{\dagger} \qquad (3.56)$$

Where a is the change to the element and U,V are the unit column vectors which are zero in all elements but one. Then, if $H^{-1}=Z$, {14},

$$\begin{aligned} Z' = (H + UaV^{\dagger})^{-1} &= H^{-1}\,(1 + UaV^{\dagger} H^{-1})^{-1} \\ &= Z - Z\,UaV^{\dagger} Z + Z\,UaV^{\dagger}\,UaV^{\dagger}Z - \ldots\ldots \qquad (3.57) \\ &= Z - ZUa\,(1 - V^{\dagger} Z\,Ua + \ldots.)\; V^{\dagger} Z \\ &= Z - Z\,Ua\,(1 + V^{\dagger}Z\,U\,a)^{-1}\, V^{\dagger}Z \end{aligned}$$

It can easily be seen that this formula can be applied to update the 32x32 block of Z' without knowing the rest of its elements.

The calculation can further be optimized by considering two hypercubes at a time.

3.6)- LANCZOS METHOD FOR H^{-2};

From above we know that the chiral order parameter can be given by the following relation,

$$\langle \bar{\psi}\,\psi \rangle = \frac{1}{N_L}\, tr\,(M_C + 2ma)$$

where N_L is no. of lattice sites. The right hand side of eq.3.56 is averaged over many configurations. The size of the matrix M_c is NxN where $N=3N_L$. Above, we described the Lanczos method to obtain all the eigenvalues of the matrix $H = i(M_c + 2ma)$. In terms of eigenvalues of the M_{KS} eq.3.56 becomes,

$$\langle \bar{\psi}\,\psi \rangle = \frac{3}{N} \sum_{K} \frac{1}{-\lambda_K + 2ma} \qquad (3.58)$$

The Lanczos diagonalisation provides all the eigenvalues of H and hence the initial eigenvalues for detH and trH^{-1} at the beginning of each sweep. Updating all the hypercubes of the lattice once is called a sweep or an iteration. After each sweep, the changed $tr(H + \Delta)^{-1}$ can be calculated as follows;

$$tr(H + \Delta)^{-1} = tr\, H^{-1} + \text{(change produced by updating during the sweep)}$$

$$\text{change} = tr(H + \Delta)^{-1} - trH^{-1} = -tr\,(H^{-2}\Delta(1 + H^{-1}\Delta)^{-1})$$

and an algorithm for calculating the H^{-2} is required. This algorithm can be obtained by differentiating the Lanczos algorithm giving the eigenvalues of H^{-1}(from eqs.3.43 to 3.50a) with respect to 2ma. The following is the summary of the values of the variables required to calculate $H^{-2}x_1$.

INITIAL VALUES

$$AA_1 = \frac{dA_1}{d(2ma)} = 0 \qquad BB_1 = \frac{dB_1}{d(2ma)}$$

$$tt_1 = \frac{dt_1}{d(2ma)} = 0 \qquad yy_1 = \frac{dy_1}{d(2ma)} \qquad (3.59)$$

$$VV_1 = \frac{dV_1}{d(2ma)} = 0 \qquad UU_1 = \frac{dU_1}{d(2ma)}$$

For further iterations the even and odd values of these matrix variables are given below;

$$AA_{2K} = AA_{2K-1} + m\,c\,B_{2K-1} + m^2 c\,BB_{2K-1}$$

$$BB_{2K} = -\beta_{2K}\,c\,BB_{2K-1}$$

$$yy_{2K} = yy_{2K-1} - AA_{2K}\,A_{2K}^{-2}\,c\,t_{2K-1} - A_{2K}^{-1}\,c\,tt_{2K-1}$$

$$UU_{2K} = UU_{2K-1} + i\,x_{2K}\,c\,B_{2K-1} + im\,x_{2K}\,c\,BB_{2K-1}$$

$$VV_{2K} = VV_{2K-1} + x_{2K}\,\beta_{2K-1}^{-1}\,tt_{2K-1} + i\,U_{2K}A_{2K}^{-1}\,\beta_{2K-1}^{-1}\,t_{2K-1}$$
$$+im(\,UU_{2K}A_{2K}^{-1}\,\beta_{2K-1}^{-1}\,t_{2K-1} + U_{2K}\,A_{2K}^{-2}\,AA_{2K}\,\beta_{2K-1}t_{2K-1} + U_{2K}A_{2K}^{-1}\beta_{2K-1}tt_{2K-1})$$

$$tt_{2K} = \beta_{2K}(AA_{2K-1}A_{2K}^{-1}\,c\,t_{2K-1} + A_{2K-1}AA_{2K}A_{2K}^{-1}\,c\,t_{2K-1}$$
$$+A_{2K-1}A_{2K}^{-1}\,c\,tt_{2K-1}) \qquad (3.60)$$

and

$$AA_{2K+1} = -\beta_{2K}\, d\, AA_{2K}$$

$$BB_{2K+1} = BB_{2K} - d\, AA_{2K}$$

$$yy_{2K+1} = y_{2K},\ tt_{2K+1} = tt_{2K},\ VV_{2K+1} = VV_{2K}$$

$$UU_{2K+1} = UU_{2K} + x_{2K+1}\, d\, AA_{2K}$$

so that,

$$H^{-2} x_1 = -T^{-1}\{ T^{-1} (2 m y_{2K+1} \beta_1^{-1} + m^2 yy_{2K+1}.\beta_1^{-1}) - VV_{2K+1} \}$$

where,

$$T = (1 - m^2 y_{2K+1} \beta_1^{-1})$$

$$2ma = m$$

$$(\gamma_{2K-1}^{-1})^{\dagger} = c$$

$$(\gamma_{2K}^{-1})^{\dagger} = d \qquad (3.61)$$

3.7)- BLOCK INVERSION: A FURTHER OPTIMIZATION:

The non-hermitian block Lanczos method with mass requires two sets of the equations (3.36 to 3.39). We used one set(3.36 and 3.37) using the techniques of section 2.5 and 2.6, for the block inversion of a big sparse matrix,a fermion matrix with mass, in section 3.3b. This uses interations between even-even and even-odd sites of the lattice and therefore produces even-even and even-odd blocks of the inverse of the fermion matrix. A further optimization can be obtained by writing the first Lanczos vector of the unused set as a linear combination of all other Lanczos vectors of the set already employed for the inversion,

$$Y_1 = \sum_{i=1}^{K} x_i R_i \qquad (3.62)$$

$$H^{-1} Y_1 = H^{-1} \sum_{i=1}^{K} x_i R_i \qquad (3.63)$$

This provides the odd-odd and odd-even blocks of the inverse of the fermion matrix in parallel with the even-even and even-odd blocks of the inverse.

By using the 3.36 and 3.37, we can calculate right hand side of

the eq.3.63 as a series as in section 2.5 and 2.6,

$$H^{-1}\sum_{i=1}^{K} x_i R_i = c_1x_1 + c_2x_2 + \ldots\ldots\ldots \quad (3.64)$$

After K iterations of the Lanczos algorithm we construct K terms in series with a remainder involving $H^{-1}x_K$ and $H^{-1}x_{K+1}$ so that,

$$H^{-1}\sum_{i=1}^{K} x_iR_i = v_K + H^{-1}\, x_K\, a_K + H^{-1}x_{K+1}\, b_K \qquad (3.65)$$

with

$$v_K = c_1x_1 + c_2x_2 + \ldots\ldots\ldots$$

Increasing the range of summation past K gives,

$$H^{-1}\sum_{i=1}^{K+1} x_i\, R_i = v_K + H^{-1}x_Ka_K + H^{-1}\, x_{K+1}\, b_K + H^{-1}x_{K+1}R_{K+1} \quad (3.66)$$

We shall use 2mai= $\alpha_K = \alpha_{K+1} = \alpha_{K-1}$, c= $(\gamma_K{}^{\dagger})^{-1}$ and 2ma=m (where necessary) , in this section. As in section 2.5, we shall use eq.2.37 to eliminate $H^{-1}x_K$ from eq.3.66 to get,

$$H^{-1}\sum_{i=1}^{K+1} x_i\, R_i = v_K + x_{K+1}\, c\, a_K - \alpha_{K+1}\, H^{-1}x_{K+1}\, c\, a_K \qquad (3.67)$$
$$- H^{-1}x_{K+2}\, \beta_{K+1}\, c\, a_K + H^{-1}x_{K+1}b_K + H^{-1}x_{K+1}R_{K+1}$$

Comparing eqs. 3.65 and 3.67, we get,

$$v_{K+1} = v_K + x_{K+1}\, c\, a_K \qquad (3.68)$$

$$\begin{pmatrix} a_{K+1} & -\alpha_{K+1}c \\ b_{K+1} & -\beta_{K+1}c \end{pmatrix} \begin{pmatrix} 1 \\ 0 \end{pmatrix} + \begin{pmatrix} R_{K+1} \\ 0 \end{pmatrix} \qquad (3.69)$$

As in section 2.5, the starting point is not unique since we could also begin with the identity,

$$H^{-1}x_1 R_1 = H^{-1} x_1 R_1 \qquad (3.70)$$

Adding eqs.3.36 and 3.70 after multiplying with r and s respectively gives,

$$H^{-1}x_1R_1 [r + \alpha_1 s] = x_1R_1 s + H^{-1}x_1R_1 r - H^{-1} x_2 \beta_1 R_1 s \quad (3.71)$$

Comparing eq.3.71 with eq.3.65 gives the starting values,

$$v_1 = x_1 R_1 s \quad P \qquad (3.72)$$

$$a_1 = R_1 r \quad P \qquad (3.73)$$

$$b_1 = -\beta_1 R_1 s \quad P \qquad (3.74)$$

where

$$P = (r + \alpha_K s)^{-1}$$

The coefficients r and s are to be determined at the end of the calculations where they can be chosen in such a way that the final remainder is very small. Write,

$$\begin{pmatrix} a_K \\ \\ b_K \end{pmatrix} = \pi_K R_1 \begin{pmatrix} r \\ \\ s \end{pmatrix} P + \rho_K \qquad (3.75)$$

where if the size of the α's and β's is LxL, the 2Lx2L matrix π_K can be calculated from the recurrence relations,

$$\pi_1 = \begin{bmatrix} 1 & 0 \\ 0 & -\beta_1 \end{bmatrix} \qquad (3.76)$$

$$\pi_{K+1} = \eta_{K+1}\, \pi_K \qquad (3.77)$$

while ρ_K from,

$$\rho_1 = \begin{pmatrix} 0 \\ 0 \end{pmatrix}, \quad \rho_{K+1} = \eta_{K+1}\, \rho_K + \begin{pmatrix} R_{K+1} \\ 0 \end{pmatrix} \qquad (3.78)$$

where

$$\eta_{K+1} = \begin{bmatrix} -\alpha_{K+1}\, c & 1 \\ -\beta_{K+1}\, c & 0 \end{bmatrix}$$

For the convergence of the series, we require,

$$\begin{pmatrix} a_K \\ b_K \end{pmatrix} \rightarrow \begin{pmatrix} 0 \\ 0 \end{pmatrix} \qquad (3.79)$$

This would happen for any choice of the initial condition if $\pi_K \rightarrow 0$. But

$$\det \pi_K = \prod_{i=1}^{K-1} \det \begin{bmatrix} -\alpha_{K+1}\, c & 1 \\ -\beta_{K+1}\, c & 0 \end{bmatrix}$$

$$= \prod_{i=1}^{K-1} \det \left(-\beta_{K+1}\, (\gamma_K^{\dagger})^{-1}\right) \quad \text{since } c = (\gamma_K^{\dagger})^{-1}$$

$$= \frac{\det \beta_K}{\det \gamma^{\dagger}_{K-1}} \cdot \frac{\det \beta_{K-1}}{\det \gamma^{\dagger}_{K-2}} \cdots\cdots\cdots \frac{\det \beta_2}{\det \gamma^{\dagger}_1}$$

so that $\pi_K \rightarrow 0$, only if one of the $\det\beta = 0$ or one of $\det\gamma^{\dagger}_{K-1} = \infty$ and we cannot have $\pi_K \rightarrow 0$. However if one eigenvalue of π_K tends to zero we can take $R_1 \begin{bmatrix} r \\ \\ s \end{bmatrix}$ to be the corresponding eigenvector and this will suffice to make the remainder term small. In this condition ρ_K will also become small if $\begin{bmatrix} R_{K+1} \\ \\ 0 \end{bmatrix} \rightarrow 0$. Since we do not know r and s until the end we must compute v_K as a linear combination,

$$v_K = \sigma_K R_1 \begin{bmatrix} r \\ \\ s \end{bmatrix} P + f_K \qquad (3.80)$$

with the initial conditions,

$$\sigma_1 = (0, x_1), f_1 = 0 \qquad (3.81)$$

Putting the values of v_{K+1} and v_K from eq.3.80 in eq.3.68, we get,

$$\sigma_{K+1} R_1 \begin{bmatrix} r \\ \\ s \end{bmatrix} P + f_{K+1} = \sigma_K R_1 \begin{bmatrix} r \\ \\ s \end{bmatrix} P + x_{K+1}\, c\, a_K \qquad (3.82)$$

giving,

$$f_{K+1} = f_K + (x_{K+1}\, c\,,\ 0)\, \rho_K \qquad (3.83)$$

$$\sigma_{K+1} = \sigma_K + (x_{K+1}\, c\,,\ 0)\, \pi_K \qquad (3.84)$$

Comparing eqs.3.40 and 3.76 for π_1 and, 3.42 and 3.81 for σ_1 gives the initial values,

$$A_1=-\beta_1,\ B_1=0,\ t_1=1$$
$$y_1=0,\quad U_1=x_1,\ V_1=0 \qquad (3.85)$$

Starting from,

$$\pi_{2K+1}=\eta_{2K+1}\,\pi_{2K}$$

and using the values of π_{2K+1} and π_{2K} from eq.3.40 and 3.41 we get,

$$\begin{bmatrix} \text{im}\,B_{2K+1} \\ A_{2K+1} \end{bmatrix} = \begin{bmatrix} -\alpha_{2K+1} & 1 \\ -\beta_{2K+1}\,c & 0 \end{bmatrix} \begin{bmatrix} A_{2K} \\ \text{im}B_{2K} \end{bmatrix}$$
$$y_{2K+1} = y_{2K}$$
$$t_{2K+1} = t_{2K} \qquad (3.86)$$

Using only even values of K, eq.3.84 becomes,

$$\sigma_{2K+1} = \sigma_{2K} + (x_{2K+1}\,c\,,\ 0\,)\,\pi_{2K} \qquad (3.87)$$

and we get,

$$U_{2K+1}= U_{2K} + x_{2K+1}\,c\,A_{2K} \qquad (3.88)$$
$$V_{2K+1} = V_{2K} \qquad (3.89)$$

With the initial conditions 3.78 on ρ, we can write,

$$\rho_{2K+1} = \begin{bmatrix} \text{im}B_{2K+1} \\ A_{2K+1} \end{bmatrix} g_{2K+1} + \begin{bmatrix} 0 \\ h_{2K+1} \end{bmatrix} \qquad (3.90)$$

$$\rho_{2K} = \begin{pmatrix} A_{2K} \\ \\ imB_{2K} \end{pmatrix} \quad g_{2K} + \begin{pmatrix} h_{2K} \\ \\ 0 \end{pmatrix} \qquad (3.91)$$

and

$$\rho_{2K+1} = \eta_{2K+1}\, \rho_{2K} \qquad (3.92)$$

Putting the values of ρ_{2K+1} and ρ_{2K} from 3.90 and 3.91 in 3.92 we get,

$$g_{2K+1} = g_{2K} - B^{-1}_{2K+1}\, c\, h_{2K} \qquad (3.93)$$

$$h_{2K+1} = [\, -\beta_{2K+1}\, c + A_{2K+1} B^{-1}_{2K+1}\, c\,]\, h_{2K} \qquad (3.94)$$

Writing,

$$f_{2K+1} = U_{2K+1}\, g_{2K+1} + W_{2K+1} \qquad (3.95)$$

and using eq.3.83, we get,

$$W_{2K+1} = W_{2K} + x_{2K+1}\, c\, h_{2K} - U_{2K+1}(g_{2K+1} - g_{2K}) \qquad (3.96)$$

For the even variables A,B, ... , we start from,

$$\pi_{2K} = \eta_{2K}\, \pi_{2K-1}$$

and a similar algorithm gives their values. The values of even and odd variables can be summarised as :-

$$\begin{pmatrix} im\, B_{2K+1} \\ \\ A_{2K+1} \end{pmatrix} = \begin{pmatrix} -\alpha_{2K+1} & 1 \\ \\ -\beta_{2K+1}\, c & 0 \end{pmatrix} \begin{pmatrix} A_{2K} \\ \\ imB_{2K} \end{pmatrix}$$

$$y_{2K+1} = y_{2K}$$

$$t_{2K+1} = t_{2K}$$

$$U_{2K+1} = U_{2K} + x_{2K+1}\, c\, A_{2K}$$

$$V_{2K+1} = V_{2K}$$

$$g_{2K+1} = g_{2K} - B^{-1}_{2K+1}\, c\, h_{2K}$$

$$h_{2K+1} = [\, -\beta_{2K+1}\, c + A_{2K+1} B^{-1}_{2K+1}\, c\,]\, h_{2K}$$

$$W_{2K+1} = W_{2K} + x_{2K+1}\, c\, h_{2K} - U_{2K+1}(g_{2K+1} - g_{2K}) \qquad (3.97)$$

and

$$A_{2K} = m^2\, d\, B_{2K-1} + A_{2K-1}$$

$$B_{2K} = -\beta_{2K}\, d\, B_{2K-1}$$

$$y_{2K} = y_{2K-1} - A^{-1}_{2K}\, d\, t_{2K-1}$$

$$t_{2K} = \beta_{2K}\, A_{2K-1} A^{-1}_{2K}\, d\, t_{2K-1}$$

$$U_{2K} = U_{2K-1} + im\, x_{2K}\, d\, B_{2K-1}$$

$$V_{2K} = V_{2K-1} + im\, U_{2K}\, A^{-1}_{2K}\, d\, t_{2K-1} + x_{2K}\, d\, t_{2K-1}$$

$$g_{2K} = g_{2K-1} - \alpha_{2K}\, A^{-1}_{2K}\, d\, h_{2K-1} + A^{-1}_{2K}\, R_{2K}$$

$$h_{2K} = B_{2K}[\, A^{-1}_{2K} A^{-1}_{2K-1} B^{-1}_{2K-1} h_{2k-1} - im\, A^{-1}_{2K}\, R_{2K}]$$

$$W_{2K} = W_{2K-1} - U_{2K}[\, g_{2K} - g_{2K-1}] \qquad (3.98)$$

with $d = (\gamma^{\dagger}_{2K-1})^{-1}$

For the inverse, from eq.3.80, we can write,

$$V_{2K} = \sigma_{2K}\, R_1 \begin{pmatrix} r \\ \\ s \end{pmatrix} (r + \alpha_{2K}\, s\,)^{-1} + U_{2K}\, g_{2K} + W_{2K} \qquad (3.99)$$

where we have used value of f_{2K} from eq.3.95. Putting values of U_{2K}, g_{2K}, W_{2K} from eqs.3.98 and choosing,

$$r = 1$$

$$s = - \frac{\text{im}\, y_{2K} R_1 + g_{2K}}{g_{2K} \alpha_{2K} + R_1}$$

we get,

$$v_{2K} = W_{2K} + V_{2K} R_1 (1 + \alpha_{2K} s)^{-1} \rightarrow H^{-1} Y_1 \qquad (3.100)$$

This algorithm is restricted in its applicability as rounding errors can spoil its convergence. We have restricted its use to calculations on small lattices where convergence is ensured.

CHAPTER 4

SU(2) FINITE DENSITY

4.1)- MATTER FIELD AND CHIRAL SYMMETRY:

In this chapter and chapter 5, we mean $\langle\bar{\chi}\,\chi\rangle$ of eq.1.78 by writing $\langle\bar{\psi}\,\psi\rangle$ and have used H to represent the fermion matrix with chemical potential, unless otherwise explicitly shown.

Comtemporary physics believes that in the normal nuclear matter, the binding forces between quarks increase with the distance separation, making it impossible to split hadrons into individual quarks. Using this picture of hadrons, strong interaction thermodynamics has shown the limit for confinement of quarks. At high density, temperature or both, the quarks become free and in this limit matter can be thought of a quark or quark-gluon plasma. This reflects a phase change from one form of matter to another.

Mott transition for electrons provides a natural analogue of the deconfinement of quarks. At high density, the Coulomb's potential which binds the electrons to the ions is partially screened by the presence of other charges and become much shorter range. At sufficiently high density, the resulting Debye screening radius becomes less than the atomic binding radius so that electrons can no longer feel the binding force to the ions and are set free. At this point,a change of phase takes place; the insulating matter becomes electrically conductive. In Q.C.D, where the gauge group is $SU(3)_{colour}$, deconfinement of the quarks is the analogue of the Mott transition for electrons, where the Coulomb's potential is partially screened by colour charges{17}.

The electric conductivity of electrons has the form,

$$\sigma_e \sim e^{\frac{E}{T}} \qquad (4.1)$$

where E is the ionization energy and T is temperature. In the ideal situation, σ_e vanishes at low temperature for insulators but becomes non-zero with an increase in the temperature, density or both, as such insulator becomes conductor. Above the Mott transiton, σ_e is significantly non-zero but, even below this point, thermal ionization can produce some conduction electrons making σ_e small but non-zero.

The colour conductivity of strongly interacting matter{17},

which is a Q.C.D. analogue of σ_e , is produced by free colour charges and constitutes a rather natural signal for the deconfinement transition. It becomes non-zero for a quark-gluon plasma while it vanishes in hadron matter. The Q.C.D. analogue of the production of locally conduction electron is the formation of quark-antiquark pairs. If we try to separate a quark from a given hadron the linearly confining potential will rise with the separation until it reaches the value of the mass of the lowest qq state. At this point, the production of an additional hadron could be possible. This might be expected to give{18},

$$\sigma_c \sim e^{-\frac{m_H}{2T}} \qquad (4.2)$$

where m_H is the mass of the qq state mentioned above. For T=0, σ_c=0. If $m_H = \infty$, so that we are in the quenched approximation and dealing with the pure gluon fields, then,

$$\sigma_c = \begin{cases} = 0 & T \leq T_C \\ > 0 & T > T_C \end{cases}$$

Our ultimate goal is to introduce matter fields into the theory, so that the colour conductivity and some of the other order parameters described below do not remain very useful. This becomes our reason to find a suitable order parameter for distinguishing the phases of the theory.

4.2)- ORDER PARAMETERS:

From the above discussion, the use of invariant order parameters in lattice gauge theory is quite obvious and these can be used to distinguish different phases of the theory. For example, the energy density E, of eq.1.82 can be used as an order parameter. The choice of a particular order parameter depends upon the nature and kind of the problem.

Pure gauge lattice action eq.1.16, possesses a global symmetry under the centre Z_N of the SU(N) gauge group . The specific state, in which, the system finds itself may spontaneously break this

symmetry just as the ordered phase of the Ising model breaks the Z_2 symmetry of its Hamiltonian. We are, therefore, looking for the gauge theory analogue of spontaneous magnetisation. It is given by average of the Polyakov loops {19},

$$\bar{L}_X(U) = \frac{1}{N} \mathrm{tr} \prod_{\tau=1}^{N} U_{X;\tau,\tau+1} \qquad (4.3)$$

consisting of the product of all the gauge group elements,U's in the time direction, taken at a given spatial site x. Since S_G is invariant under the Z_N transformation, the average Polyakov loop taken over the lattice and all configurations gets a factor $\exp\{2r\pi i/N\}$, with $0 \leq r \leq 1$ and serves as an indicator for spontaneous symmetry breaking. It is zero for Z_N symmetric state and non-zero if symmetry is broken. If $\bar{L}$ measures the free energy F of a static quark, then {19},

$$\bar{L} \sim e^{\frac{-F}{T}} \qquad (4.4)$$

In the confinement phase,

$$F = \infty \quad \text{and} \quad \bar{L} = 0 \qquad (4.5)$$

while in the deconfinement regime,

$$F = \text{finite} \quad \text{and} \quad \bar{L} \neq 0 \qquad (4.6)$$

4.3)- THEORY WITH MATTER FIELDS:

With the introduction of the matter fields(light quarks) into the theory, the full lattice action,

$$S = S_{\text{gauge fields}} + S_{\text{fermions}} \qquad (4.7)$$

no longer respects the symmetry of the centre, Z_N. The average Polyakov loop L remains finite at finite temperature, density or both in the presence of matter fields. The distinction between the confinement and deconfinement regimes becomes more qualitative

and we have to look for another order parameter . The failure of colour conductivity as an order parameter, in the presence of matter fields has been discussed above.

For the full theory, it has already been noted, that in the massless limit, the free Q.C.D. Lagrangian (eq.1.55) is invariant under the chiral transformation (eq.1.52).But, even in the zero mass quark limit, the chiral invariance may be broken spontaneously. This would correspond to the spontaneous generation of an *effective mass* for the quarks and this is analogous to the effective mass of an electron in a conductor as compared to its mass in the vacuum. In the confinement phase, the chiral symmetry is indeed broken so that the u and d quarks have an effective mass of about 300Mev. In the deconfinement plasma, chiral symmetry is again restored (via the mechanism proposed by Kogut et al{12}). Thus the transition from the confined to deconfined phase is signalled by chiral symmetry. The order parameter for chiral symmetry is the chiral condensate given by eq.1.78. It may well be the however that with the global Z_N symmetry broken by the introduction of light quarks, the chiral transition becomes the basic mechanism which makes deconfinement a genuine transition{18}. As we are to introduce fermions in the theory, the chiral condensate has been found to be a very useful order parameter and we have used it for signalling different phases.

4.4)- DYNAMICAL FERMIONS AT FINITE BARYON DENSITY:

Recently many calculations have explained the phase diagram of SU(N) Q.C.D. at finite temperature and density. At zero chemical potential, there is a clear signal for a phase transition with a critical temperature. There are problems, however, at the other extreme where the effect of the finite density on the thermodynamics of zero temperature has to be considered. The standard ideas present the following scenario at T=0. Let us consider a state with a non-zero fermion number which has the lowest energy per quark. The chemical potential μ is a source of quarks for such a state and μ_c is the threshold for producing quarks.

In the infinite lattice limit, at T=0 and $\mu < \mu_c$, all the physical observables such as $<\bar{\psi}\psi>$, agree with their values at μ=0. As soon as we approach μ_c, thermodynamic processes start and quarks are added to the system, increasing the density. At large values of μ, we expect the restoration of chiral symmetry and that this will be related to the mass of the proton via the chemical potential, for SU(3), by, {12},

$$\mu_c = \frac{1}{3} M_P \qquad (4.8)$$

However, the above picture does not fit the numerical results obtained in the strong coupling limit of Lattice Q.C.D. in Ref.{21}. The results of this reference are mainly in the quenched approximation, but it notes that the results for the SU(2) gauge group for quenched and unquenched theories differ only in the size of error bars. For SU(3), some results have been presented for a few values of μ and m_q, using the full theory with the complex Langevin algorithm and these so far agree with the quenched theory. The conclusions drawn from this reference can be summarized as below:-

1)- At a fixed quark mass, the chiral condensate $<\bar{\psi}\psi>$ is constant and then goes to zero (i.e, it is restored) with increasing μ.
2)- As the quark mass m_q is decreased, μ_c decreases and at the zero mass quark limit, chiral symmetry is restored for some arbitrary $\mu>0$, which signifies a zero mass baryonic state.
3)- As a result, μ_c has been related to the pion mass by the following relation, (for m_q-->0),

$$\mu_c = \frac{1}{2} m_\pi \qquad (4.9)$$

because the pion mass goes to zero while the mass of a baryonic state is expected to stay constant as the quark mass goes to zero. Hence the mass of a baryonic state can be given as, $(3/2)m_\pi$.

The relation of μ_c to m_π is not a surprise{22}, but the production of a zero mass baryonic state is really puzzling. The reference suggests that the possible sources of error might be as follows:-

1)- Small size lattices -(Finite size effects)
2)- Big fermion bare masses.
3)- The strong coupling limit of QCD.
4)- The quenched approximation.

There are reasons to suspect the quenched approximation.In fact, Gibbs{23} via the eigenvalue distribution of the propagator matrix has shown that indeed a transition at half the pion mass in the quenched theory exists but above $\mu_c=(1/2)m_\pi$, the chiral condensate is not exactly zero. There is a small residual condensate at $m_q=0$, where m_q is the quark mass. He argued that there can be no deconfinement

from confined phase at $\mu=0$ at non-zero density in the quenched approximation since the behaviour of the Polyakov loops{19}, are unaffected by the chemical potential and yet it can be argued that there cannot be chiral symmetry restoration without deconfinement. He also used a U(1) one dimensional model at finite density to illustrate his conclusions and argued that same would hold for high dimensions to prove that the quenched and unquenched theories;

a)- agree $m_q > 2\,\mathrm{Sinh}\mu$

b)- disagree $m_q < 2\,\mathrm{Sinh}\mu$

4.5)- EIGENVALUE DISTRIBUTION AT ZERO DENSITY:

To calculate the chiral condensate on a fixed size lattice, we need to calculate the inverse of the fermion matrix as shown in eq.1.78. As given earlier, at zero chemical potential, the fermion matrix is anti-hermitian. For this reason, on a complex plane, the eigenvalues are expected to appear only along the imaginary axis. At non-zero chemical potential, the fermion matrix becomes non-hermitian and the eigenvalues are distributed around the imaginary axis with a $\pm\lambda$ symmetry, due to chiral symmetry (eq.1.57a). As the fundamental representation of SU(2) is pseudoreal, an additional symmetry λ,λ^*, is also available for this gauge group.

At zero density, the chiral condensate can be given as{13},

$$\langle\bar{\psi}\psi\rangle \sim \frac{1}{2}\sum_K \left(\frac{1}{i\lambda_k+2ma} + \frac{1}{-i\lambda_k+2ma} \right) \qquad (4.10)$$

$$= \sum_k \frac{2ma}{\lambda_k^2 + (2ma)^2} \qquad (4.11)$$

For large lattices,

$$\langle\bar{\psi}\psi\rangle \sim \int_{-\infty}^{+\infty} d\lambda \, \frac{2ma\,\rho(\lambda)}{\lambda_k^2 + (2ma)^2} \qquad (4.12)$$

where 2ma is the quark mass(scaled) in the lattice units while $\rho(\lambda)$ is the normalized eigenvalue spectral density.

As 2ma --->0,

$$\langle \bar{\psi}\psi \rangle \sim \rho(0) \qquad (4.13)$$

and we require eigenvalues close to zero.

4.6)- SU(2) FINITE DENSITY RESULTS:{27}

For SU(3), the chiral order parameter can be given as,

$$\langle \bar{\psi}\psi \rangle = \frac{\langle \mathrm{tr}\, H^{-1} e^{i\phi} \rangle}{\langle e^{i\phi} \rangle} \qquad (4.14)$$

For SU(2), ϕ=0, so that the chiral condensate is real and positive,

$$\langle \bar{\psi}\psi \rangle = \frac{\langle \mathrm{tr}\, H^{-1} \rangle}{\langle 1 \rangle} \qquad (4.15)$$

where,

$$\langle \mathrm{tr}\, H^{-1} \rangle = \int dU\, \mathrm{tr} H^{-1}\, e^{S_{eff.}} \qquad (4.15a)$$

and via eq.eq.1.74 and 1.77, detH is the contribution of the dynamical fermions to the effective action if this contribution is replaced by $\mathrm{tr}H^{-1}\mathrm{det}H$, eq.4.15 becomes,

$$\langle \bar{\psi}\psi \rangle = \frac{\langle 1 \rangle}{\langle (\mathrm{tr}\, H^{-1})^{-1} \rangle} \qquad (4.16)$$

This representation for the condensate has a driving force which should have a weaker repulsion of the smaller eigenvalues compared to that of eq.4.15. We present results for both the driving forces.

4.7)- THE FERMION WEIGHT |H|:

We carried out calculations using the Lanczos algorithm for finite density with full theory for SU(2) gauge group at small quark masses to evaluate the chiral condensate on a 4^4 lattice. The length of the lattice in the time direction represents the inverse of the temperature{10}.We used strong and intermediate coupling for our

calculations.

To understand the behaviour of the chiral condensate in terms of the distribution of smaller eigenvalues of the fermion matrix, we present the following summary of the models from ref.{24}. We show an analogy between the chiral condensate $<\bar{\psi}\psi>$ in terms of the eigenvalues of the fermion matrix for SU(2) and an electric field E arising from unit positive charges at (x_i,y_i) where the ith eigenvalue of the fermion matrix $\lambda = x_i + iy_i$ and the electric field $E \cong <\bar{\psi}\psi>$ is measured at $((x=m_q),0)$, where m_q is the quark mass. However this analogy is only valid in case when we use eq.4.15 as the representation for the chiral condensate.

4.7a)- THE MODELS FOR THE CHIRAL CONDENSATE:

on a large lattice, the chiral condensate can be given as,

$$<\bar{\psi}\psi> = \int dx \int_{-\infty}^{+\infty} dy\, \rho(x,y)\, \frac{1}{m_q + x + iy} \qquad (4.17)$$

where x and y represent the real and imaginary parts of the eigenvaues of the $\not{D}$ part of the fermion matrix and ρ is the spectral density.

Supposing that ρ is independent of y, so that $\rho(x,y) \cong f(x)$,

$$<\bar{\psi}\psi> = \int f(x)\, dx \int_{-\infty}^{+\infty} dy\, \frac{1}{m_q + x + iy}, \qquad (4.18)$$

then,

$$= \int f(x)\, dx\ (m_q+x) \int_{-\infty}^{+\infty} \frac{dy}{y_i^2 + (m_q+x)^2} = \begin{cases} \pi \int f(x)\, dx & \text{if } x > -m_q \\ -\pi \int f(x)\, dx & \text{if } x < -m_q \end{cases} \qquad (4.19)$$

CASE(a): EIGENVALUES FORM A UNIFORMLY POPULATED STRIP OF WIDTH 2L:

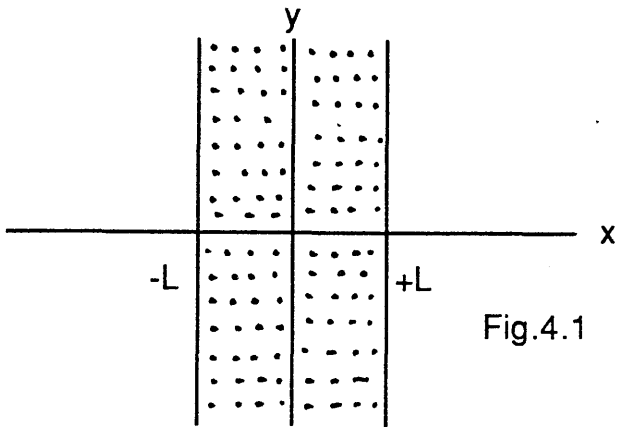

Fig.4.1

then f(x) = ρ = constant. Fig.4.1 represents the case. There are two possible situations;

a(i)- $L < m_q$

$$\langle\bar{\psi}\,\psi\rangle = \rho \int_{-L}^{+L} dx\,\pi = 2\pi\rho L \qquad (4.20)$$

a(ii)- $-L < m_q < L$,

$$\langle\bar{\psi}\,\psi\rangle = \rho\,[\int_{-L}^{-m} -\pi\,dx + \int_{-m}^{L} \pi\,dx\,] = 2\pi\rho m \qquad (4.21)$$

Hence if the quark mass lies inside the uniformly populated strip, $\langle\bar{\psi}\psi(m_q=0)\rangle = 0$.

CASE(b)- EIGENVALUES FORM TWO UNIFORMLY POPULATED SYMMETRIC STRIPS:

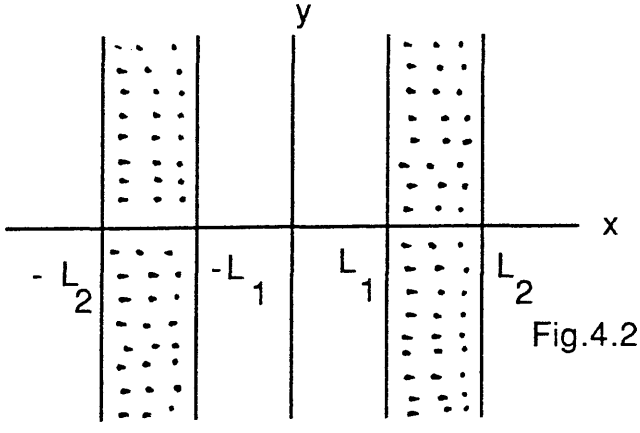

Fig.4.2

Fig.4.2 is the pictorial representation of this case. There are

three possible locations of the quark mass on the real axis. With a similar treatment as given above, we get,

$$\text{b(i)-}\quad -L_1 < m_q < L_1, \qquad \langle\bar{\psi}\,\psi\rangle = 0 \qquad (4.22)$$

$$\text{b(ii)-}\quad L_1 < m_q < L_2, \qquad = 2\pi\rho(m_q - L_1) \qquad (4.23)$$

$$\text{b(iii)-}\quad -L_2 > m_q > L_2, \qquad = 2\pi\rho(L_2 - L_1) \qquad (4.24)$$

4.7b)-THE TWO DIMENSIONAL ELECTROSTATIC MODEL:

The eigenvalues are considered as unit positive charges at (x_i, y_i) producing an electric field E on the real axis. We calculate $\langle\bar{\psi}\psi(x=m_q, 0)\rangle$ using Gauss' law,

$$\int \vec{E} \cdot d\vec{l} \times \hat{k} = 2\pi \int \rho \, ds \qquad (4.25)$$

where k is the unit vector along the outward normal perpendicular to the plane containing E and dl in fig.4.3.

(C)- UNIFORMLY POPULATED SINGLE STRIP:(Fig.4.3)

As mentioned above, we consider that the quark mass could lie at different places on the real axis. We make a Gaussian box of length $2m_q$(from $-m_q$ to m_q) and finite height 2Δ as shown in fig.4.3. The possible situations and the resulting electric field which can occur are:-

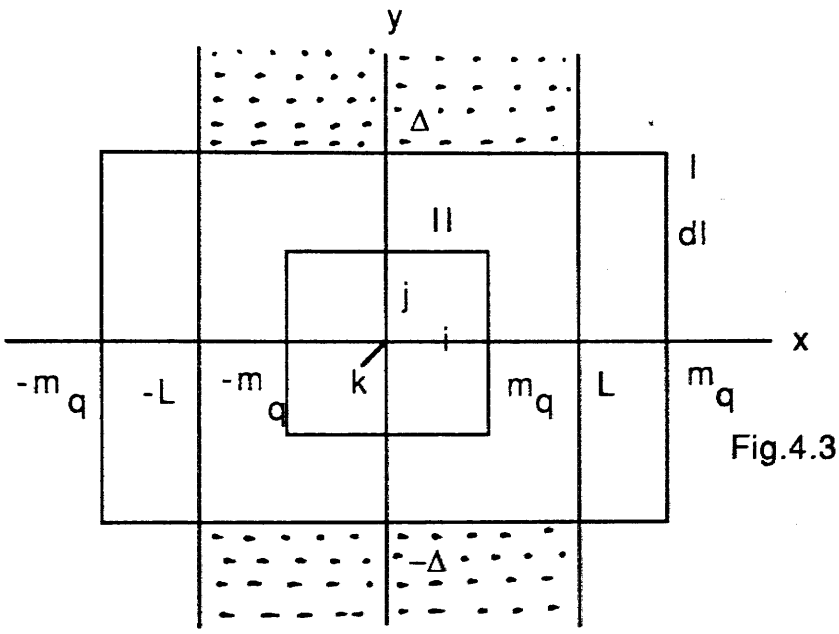

Fig.4.3

c(i)- $m_q \geq L$,

$$\int 2E\,dl = 4E\,\Delta = 2\pi\rho\,(2\Delta \times 2L)$$

$$E = 2\pi\rho L \qquad (4.26)$$

c(ii)- $m_q \leq L$,

$$\int_{-\Delta}^{+\Delta} 2E\,dl = 4E\,\Delta = 2\pi \int \rho\,ds$$

$$E = \frac{\pi f'(\Delta, m_q)}{2\Delta} \qquad (4.27)$$

with $f'(\Delta, m_q) = \rho.\ 2\Delta.2m$ where $f'(\Delta, m_q)$ denote the number of the eigenvalues inside the box.

(d)- TWO SYMMETRICAL STRIPS UNIFORMLY POPULATED:

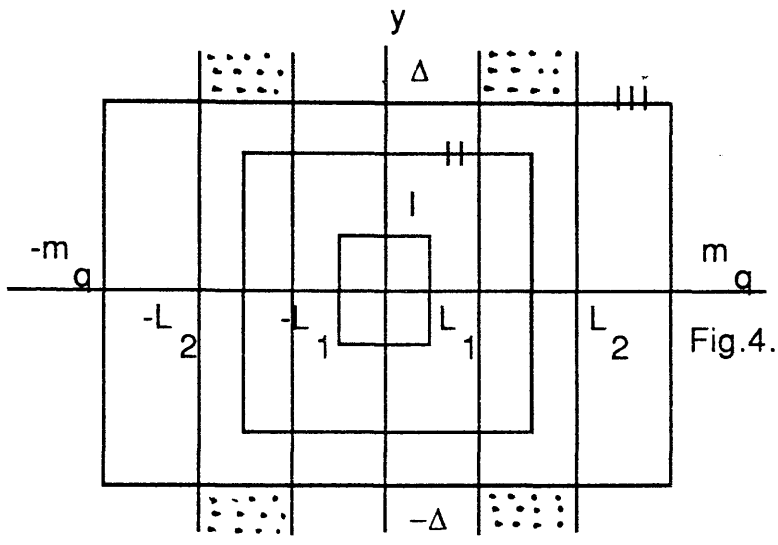

Fig.4.4

Three possible Gaussian boxes for the location of mass on the x-axis(real axis) discussed below are shown in the fig.4.4.

d(i)- $0 < m_q < L_1$, $E = 0$ (4.28)

d(ii)- $L_1 \leq m_q \leq L_2$

$$E = \frac{\pi f(\Delta, m_q)}{2\Delta} \qquad (4.23a)$$

d(iii)- $m_q > L_2$, $E = 2\pi\rho(L_2 - L_1)$ (4.29)

An analogy between cases (a,b) and (c,d) is obvious. An immediate consequence, as can be noted from eqs.4.21 and 4.22, is that $\langle\bar{\psi}\psi(m)\rangle$, in the zero mass quark limit, is non-zero if and only if, there is an eigenvalue delta function on the imaginary axis and E will be non-zero.

Before dicussing the figures with eigenvalue distribution, the following points for these distributions should be noted:-

1)- As mentioned earlier, at zero chemical potential, the eigenvalues are expected to appear along the imaginary axis.

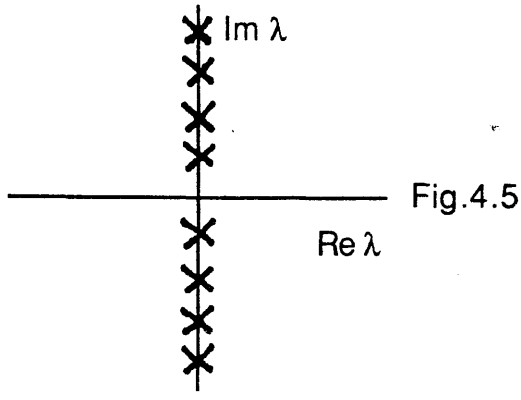

Fig.4.5

2)- For a finite lattice, such as 4^4 lattice, the effect of the chemical potential is felt much earlier than it would be for an infinite lattice discussed in section 4.4. In fact, it is immediate for a finite lattice. At non-zero chemical potential, with fixed quark mass, coupling constant and N_f=number of flavours, the eigenvalues move off the imaginary axis perpendicularly and form a single strip as shown in fig.4.6. As noted earlier, the eigenvalues are distributed with $\pm\lambda,\lambda^*$, symmetry round the imaginary axis.

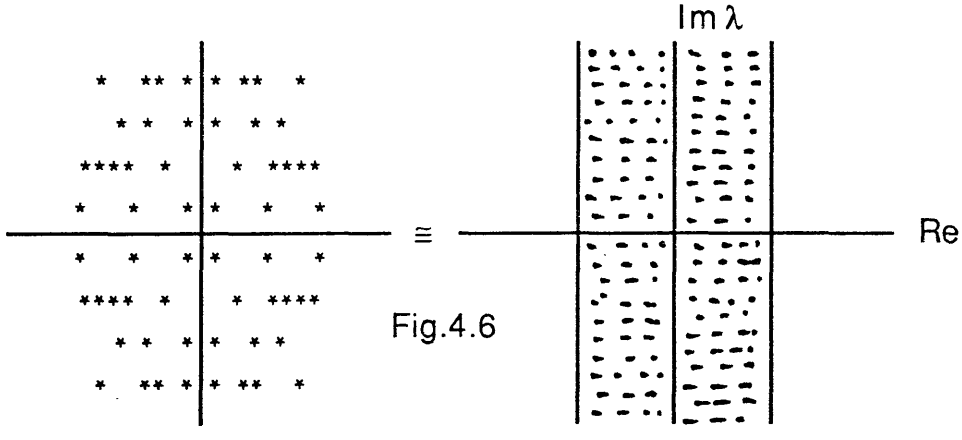

Fig.4.6

3)- As we increase the chemical potential μ, the width of the strip increalses monotonically with it. At large μ, the eigenvalues form two uniform symmetrics around the imaginary axis leaving the region around λ=0, completely depleted of eigenvalues as shown fig.4.7.

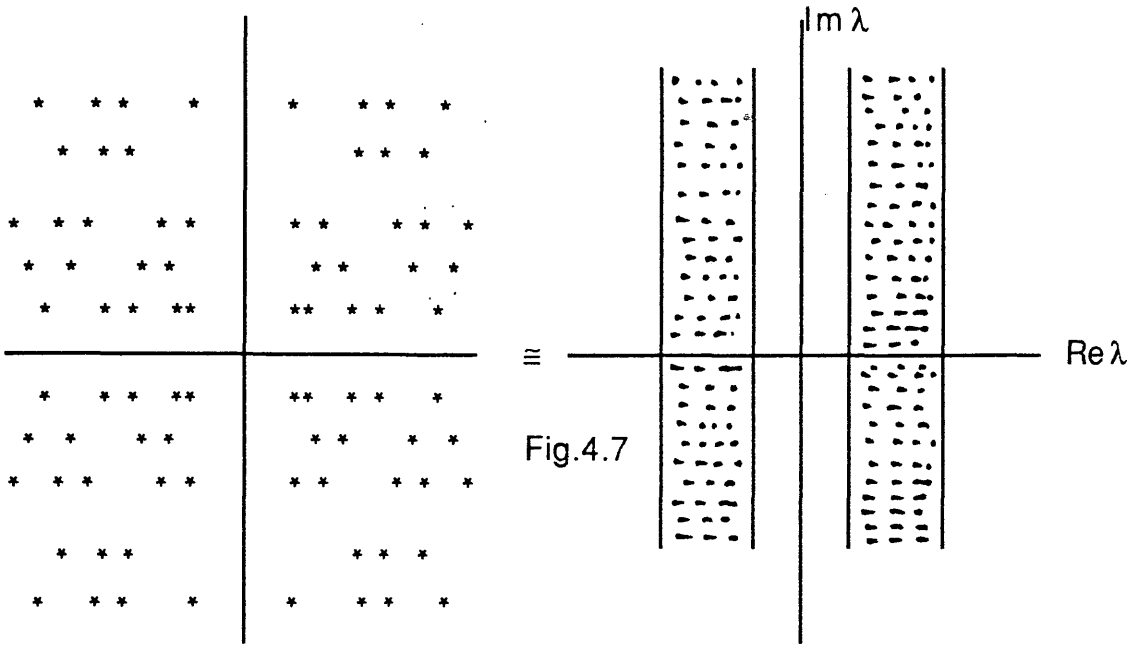

Fig.4.7

4)- The inclusion of dynamical fermions means that the fermion determinant of eq.1.88 is included and can be given by,

$$\text{Det}\,(M_c + 2ma) = \prod_i [\,\lambda_i^2 - (2ma)^2] \qquad (4.30)$$

Whenever an eigenvalue comes close to the location of the quark mass, the configuration containing such as eigenvalue is rejected by the Metropolis algorithm. Therefore, we might expect a gap to appear around the location of the quark mass on the real axis, when mass enters the strip of eigenvalues. We call this the fermionic repulsion of the zero modes. Fig.4.28 shows such a situation at large μ.

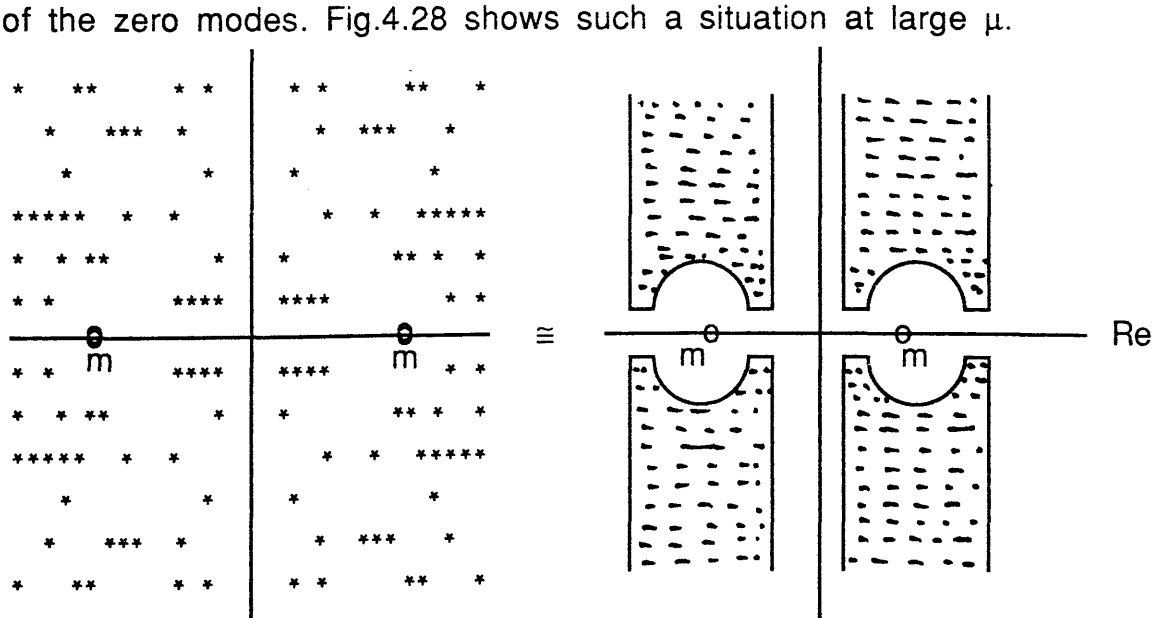

Fig.4.28

With these expectations and observations, we proceed to discuss our results.

The eigenvalues of all the distributions presented, in this chapter are for the fermion matrix $2(M_c-m_q)$.

For all the figures presented, the bare quark mass,m_q, is twice the mass shown on each figure which is a consequence of the rescaling of section 1.7a. Fig.4.8 and 4.9, show the eigenvalue distribution of the fermion matrix for the quark masses 0.1 and 0.0125, at zero chemical potential, N_f =4 and β=1.7. The eigenvalues only appear along the imaginary axis as expected.

For fig.4.10, we have calculated explicitly $<\bar{\psi}\psi>$ at increasing values of the chemical potential at fixed m_q=0.4, β=.5 and N_f=4. Later, we shall compare the conclusion drawn from this plot, with the one drawn from eigenvalue distribution plots of the fermion matrix. In this figure chiral condensate decreases with an increase in μ and goes to zero or is restored at μ=1.0 in lattice units. The phase transition is second order and it is very difficult to obtain the correct value of μ_c, but it is approximately 0.4.

Figs.4.11 to 4.18, show the eigenvalue distribution with increasing chemical potential. The values of the quark mass, β and N_f are the same as for fig.4.10. The first thing to note in these figures is that the eigenvalue distribution is symmetric along the imaginary axis with no eigenvalue delta function on the imaginary axis.

As previously mentioned, while using the analogy between $<\bar{\psi}\psi>$ and electrostatic field intensity E , it is assumed that quark mass lies on the real axis so that for fig.4.11, the quark mass is outside the strips. Using this analogy, when we make a Gaussian box of length $2m_q$ and some finite height, it contains some eigenvalues. According to case d(iii) of this section, $<\bar{\psi}\psi> \cong E \neq 0$, so that, chiral symmetry is broken.

It can be seen that as we increase the chemical potential, the gap along the imaginary axis keeps on widening, while a gap also starts to appear along the real axis. The situation is unchanged until fig.4.15, where quark mass enters the strip.In this figure, the fermionic repulsion of zero modes is very prominent. The Gaussian box still contains eigenvalues and chiral symmetry is broken. In figs.4.16 and 4.17 we can make Gaussian boxes free from eigenvalues but for fig.4.18 the signal is clear, the region around λ=0 is completely free from eigenvalues and chiral symmetry is clearly restored at μ=1.0.

The average plaquette is measure of the equilibrium state of

the thermodynamic system{25}. Fig.4.19 gives a history of the chiral condensate and the Average plaquette, versus sweep number, where μ is altered after 5 or 10 sweeps. The system is in equilibrium since the Average plaquette is approximately constant and chiral symmetry is found to be restored at μ=1.0.

It is clear from the above discussion, that we can rely on the chiral symmetry signals given by the eigenvalue distribution of the fermion matrix.

To demonstrate the problem of the zero mass baryonic state mentioned earlier, we consider the chiral condensate as a function of the quark mass with the chemical potential, β and N_f fixed.

Fig.4.20 presents a history of explicitly calculated $<\bar{\psi}\psi>$ and Average plaquette versus sweep number with a changing m_q. This figure is important in the sense that it is the first to indicate the problem. Later on, we shall confirm the result by the eigenvalue distribution graphs of the fermion matrix. The chemical potential, β, and N_f are fixed at the values, 0.1,1.7 and 4 respectively. We have plotted $<\psi\psi>$ at three different quark masses as shown in the figure. $<\psi\psi>$ tends to vanish as the quark mass goes to zero,i.e., for all other parameters of the theory fixed,

$$<\bar{\psi}\,\psi> \text{ ----> } 0, \text{ as } m_q \text{----->} 0$$

This is a signal that μ=0.1 will be sufficient to restore chiral symmetry in the vanishing quark mass limit. In other words, an arbitrary $\mu \neq 0$, may restore chiral symmetry in the zero mass quark limit.

From above we know that the chiral character of the theory can also be signalled by the eigenvalue distributions of the fermion matrix. Fig.4.21 to 4.23, show the eigenvalue distribution for five superimposed configuration at quark mass $[(1/2)m_q]$ of 0.05, 0.0125 and 0.00625 with again fixed μ= 0.1, β= 1.7 and N_f= 4, same as for fig.4.20. In order to examine our results, we would like to discuss these figures individually. Again, we note that there is no eigenvalue delta function along the imaginary axis and the strips are symmetric around the imaginary axis.

As given above, fig.4.21 is a plot of the eigenvalues on a complex plane at quark mass 0.1 in lattice units. The quark mass lies outside the strip as schematically shown in the fig.4.21a.

Fig.4.21 ≅

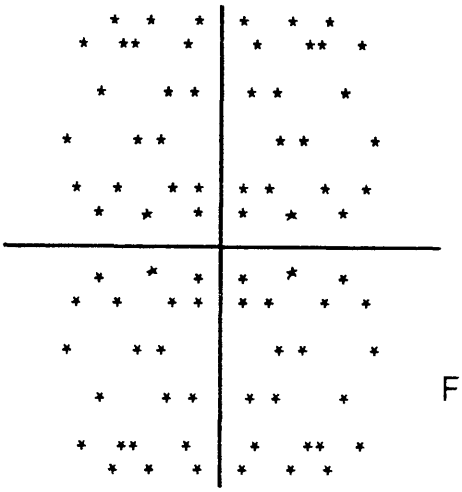

≅

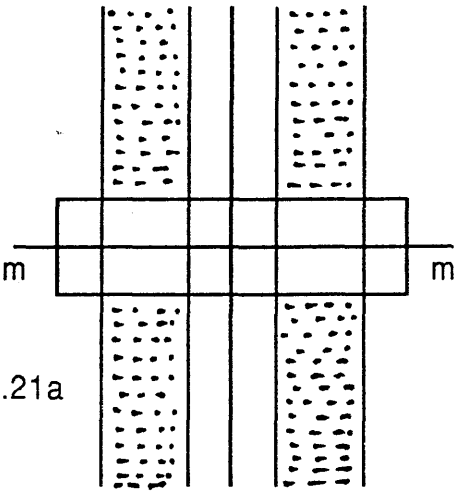

Fig.4.21a

On making a Gaussian box of the length $2m_q$ and some finite height, some eigenvalues enter the box and chiral symmetry is broken, as discussed earlier. As the quark mass lies outside the strip, some eigenvalues are very close to the real axis.

In fig.4.22, quark mass 0.0250 lies inside the strip of eigenvalues. The fermion repulsion of the zero modes is clear near the location of the quark mass as schematically shown in fig.4.22a.

Fig.4.22 ≅

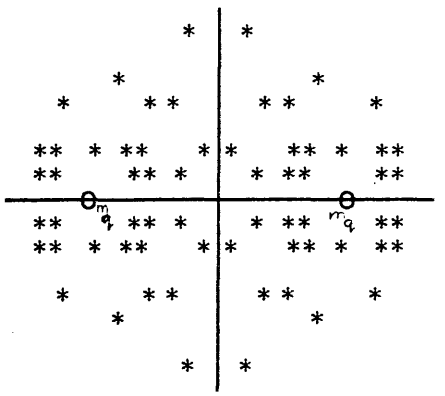

≅

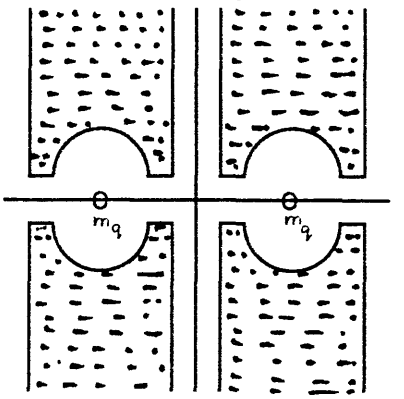

Fig.4.22a

One important thing to note is that the eigenvalues can approach the real axis between the positions of the quark mass.If we superimpose more and more configurations, the Gaussian box, according to case d(ii), may contain eigenvalues and chiral symmetry might still be broken. However, it should be noted that there are persistent gaps along the real and imaginary axis, whose growth will restore the chiral symmetry.

As schematically shown in fig.4.23a, the quark mass m_q has moved further inside the strip towards the imaginary axis.

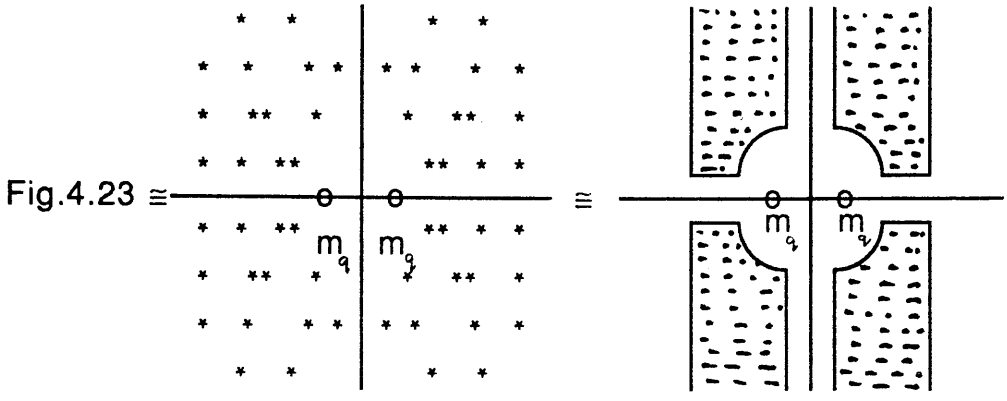

Fig.4.23a

We can note that the gaps along the real and imaginary axis have grown. These gaps and the fermion repulsion of zero modes make the region near $\lambda=0$, free from eigenvalues. We can make a Gaussian box containing no eigenvalues. The chiral symmetry is, presumably, restored according to eq.4.25.

Before discussing the zero mass quark limit, the following points should be noted:-

1)- The persistent gaps along the real and imaginary axis.

2)- The eigenvalue distributions do not seem to be changing very much other than possibly fermionic repulsions as m_q decreases and enters the strip; It looks insensitive to a decreasing quark mass.

In the situation where the quark mass goes to zero with all the parameters of the theory fixed at their values given above, due to the gaps mentioned above, a Gaussian box would contain no eigenvalue as shown in fig.4.24 and $<\bar{\psi}\psi>$ vanishes. It means that in the zero mass quark limit, chiral symmetry will be restored for any arbitrary chemical potential.

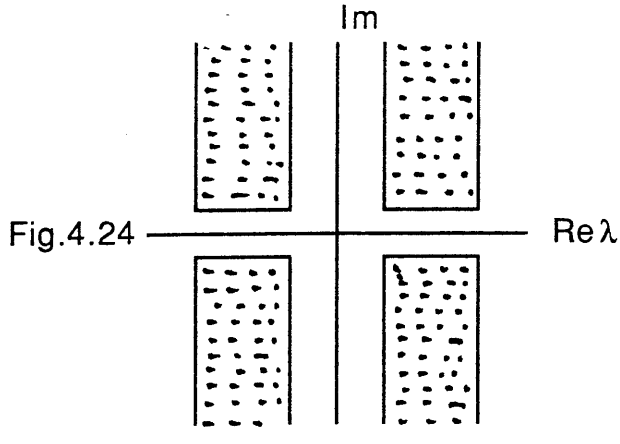

4.8)- THE FERMIONIC WEIGHT TrH^{-1} detH:

For this fermionic weight, $<\bar{\psi}\psi>$ is given by eq.4.16 and as mentioned earlier, it has a driving force which should have a weaker repulsion for smaller eigenvalues.

The first thing to note in this case is that, the analogy between chiral condensate and electrostatic field can no longer be utilized but at least we can check the weaker fermionic repulsion of the zero modes predicted in section 4.7.

Figs.4.25 and 4.26 present eigenvalue distributions for this weight at two quark masses 0.1 and 0.0125. The values of β, N_f and μ, are fixed at the same values used for figs.4.21 and 4.23, which are their counterpart for the first representation of chiral condensate given by eq.4.28.

It can be seen that as the mass enters the strip in fig.4.26, the fermionic repulsion of zero modes is weaker and eigenvalues come very close to the location of the mass.

Fig.4.27 gives a history of the chiral condensate versus sweep number for this fermionic weight at the two masses used for figs.4.25 and 4.26. Chiral symmetry seems to be restored at the smaller quark mass limit.

Table1, summarizes the differences in the calculated values of the chiral condensate for both the weights but the correct equilibrium results should be same for each weight. The error quoted is statistical. Presumably many more sweeps are required to attain true equilibrium measurement. However the difference in weights is reflected via these results for weight $trH^{-1}|H|$ as compared to that of $|H|$.

TABLE

$<\bar{\Psi}\Psi>$

$(1/2)m_q$	$\|H\|$	$trH^{-1}\|H\|$
0.05	0.169±0.033	0.234±0.027
0.0125	0.049±0.018	-
0.00625	0.014±0.002	0.0315±0.010

Eigenvalue distribution (4 configurations superimposed)

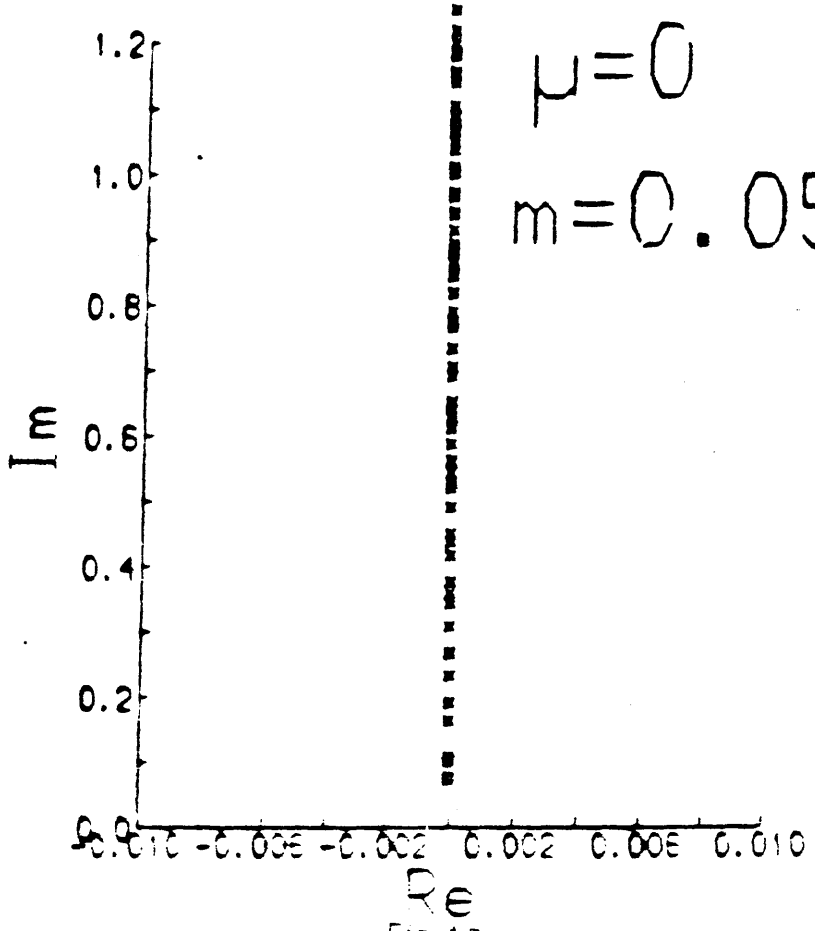

Fig.4.8

Eigenvalue distribution (4 configurations superimposed)

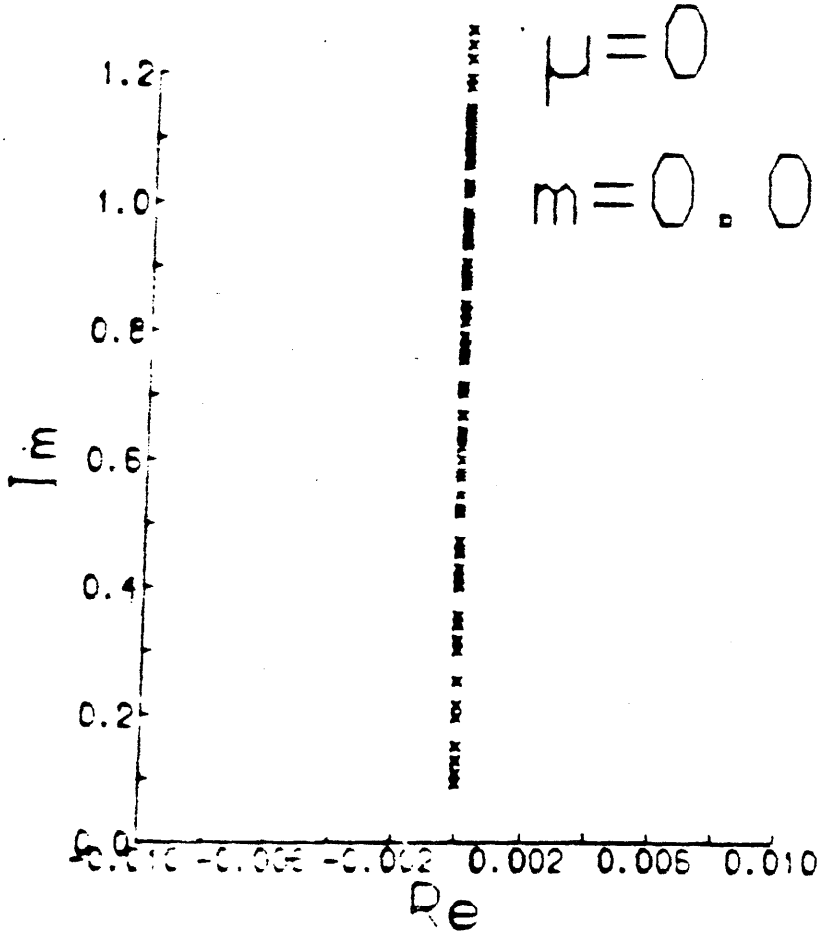

Fig.4.9

$\langle \bar{\psi}\psi \rangle$ against μ for $\beta = 0.5$ at $m = 0.2$, with line from Dagotto, Moreo and Wolff, 1986.

Fig 4.10

Eigenvalue distributions for β = 0.5 at m = 0.2 for various μ

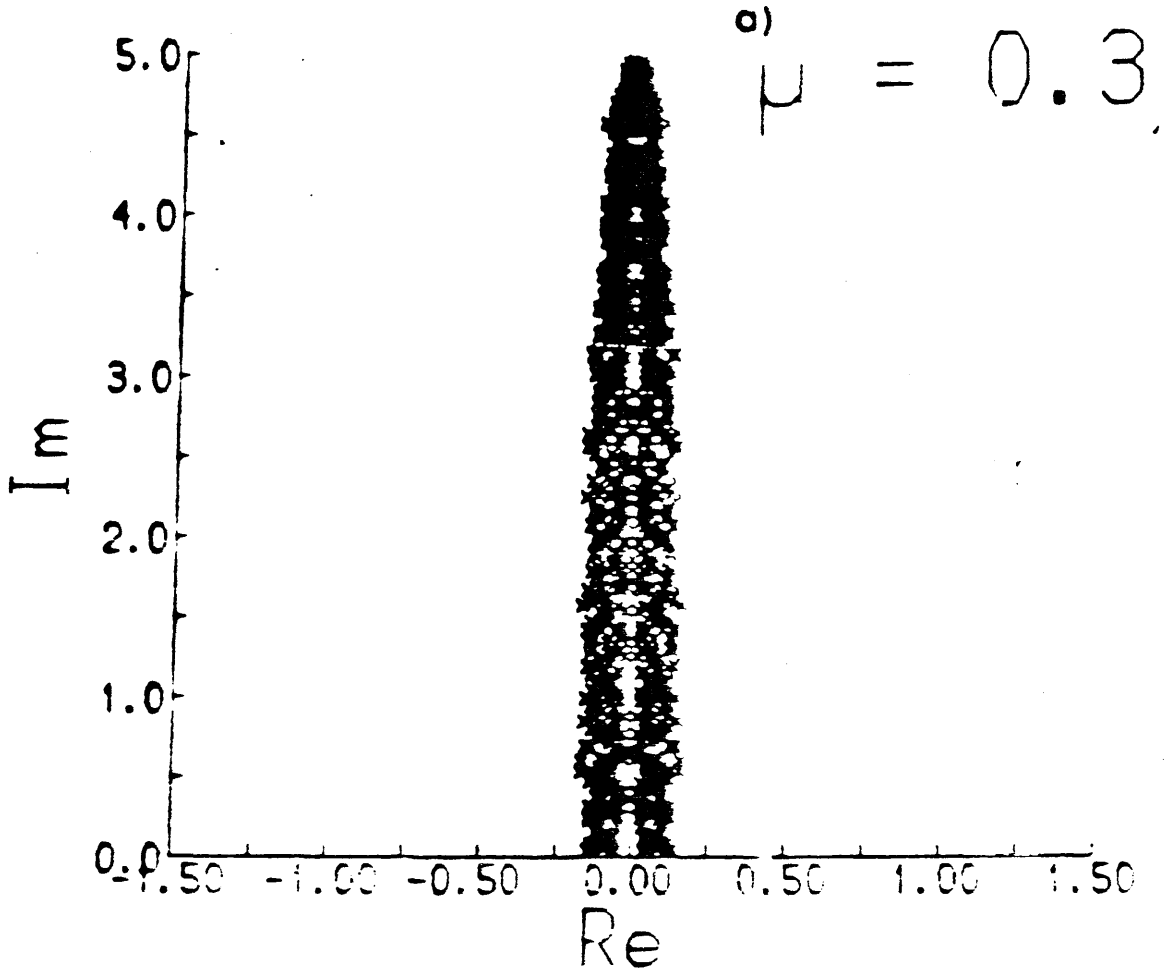

Fig.4.11

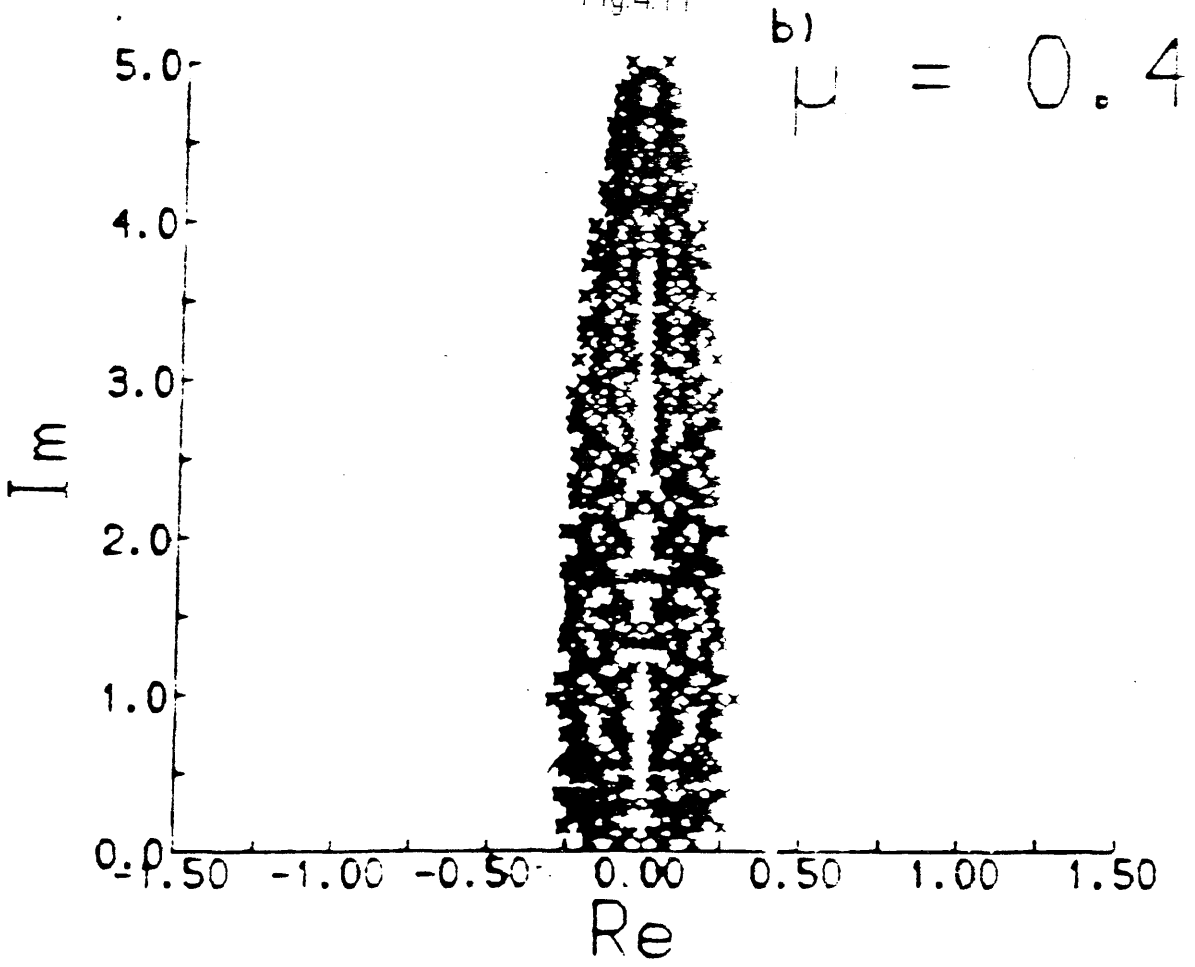

Fig.4.12

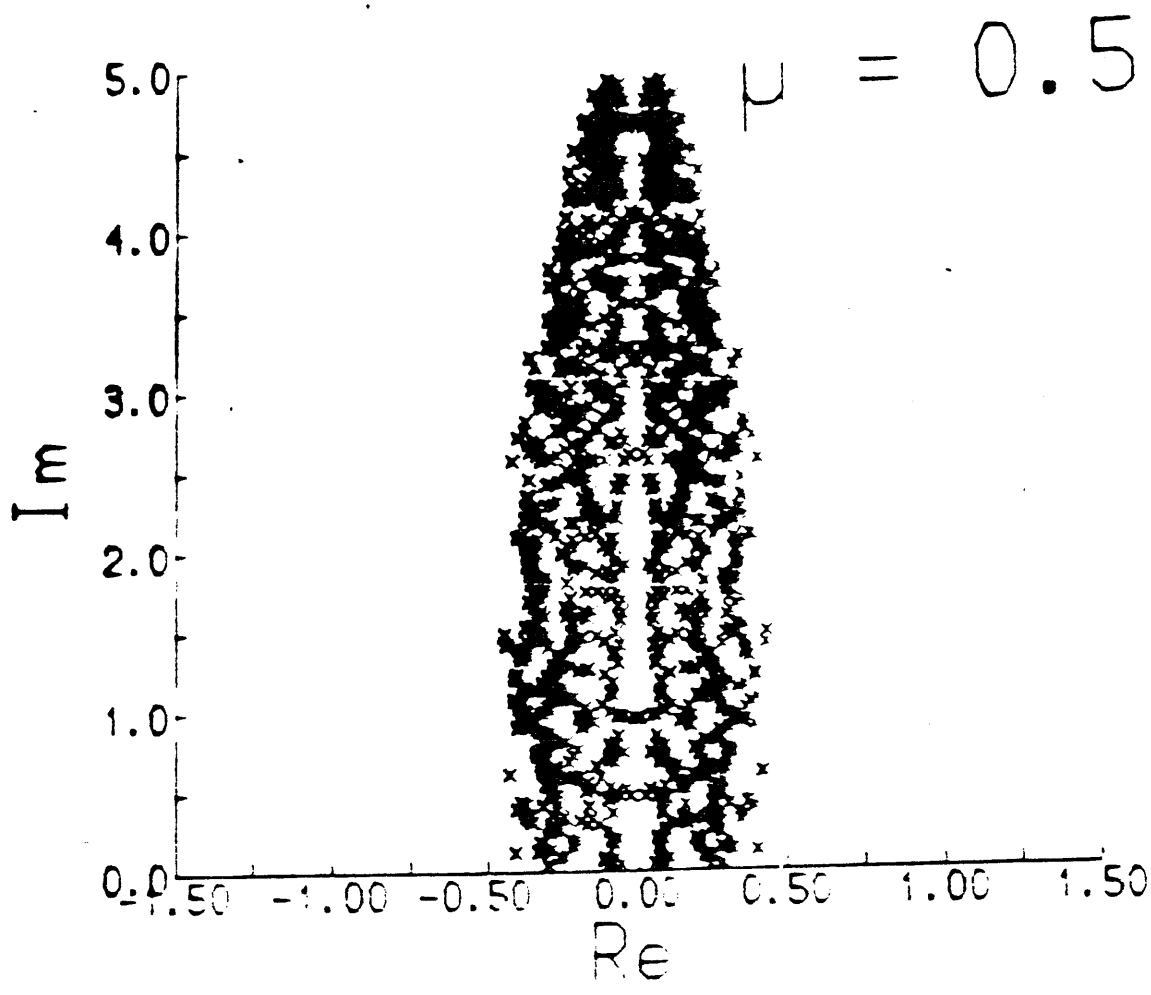

Fig.4.13

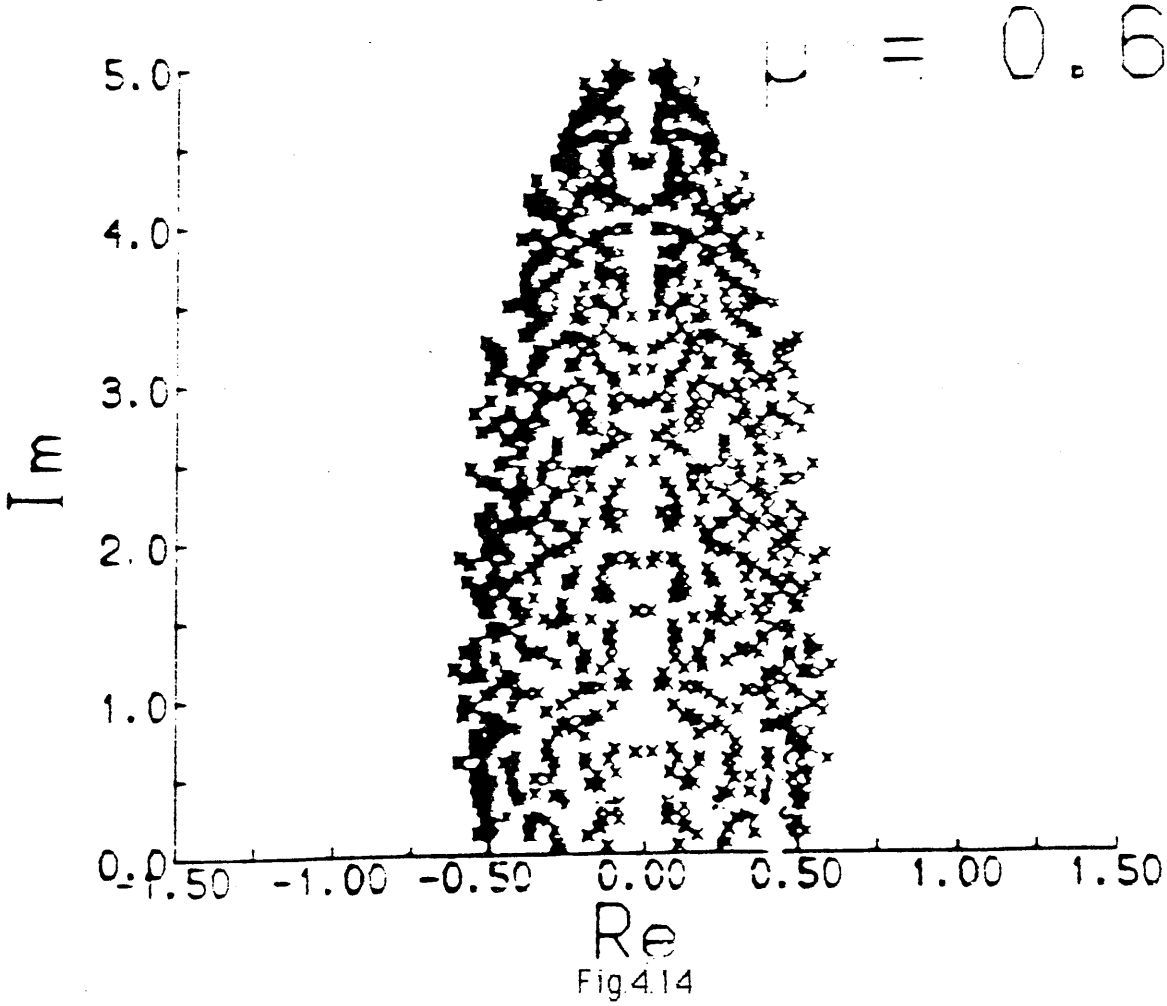

Fig.4.14

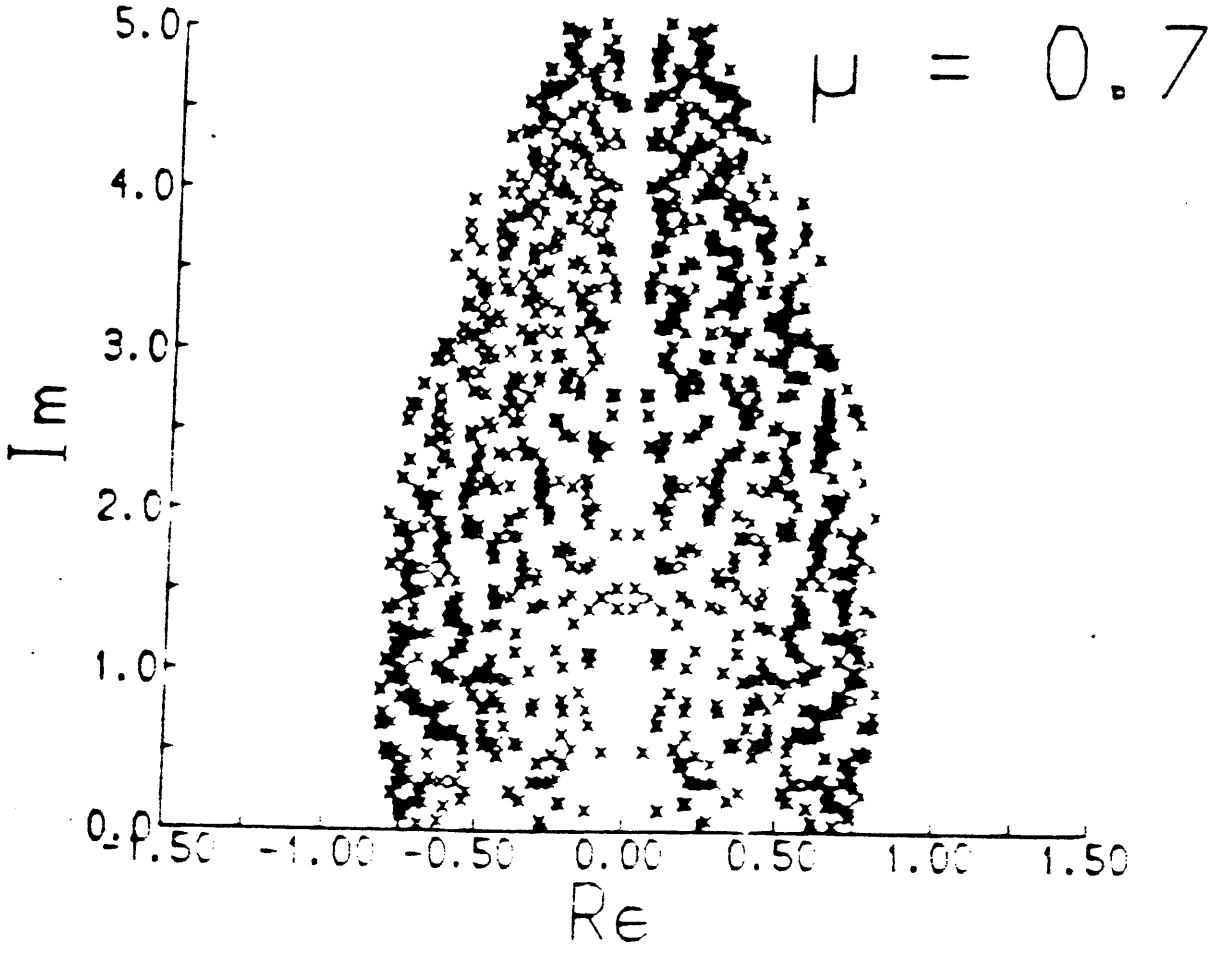

Fig 4.15

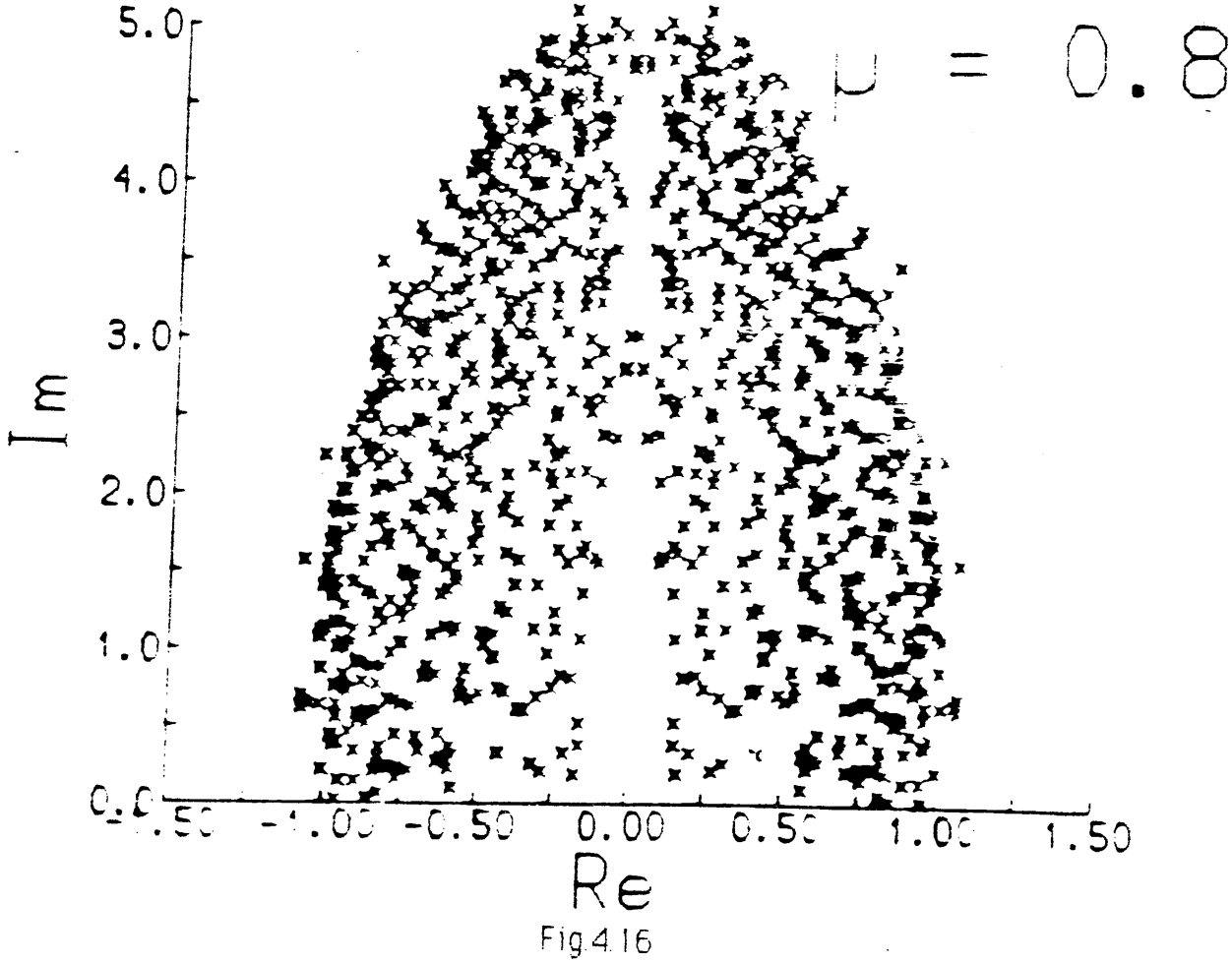

Fig 4.16

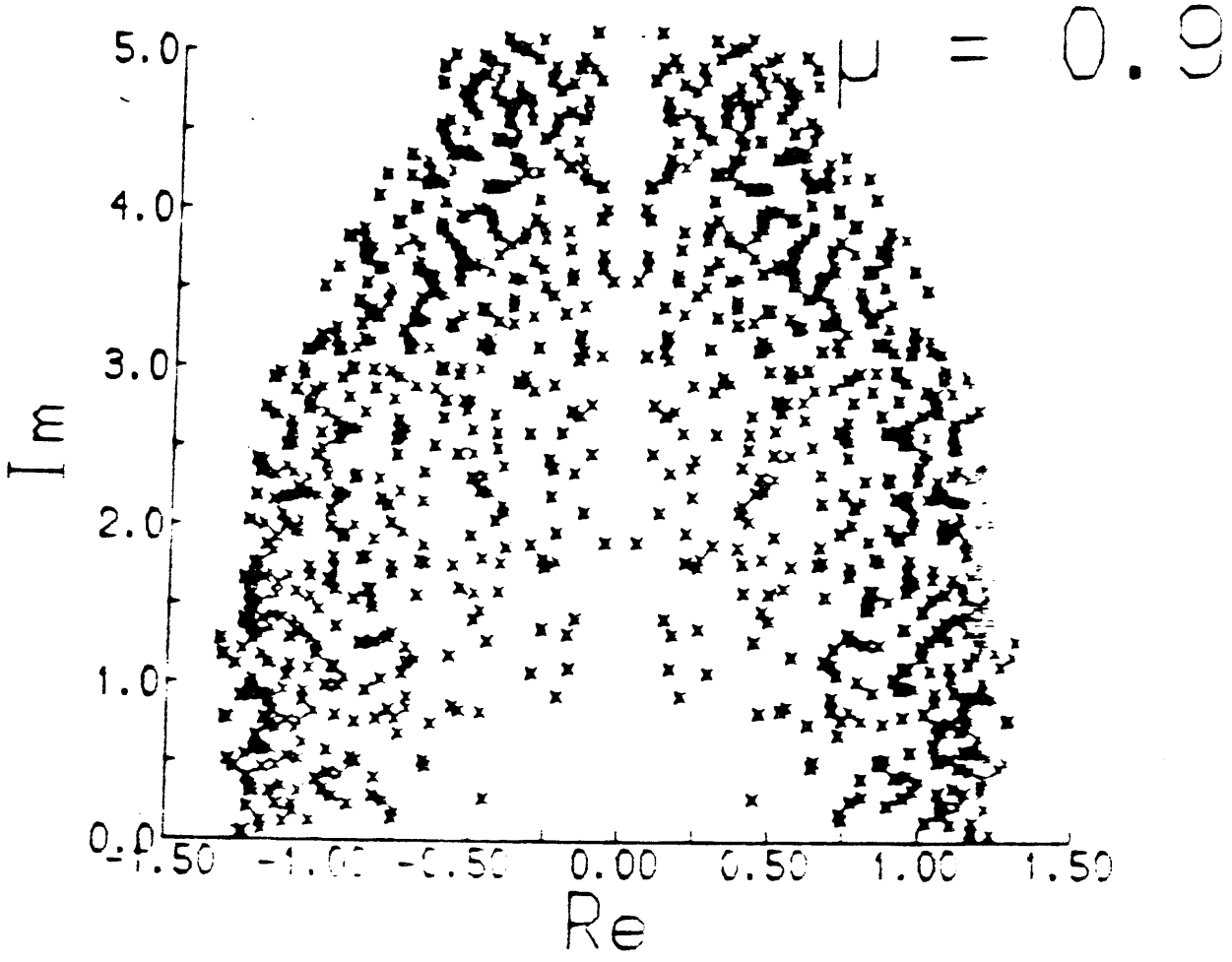

Fig.4.17

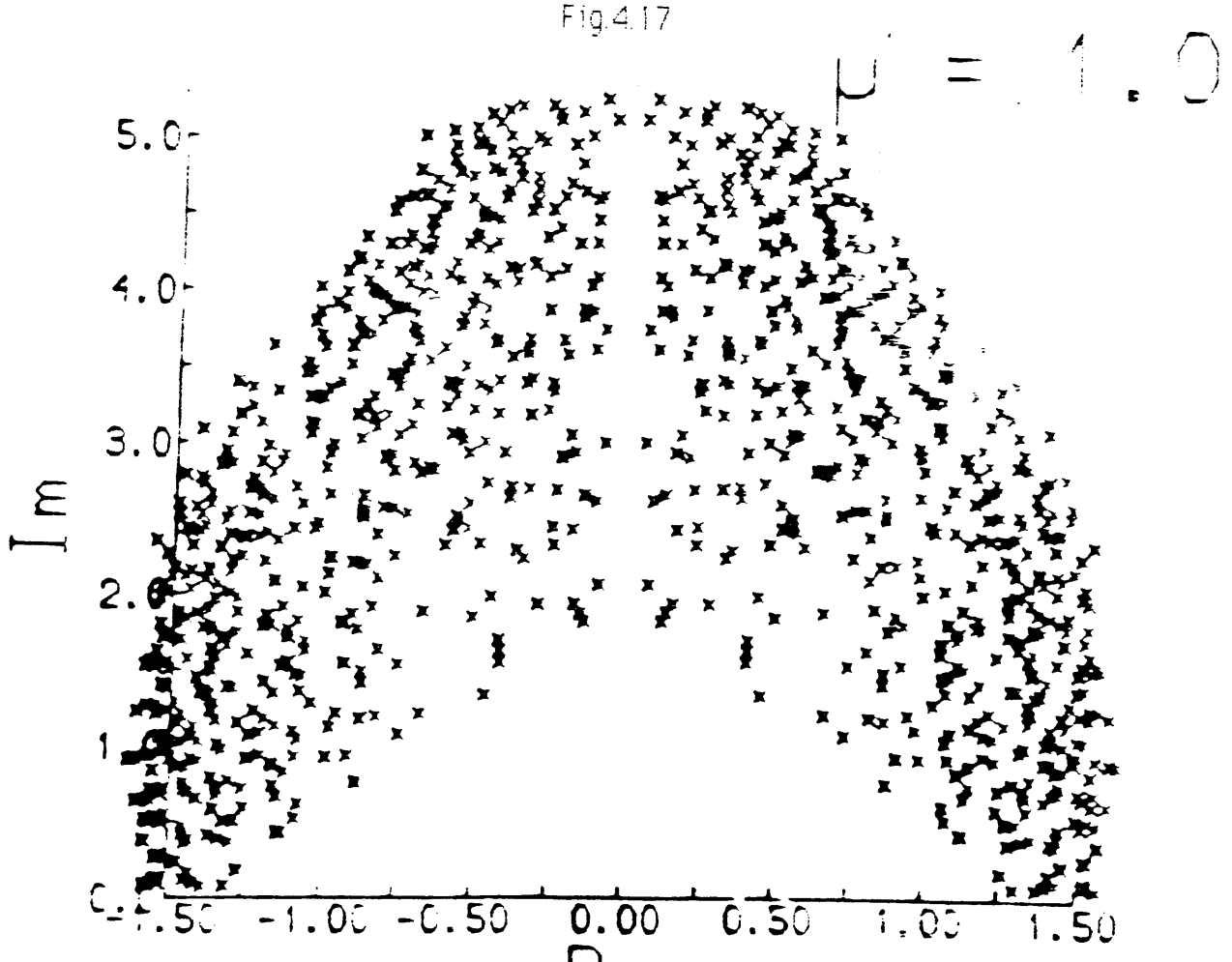

Fig.4.18

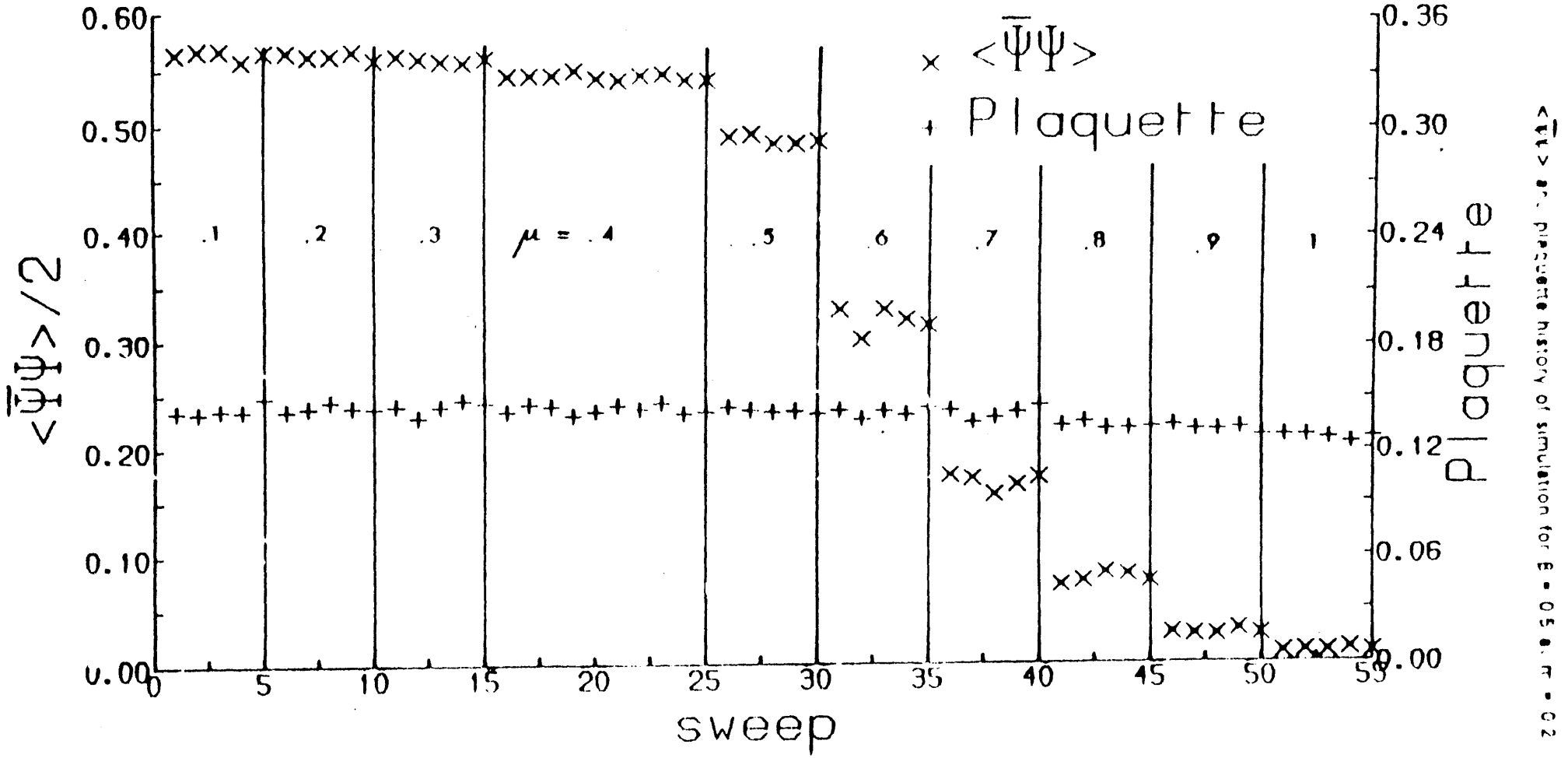
0.60
0.50
0.40
0.30
0.20
0.10
0.00
<ψ̄ψ>/2
0.36
0.30
0.24
0.18
0.12
0.06
0.00
Plaquette
<ψ̄ψ>
Plaquette
.1
.2
.3
μ = .4
.5
.6
.7
.8
.9
1
0
5
10
15
20
25
30
35
40
45
50
55
sweep
<ψ̄ψ> and plaquette history of simulation for β = 0.5 , κ = 0.2

Fig.4.19

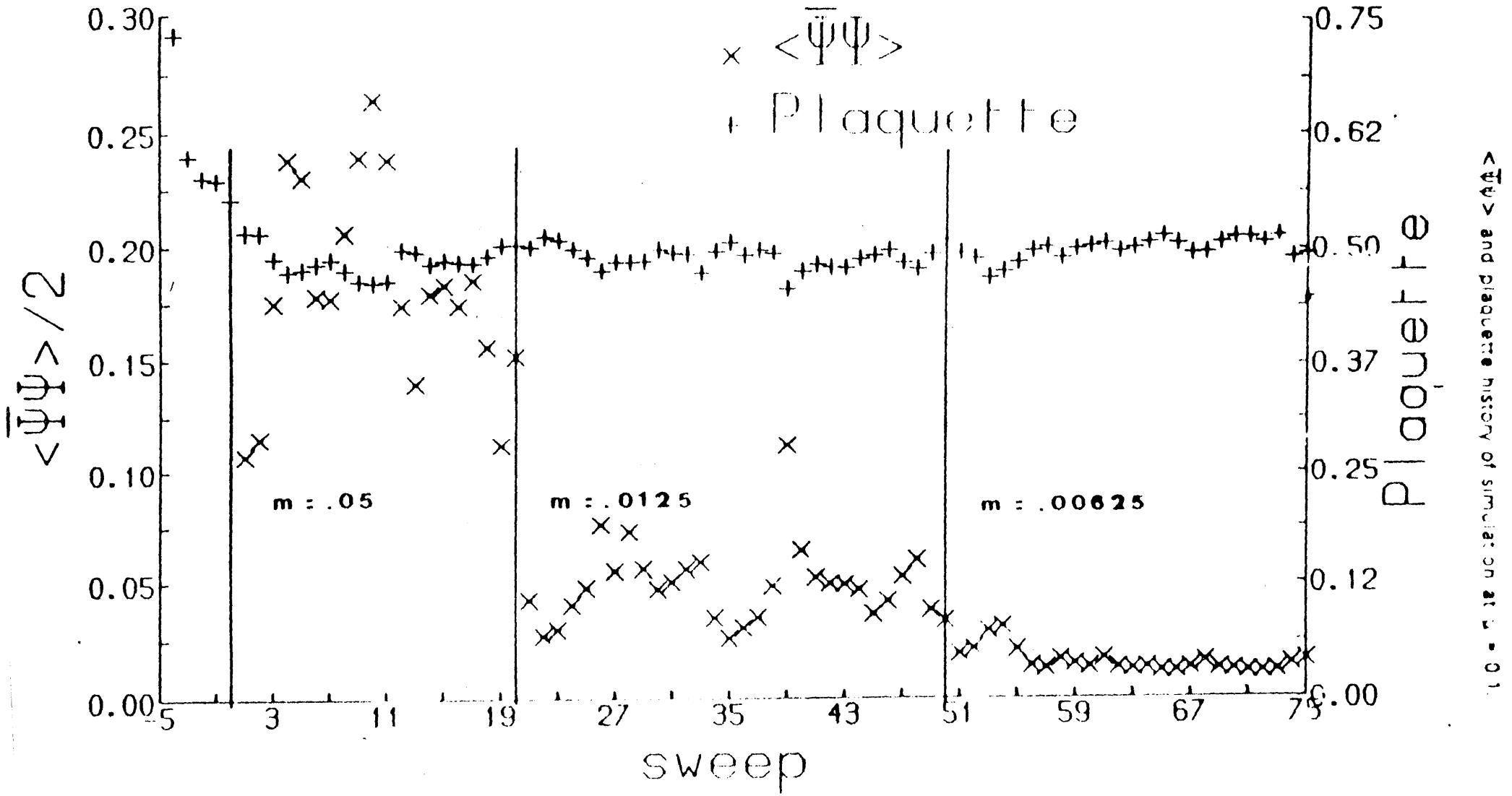
0.30
0.25
0.20
0.15
0.10
0.05
0.00
0.75
0.62
0.50
0.37
0.25
0.12
0.00
<ψ̄ψ>/2
<ψ̄ψ> and plaquette history of simulation at m = 0.1
plaquette
<ψ̄ψ>
plaquette
m = .05
m = .0125
m = .00625
-5
3
11
19
27
35
43
51
59
67
75
sweep

Fig 4.20

Eigenvalue distribution (5 configurations superimposed)

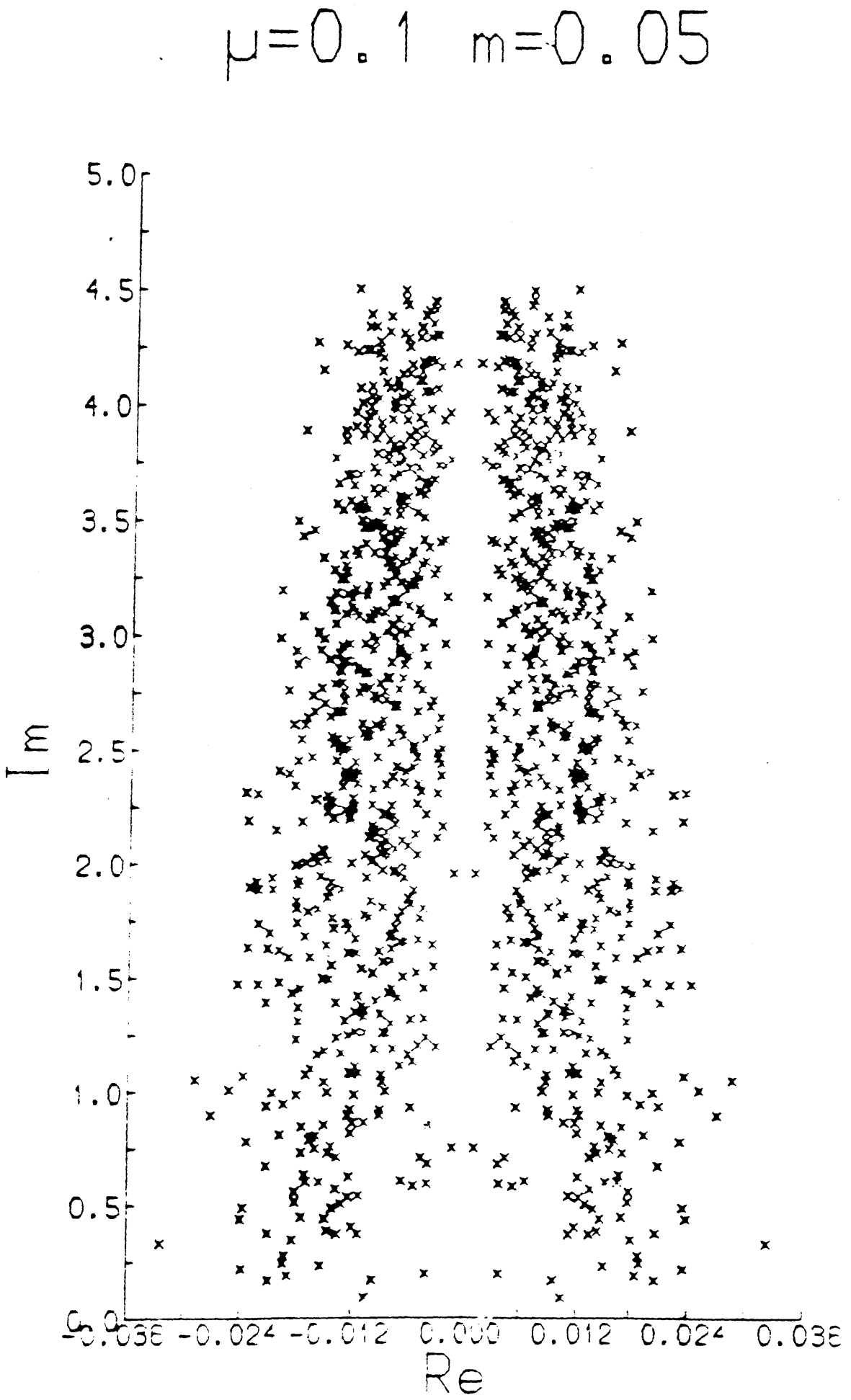

Fig.4.21

Eigenvalue distribution (5 configurations superimposed)

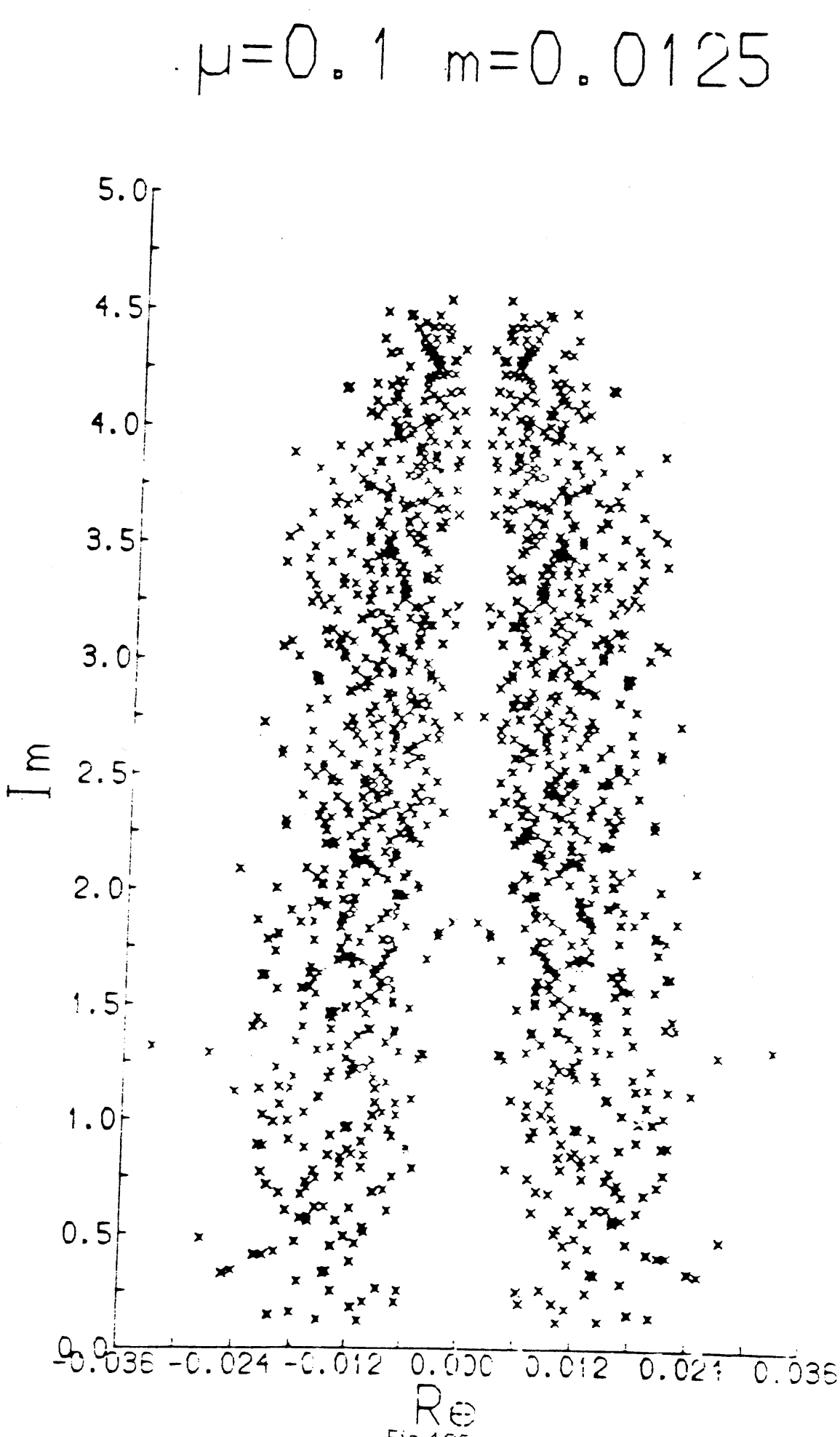

Fig 4.22

Eigenvalue distribution (5 configurations superimposed)

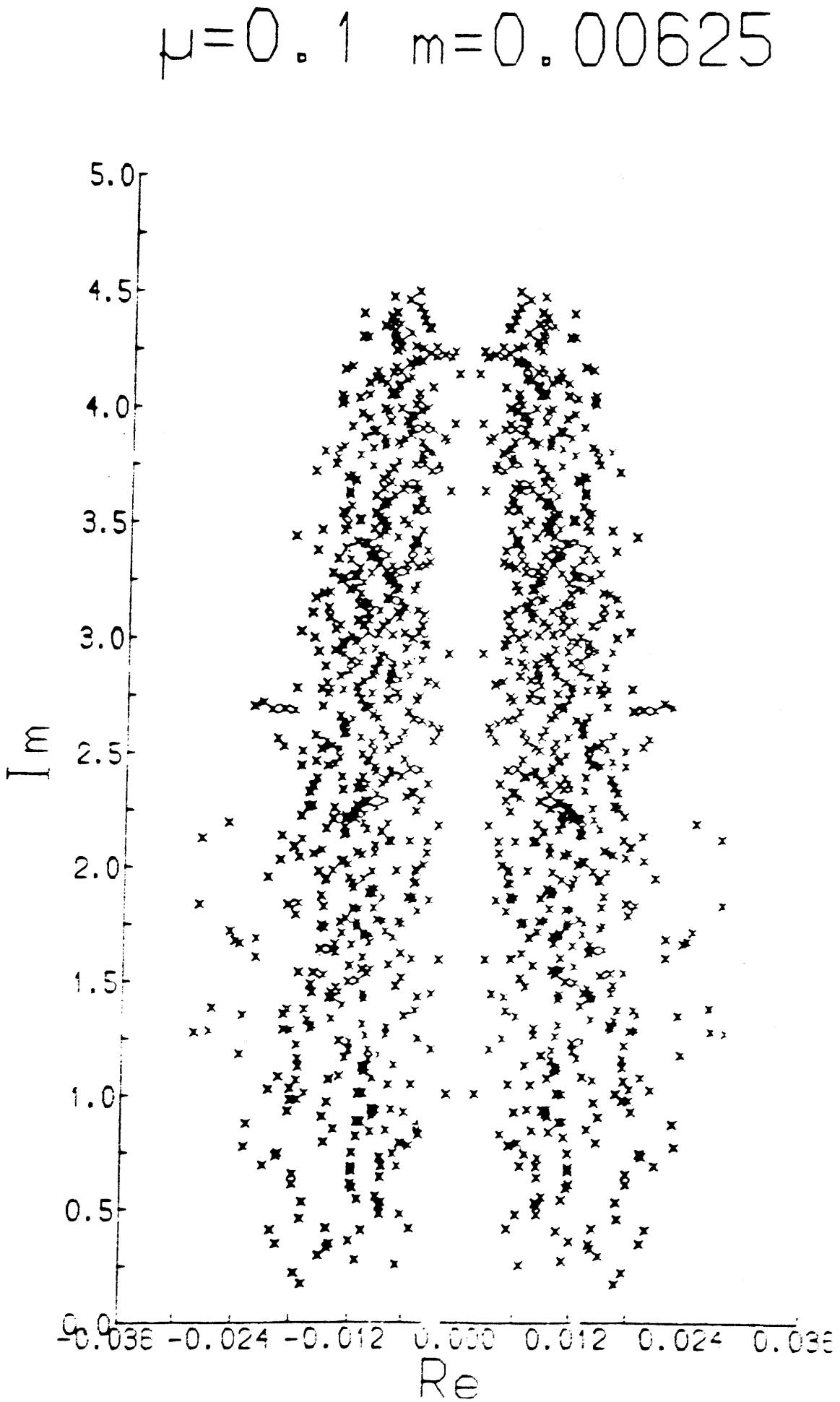

Fig 4.23

Eigenvalue distribution with new weight (4 configurations superimpo

$\mu = 0.1 \quad m = 0.05$

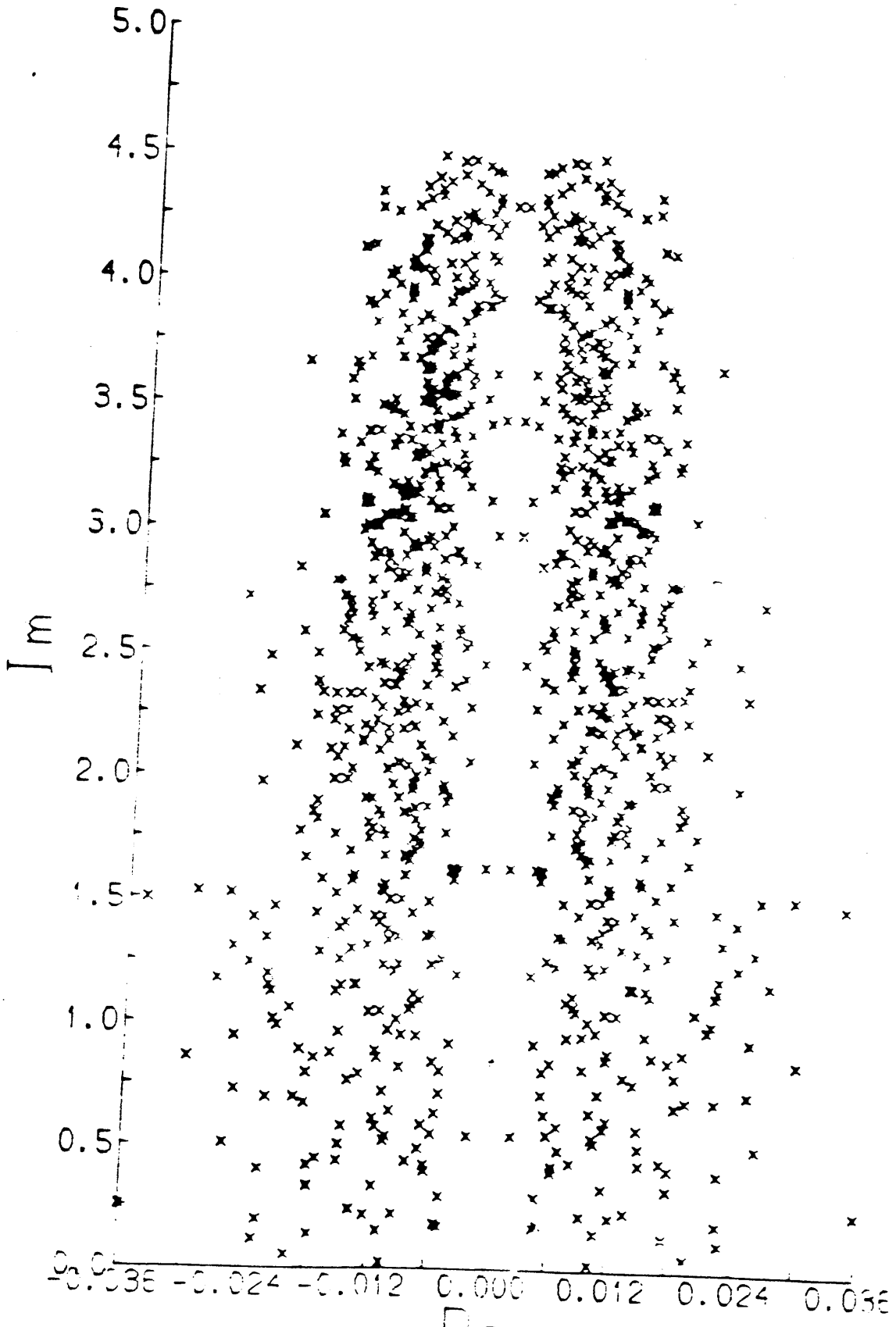

Fig 4.25

Eigenvalue distribution with new weight (4 configurations superim

$\mu = 0.1 \quad m = 0.00625$

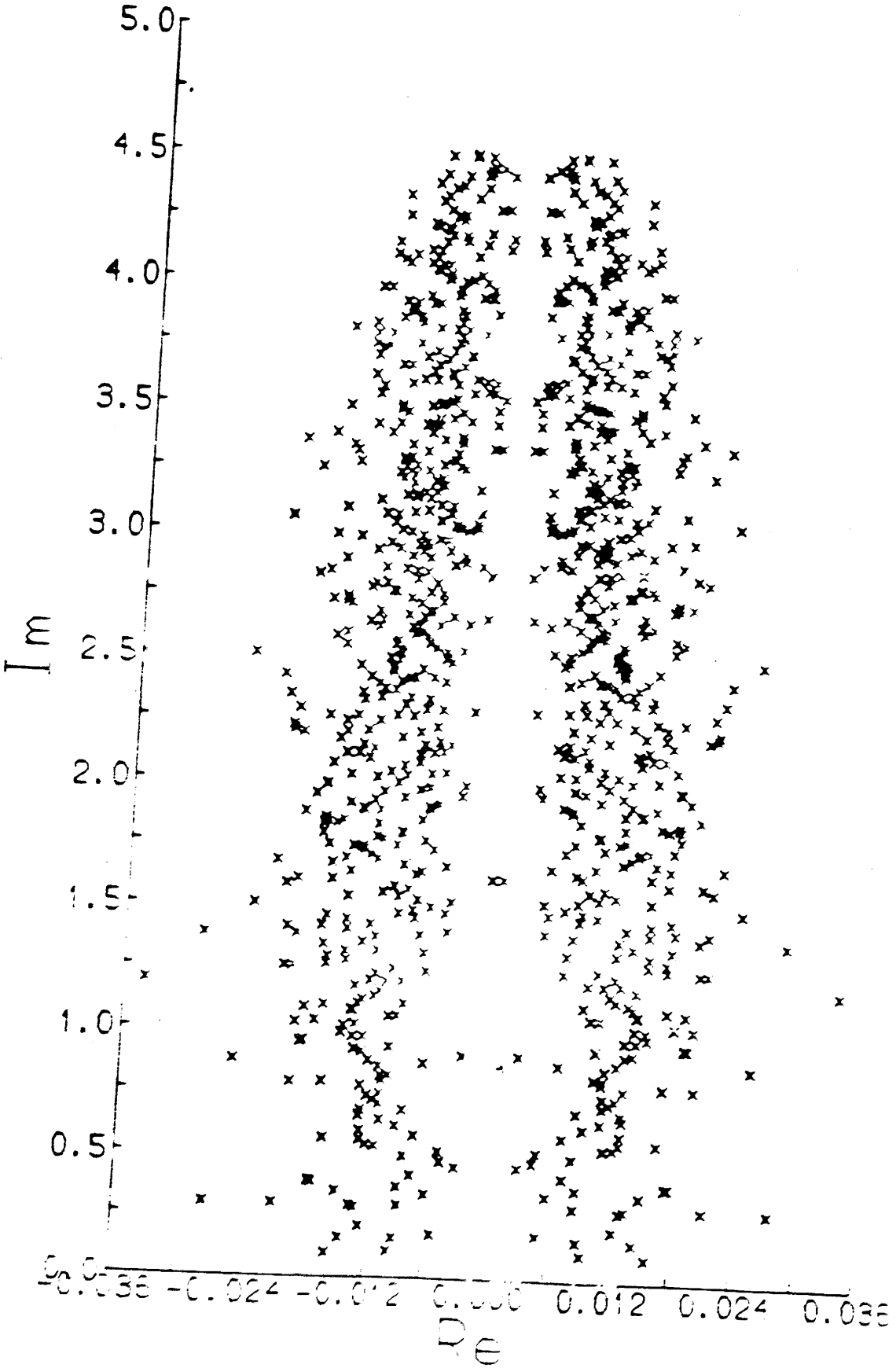

Fig 4.26

Fig. 4.8 $\langle \bar{\psi}\psi \rangle$ history of simulation with new weight at $\mu = 0.1$.

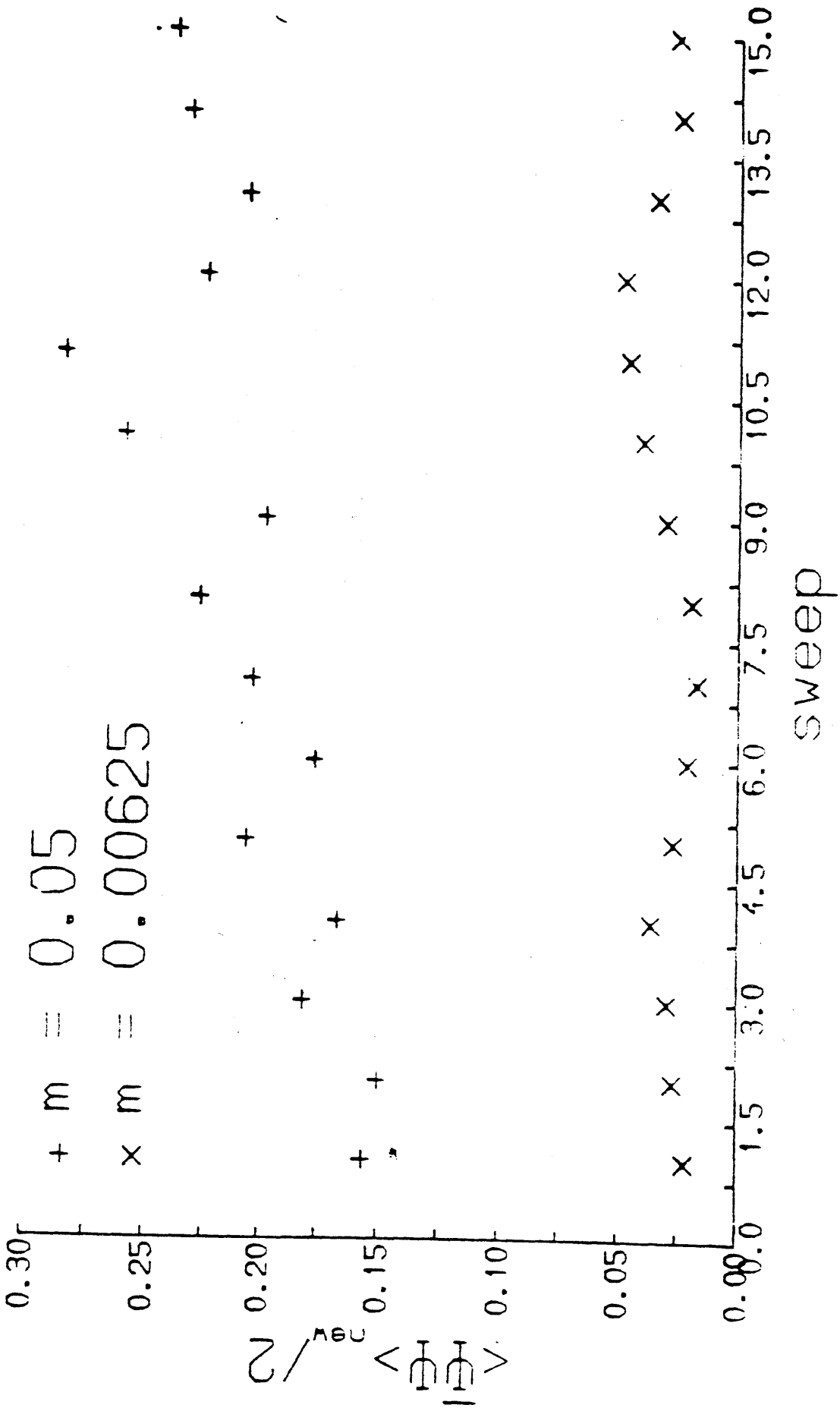

Fig 4.27

CHAPTER 5

FINITE DENSITY USING SU(3)

5.1) - FINITE DENSITY Q.C.D.:

From the last chapter, we are, now, aware of the problem of the production of a zero mass baryonic state and the consequent relation of μ_c to the pion mass instead of the nucleon mass. One of the main sources of error, was claimed to be the use of the quenched approximation and in the last chapter, we used the SU(2) gauge group for the full theory, to calculate $<\overline{\psi}\ \psi>$ at finite density. We found results similar to those obtained by the quenched approximation. In fact, this is not unexpected, as SU(2) does not differentiate between a pion and a nucleon. Moreover, as mentioned earlier, the fundamental representation of SU(2) is pseudo-real and consequently, the fermion determinant is real and positive. As we use a real and positive quantity as a weight for carrying out Monte Carlo simulations for generating statistically independent and important configurations , there is no problem as for as the SU(2) gauge group is concerned. The quenched theory approximates the fermion determinant with a constant quantity and it may be one of the reasons that the full and quenched SU(2) theory results are similar. The SU(2) group is useful in the sense, that it makes computor simulations easy but in fact the true group for QCD is the SU(3). As mentioned above, SU(2) is pseudo-real but SU(3) is not and as a result the SU(3) fermion determinant with non-zero μ is complex and the approximation of a complex quantity to a positive and real one by the quenched theory is somewhat awkward. Hopefully by including SU(3) determinant (taking up the full theory) the transition at $\mu_c=(1/2)m_\pi$, will be smoothed out and only the true transition at $(1/3)m_P$, will remain.

Fig.5.1 has been taken from reference{19} and it shows how the argument of the complex determinant changes with μ for a fixed gauge field configuration.It clearly shows that it is not legitimate to ignore the complex phase.

An arbitrary element U of SU(3) can be generated from Gell-Mann's eight λ matrices via the relation,

$$U(\varepsilon_1, \varepsilon_2, ...\varepsilon_8) = \exp(i\varepsilon_\alpha \lambda_\alpha) \qquad (5.1)$$

where the ε's are the parameters of the group.

5.2)- MONTE CARLO SIMULATION WITH DYNAMICAL FERMIONS:

5.2a)- DISCUSSION AND RESULTS:

As already mentioned, the weight with which the configurations via computor simulations are generated should be a real and positive quantity. The weight generally used for generating SU(3) configurations is,

$$W(U) = |\det H| e^{-\beta S_G} \qquad (5.2)$$

We write the complex phase explicitly and for SU(3) we therefore calculate,

$$\langle \bar{\Psi} \Psi \rangle = \frac{1}{N} \frac{\langle \mathrm{tr}\, H^{-1} e^{i\phi} \rangle}{\langle e^{i\phi} \rangle} \qquad (5.3)$$

As the complex conjugate configuration has similar contribution, we can replace the expressions for the numerator and denominator in eq.5.3 by their real parts but it will be wiser to calculate the imaginery parts also since, if the imaginery parts are becoming smaller, it indicates that the Monte Carlo is working. As discussed earlier the penality of ignoring the complex phase is then to get the results similar to the quenched theory or of SU(2) of the previous chapter.

Eq.5.3 can be written as ,

$$<\bar{\Psi}\Psi> = \frac{\mathrm{Re}<\mathrm{tr}\, H^{-1} e^{i\phi}>}{\mathrm{Re}<e^{i\phi}>} = \frac{<\mathrm{NUM}>}{<\mathrm{DEN}>} \qquad (5.4)$$

The expectation value of an observable can be written as,

$$<X> = \frac{1}{N}\sum_i x_i = \int_{x_{min}}^{x_{max}} x\,\rho(x)\,dx \qquad (5.5)$$

where $\rho(x)$ is normalised distribution function. Now if,
1)- $\rho(x)$ is a symmetric function of x ($\Rightarrow$ $x_{max} = -x_{min}$) then ,

$$<x> = 0 \quad .....(5.6)$$

2)- $\rho(x)$ is an non-symmetric function of x then,

$$<x> \neq 0 \quad .....(5.7)$$

There are four possible cases for the behaviour of $<\bar{\psi}\psi>$.

1)- <NUM>—/—> 0, but <DEN>——> 0,.

It means that the distribution function corresponding to the numerator is antisymmetric. If <DEN> is exactly zero, the fluctuations in the complex phase will be random. But if <DEN> is small, the phase can be calculated after a lot of computation. According to Gibbs {23} analysis in this region, the mass is inside the strip of the eigenvalues and chiral symmetry might be broken.

2)- <NUM>——>0, <DEN>—/—> 0.

Hopefully the system is in the chirally symmetric phase. The normalized distribution function corresponding to denominator is assymmetric.

3)- <NUM>—/—>0, <DEN>—/—>0.

The normalized distribution function corresponding to

numerator and denominator are antisymmetric. The Monte Carlo procedure will be working very well {23}.Now if it is so that there is a strong correlation between the numerator and denominator so that effect of phase of the determinant is exactly cancelled then we shall retain the quenched or SU(2) full theory results.

4)- < NUM >—>0, < DEN >—>0.

The expression eq.5.4 is in (0/0) indeterminant form. L' Hospital's rule might be applicable,i.e,

$$Lt_{\phi \to 2\pi\kappa} \frac{<NUM>}{<DEN>} = \frac{<NUM>'}{<DEN>'} \qquad (5.8)$$

but there is no clear method for implementing this scheme.

RESULTS

In all cases,measurements were taken during 5 sweeps at each value of μ. Runs were first perfomed at μ=0.3, for m_q=0.1 and β = 1.5(strong coupling). At this value of μ the quark mass lies outside the strip of eigenvalues and a very clear signal is obtained for <NUM> and <DEN>, both $\neq$ 0. The distribution function for cosϕ is asymmetric strongly towards 1 and is shown fig.5.2. A clear measurement of $<\bar{\psi}\psi>$ can be made and it is ~ 200 in lattice units, unchanged from its value at μ=0.

The region of interest is where m_q enters the strip. We present the initial results at finite density using the SU(3) gauge group on 4^4 lattice, with $\mu = 0.5$, $m_q = 0.1$, (both in lattice units) and β =1.5.

We first take the successive average of the numerator and denominator. Measurements were taken after each hypercube was updated, i.e, 32 measurements per sweep on a 4^4 lattice. These measurements were found to be uncorrelated.

Fig.5.3 shows a plot of $<trM^{-1}>$ as a function of successive measurements. It rapidly becomes essentially constant ~ 75 and

corresponds to the quenched measurement.

Fig.5.4 and 5.5 show the history of the imaginary parts of <NUM> and <DEN>. Note the fluctuations in each plot when only a small number of measurements are included. This reflects the fact that there are large fluctuations between each measurement. The plots are consistent with the imaginary parts going to zero but indicate that more measurements are required before a true equilibrated value for the condensate can be obtained (if that is possible).

We have plotted the real parts of <NUM> and <DEN> in figs.5.6 and 5.7. Again it is clear that more measurements are required but these plots are still consistent with tending to zero as more measurements are included. If so, the corresponding distribution functions should be symmetric. Note, the quark mass is in the strip of eigenvalues (Fig.5.17). We are facing the situation of case 4 described above.

In fig.5.8 we show the history of the condensate. We expect $<\bar{\psi}\psi>$ ~200 in the broken phase, whereas the quenched theory gives ~75. Hence there is no clear signal of the inclusion of fermion loops modifying the situation found in the quenched analysis.

However, these results can be altered by changing the sampling criterion or order. It is more meaningful to examine the distribution functions for <NUM> and <DEN>. These are shown in figs.5.9 to 5.18.

Fig.5.9 is a plot of $\rho(\sin\phi)$, normalised to 1 with $\mu = 0.5$,i.e,

$$\int \rho(\sin\phi)\, d(\sin\phi) = 1 \quad \text{with}$$

$$\mathrm{Im}\langle \mathrm{DEN} \rangle = \int x\, \rho(x)\, dx \qquad (5.9)$$

It is clearly trying, within statistical errors, to be symmetric, as is Im<NUM> plotted in fig.5.10. These plots are encouraging in that we require these expectation values to vanish. This is contrary to the analysis of ref.[26] which found no convincing evidence for their vanishing.

However, study of the real parts of <NUM> and <DEN> as shown

in figs. 5.11 and 5.12, also shows very symmetric distribution functions. This, together with the earlier analysis described above, is consistent with <NUM> and <DEN> each becoming very small or zero.

We have repeated the above analysis at μ=0.9 as shown in fig.5.18 with similar results. In this case the quark mass is just leaving the strip of eigenvalues and entering the cavity. One would expect that the condensate vanishes, but again one is left in an indeterminate conclusion. We encounter the same problem at μ=0.4 as shown in fig.5.17.

Increasing μ further to 1.0 leads to the results shown in fig.5.13 to 5.16. Here we see that the Monte Carlo procedure has worked. The distribution functions for Im<NUM> and Im<DEN> shown in figs.5.13 and 5.14 are symmetric whereas the for Re<DEN>, fig.5.15 is clearly antisymmetric, $\langle\cos\phi\rangle \neq 0$. The distribution for Re<NUM> is symmetric and hence the condensate is zero.

The picture we obtain is as sketched in fig.5.19.

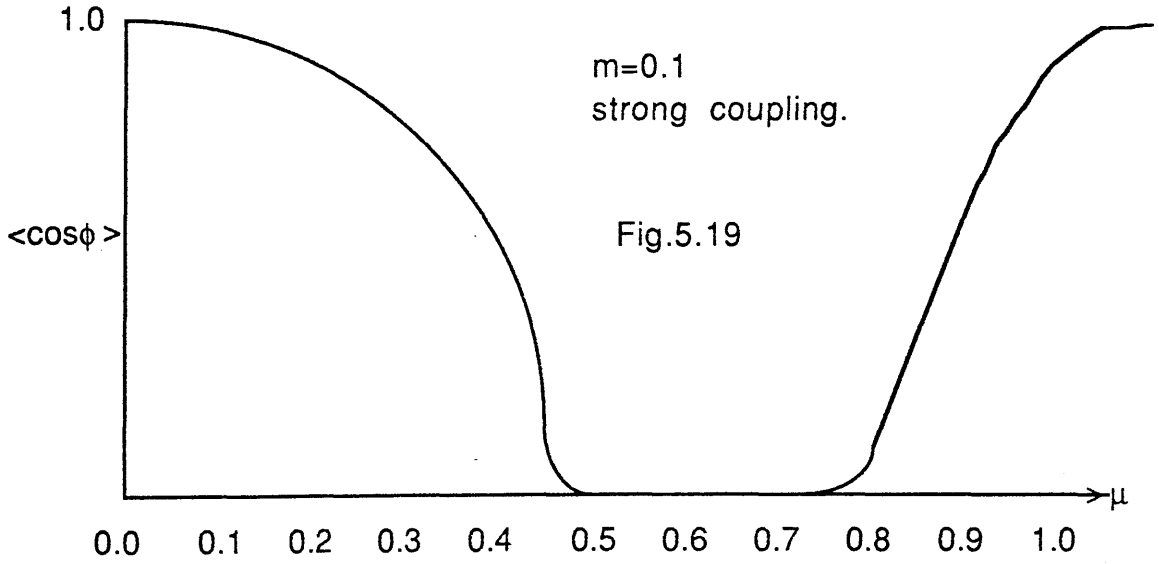

Fig.5.19

There is a clear evidence that a phase transition in the chiral condensate does exist with $0.3 \leq \mu_c \leq 1.0$. This statement is stronger than that obtained in the quenched approximation in that there is the clear possibility that the spurious transition in the quenched calculation can be removed via the inclusion of fermion loops.

During these simulations we also measured the eigenvalues of the fermion matrix at the end of each multilap sweep. From these

measurements we can make the following conjecture. In measurements of the phase transition at finite temperature and $\mu=0$ we have the theorem of Gauss. As described in chapter4 , the phase transition corresponds to the eigenvalues near the Reλ axis moving away. We conjecture that a similar mechanism will signal the onset of the phase transition at non-zero density. For m_q outside the strip, the eigenvalues are evenly distributed close to $Re(\lambda) = 0$. Note, in Fig.5.20 which summarizes the eigenvalues for 5 configurations superimposed (which is really only valid in the quenched analysis) there is a slight decrease in density around the origin of elliptical shape within approximately $-0.2 < Re\ \lambda < 0.2$, $0 < Im\lambda < 2.2$. As μ increases to 0.8 we reach the situation shown in fig. 5.21 where there has been a clear shift around the mass. We conjecture that this signals that the phase transition is at $\mu_c \cong 0.5$.

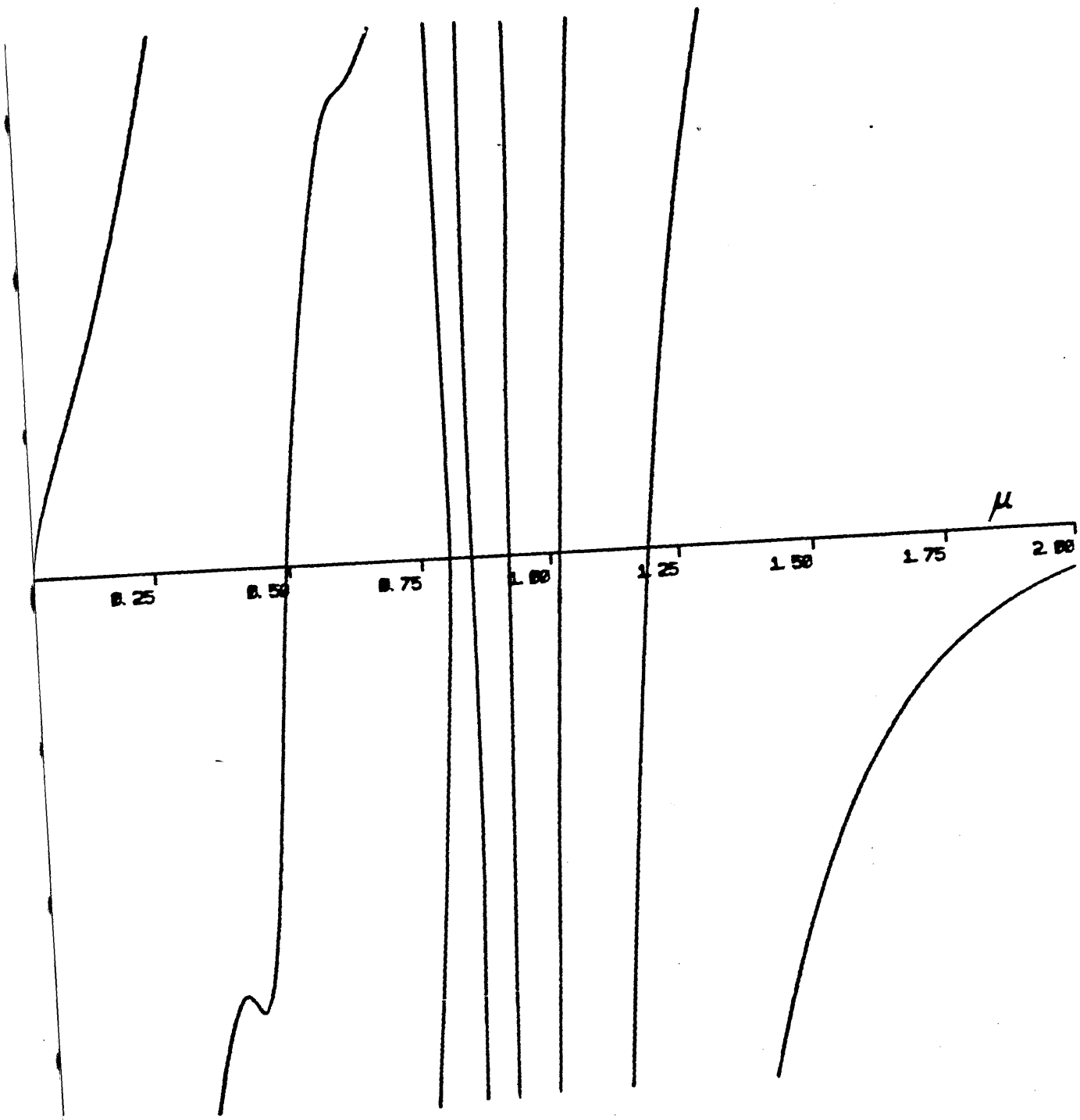

Fig. 5.1

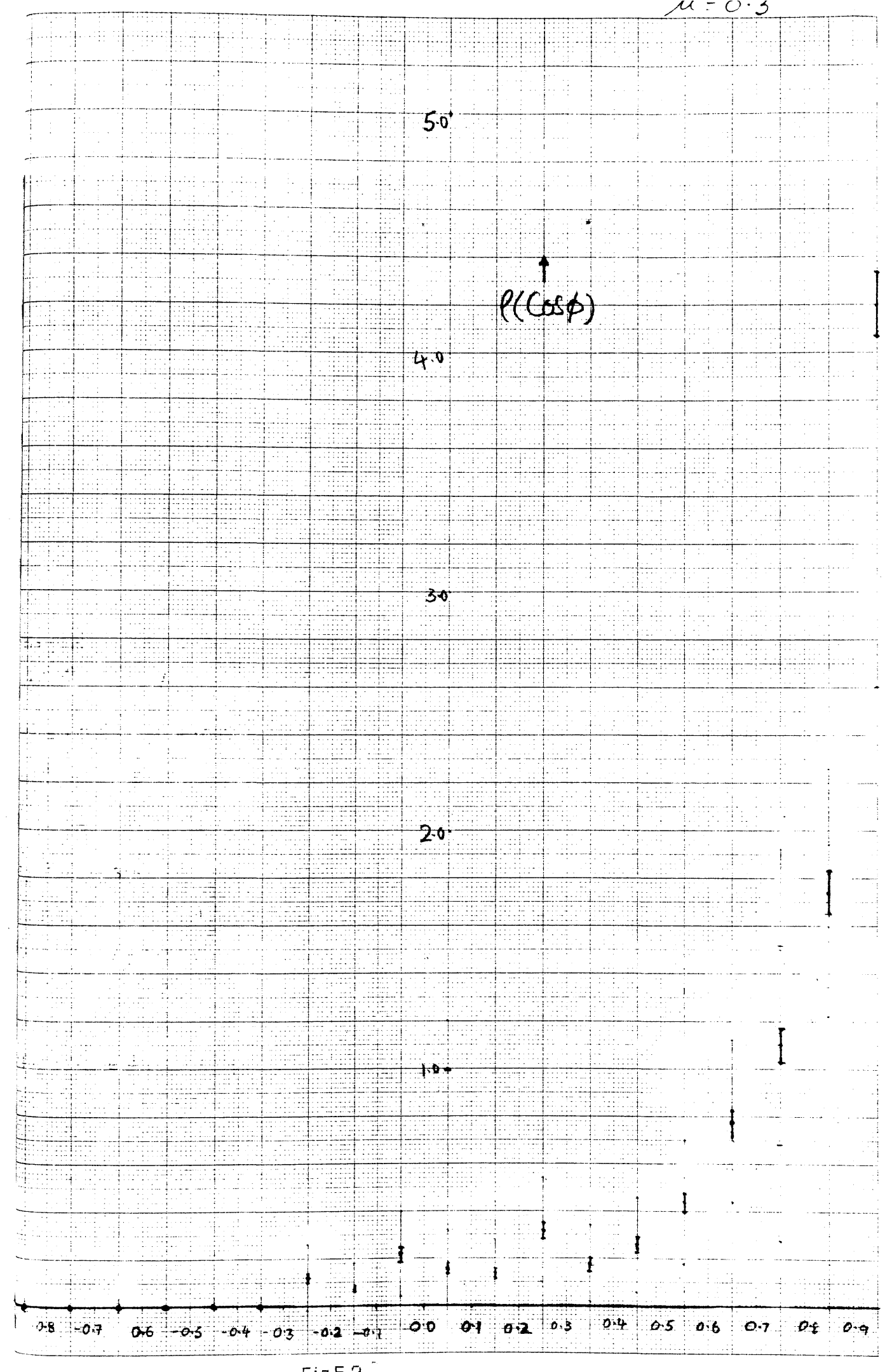
μ = 0·3
5·0
ℓ((cosϕ)
4·0
3·0
2·0
1·0
-0·8
-0·7
-0·6
-0·5
-0·4
-0·3
-0·2
-0·1
0·0
0·1
0·2
0·3
0·4
0·5
0·6
0·7
0·8
0·9

Fig 5.2

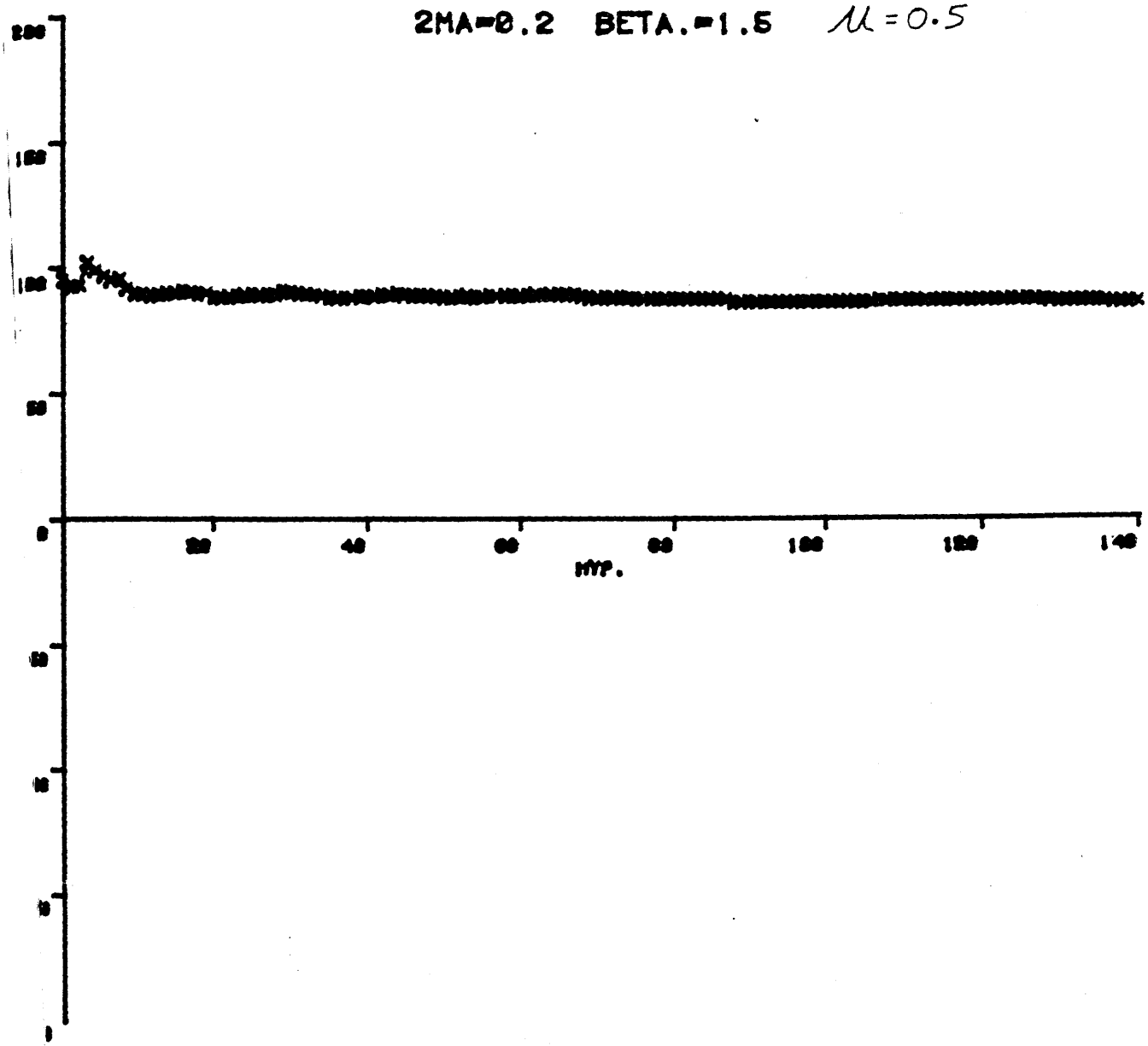

Fig.5.3

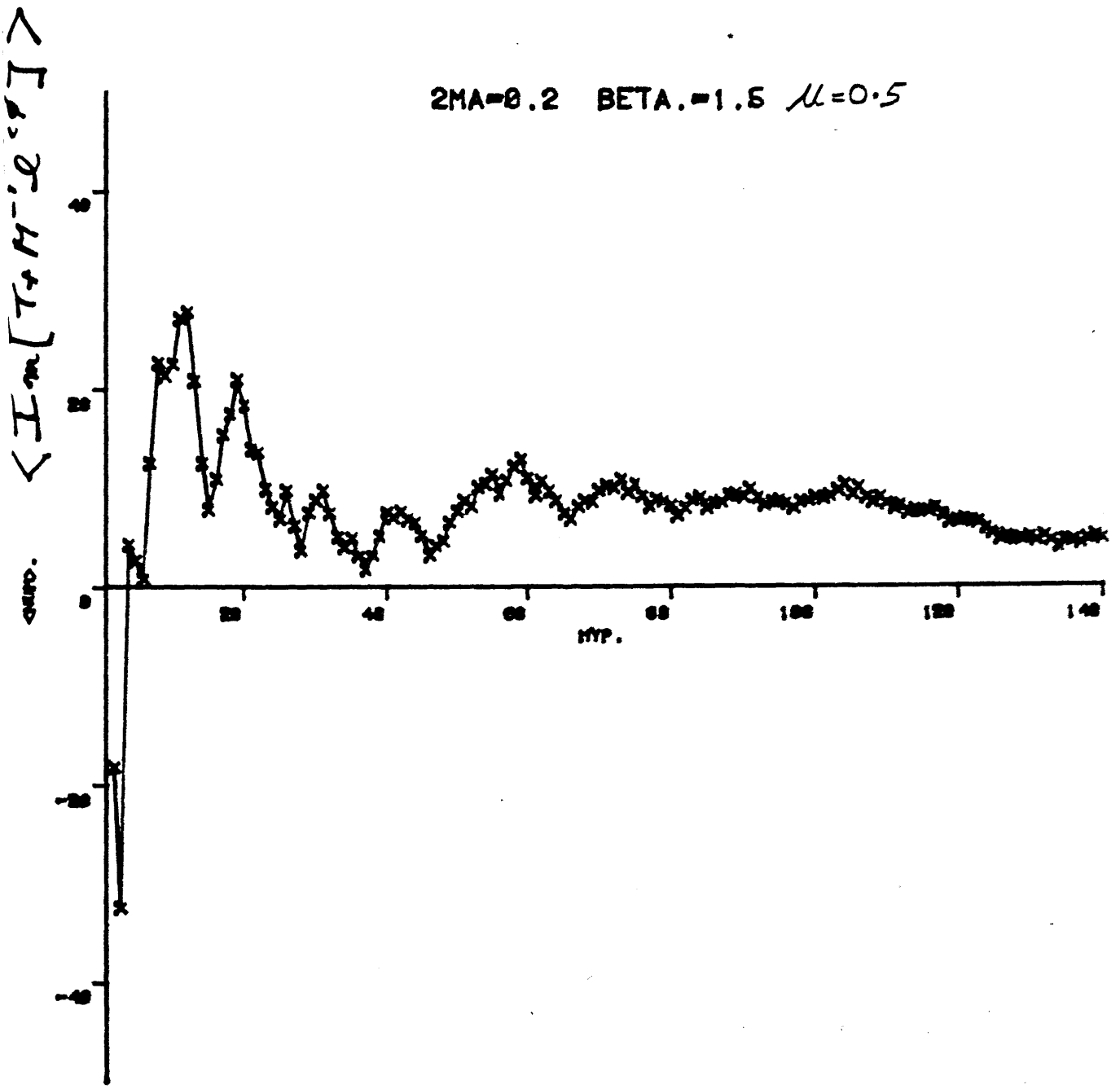

Fig.5.4

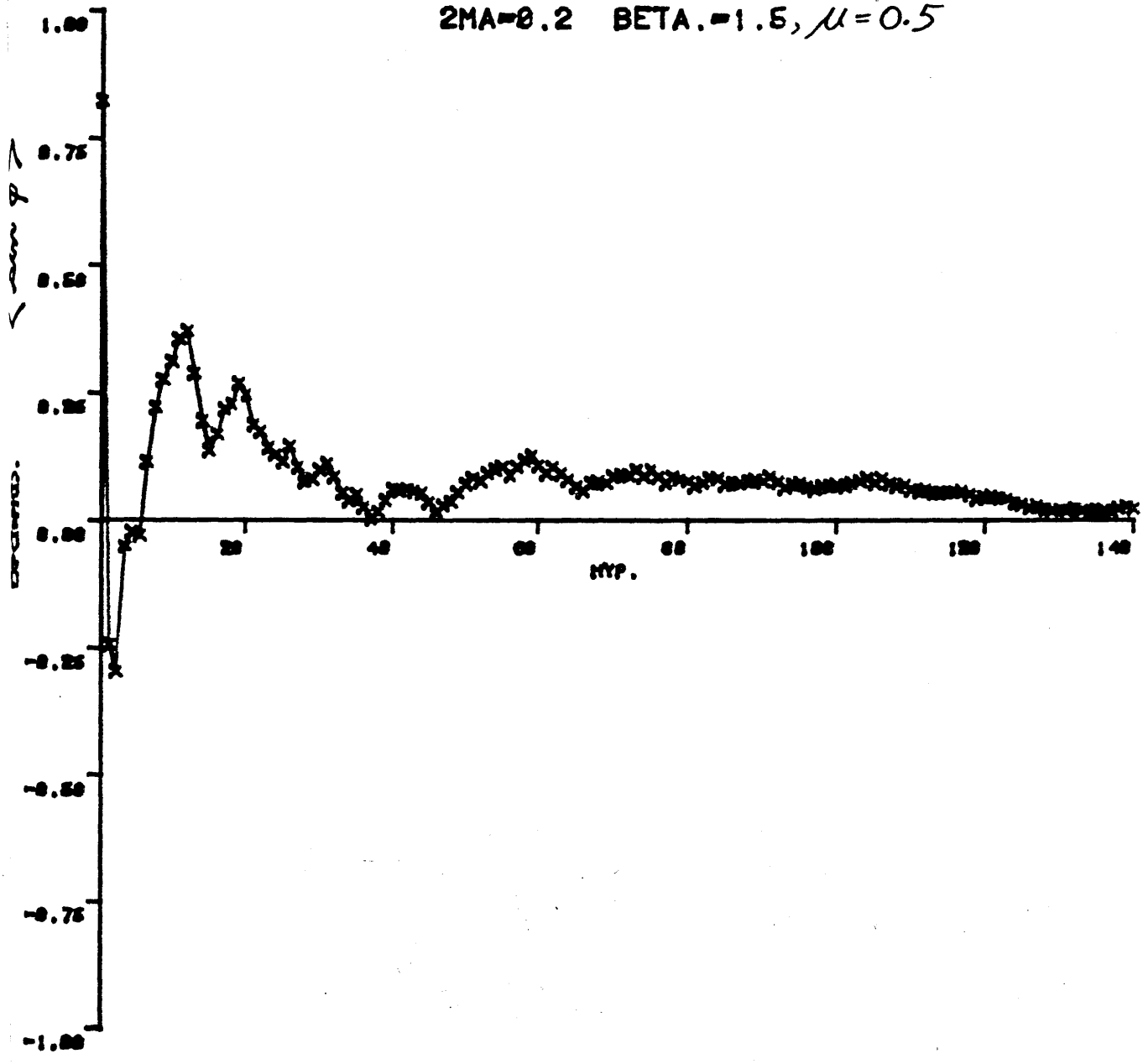

Fig.5.5

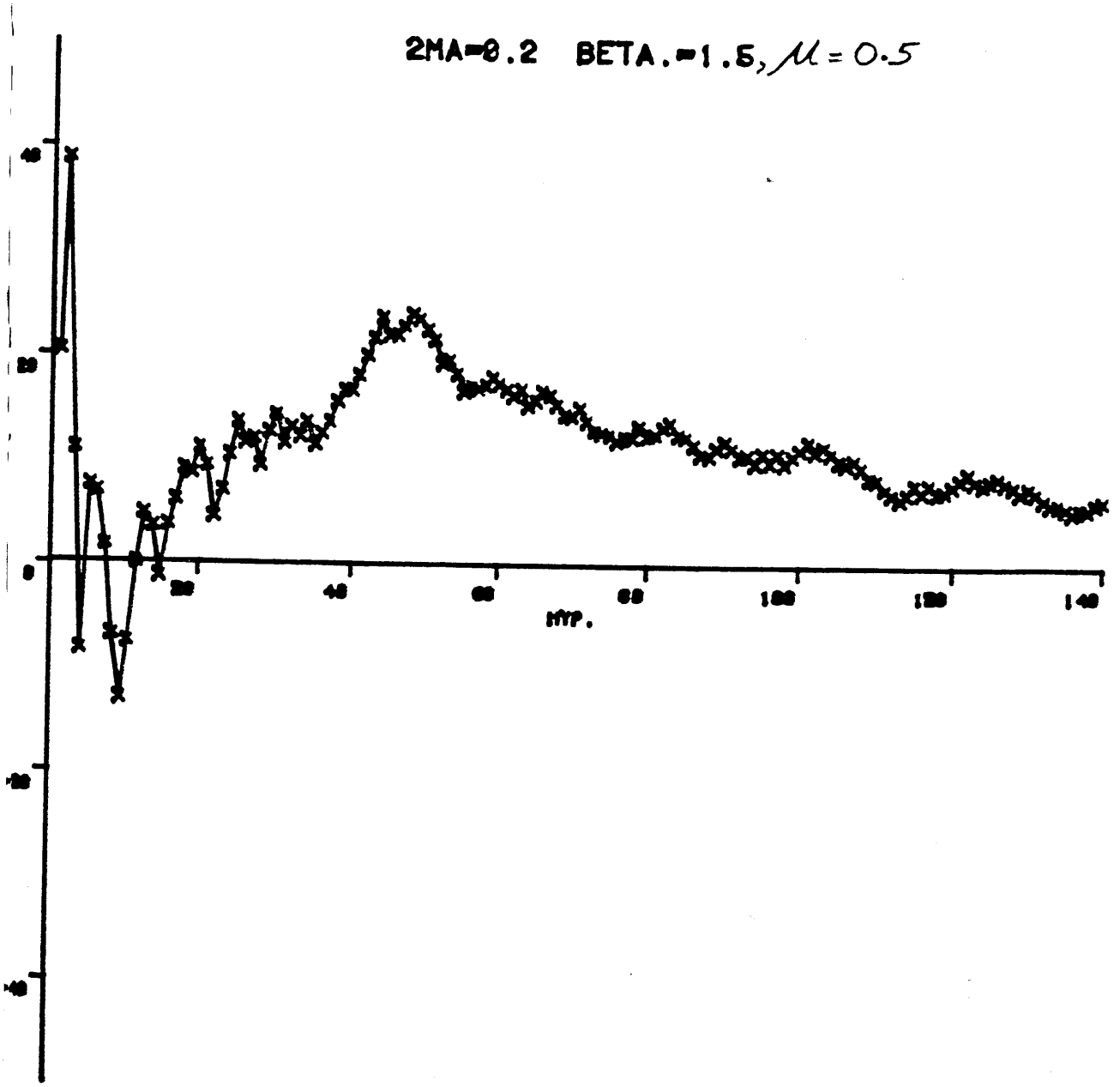

Fig.5.6

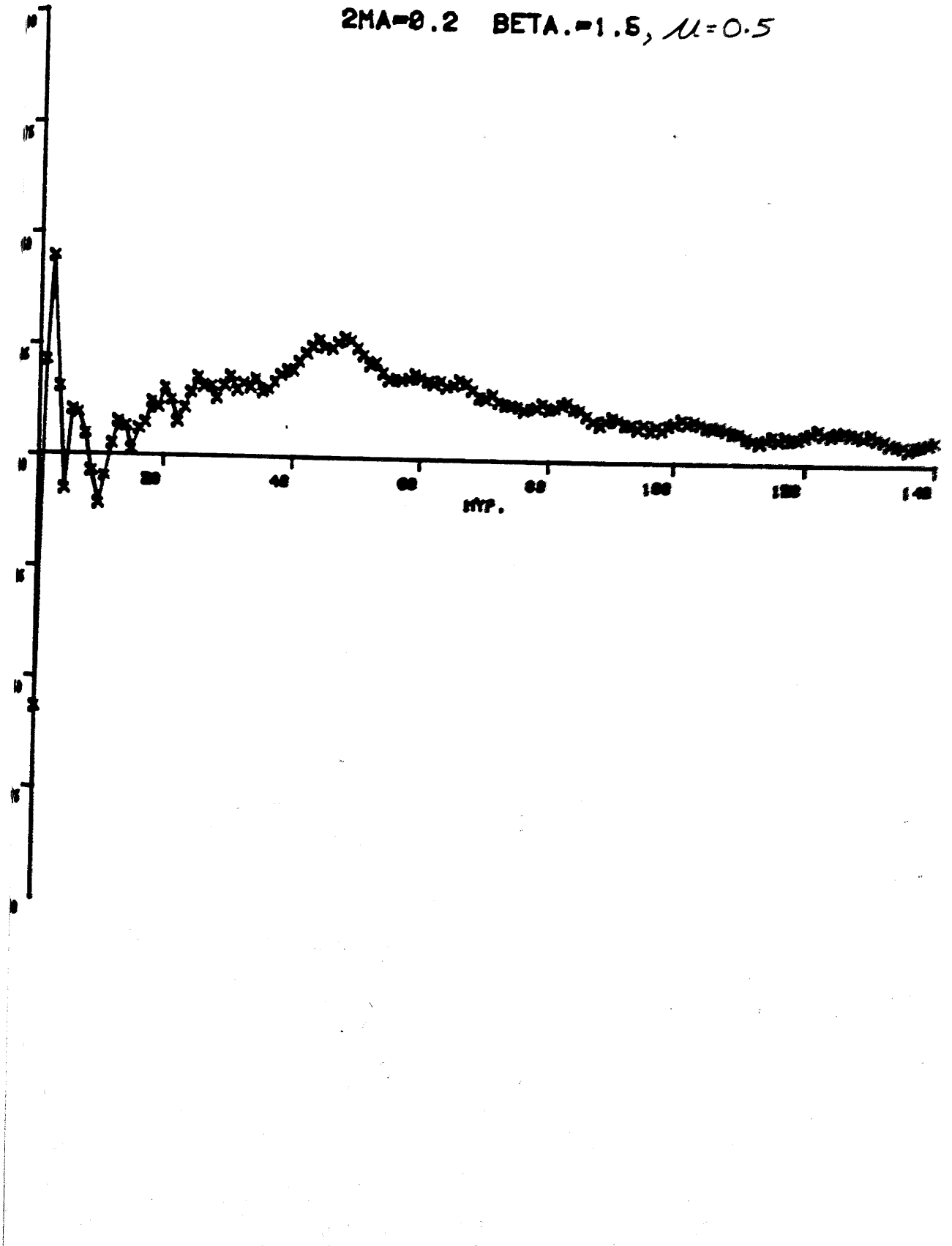

Fig 5.7

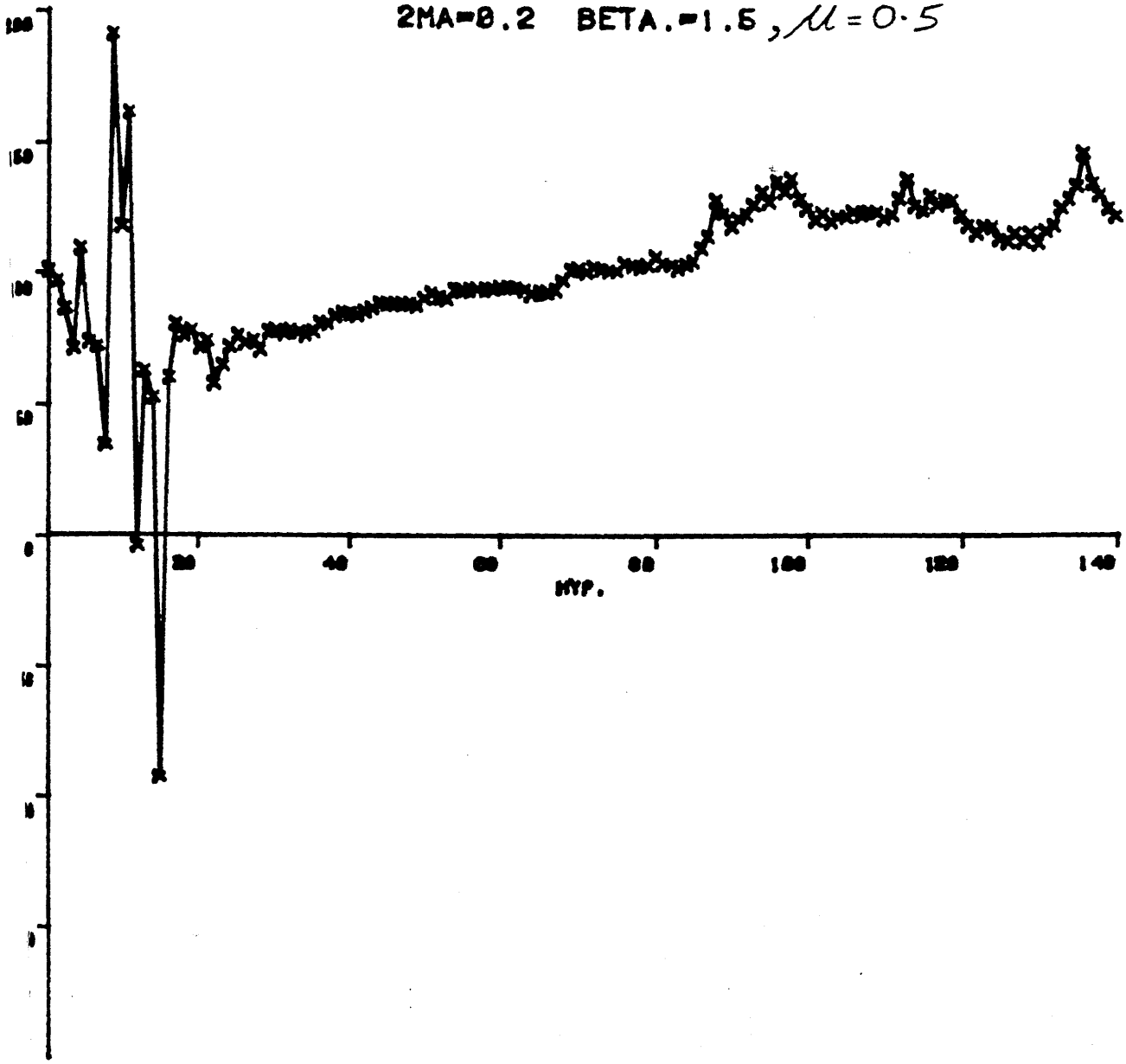

Fig.5.8

EMICAL POT. = 0.5
A = 0.2
ETA = 1.5

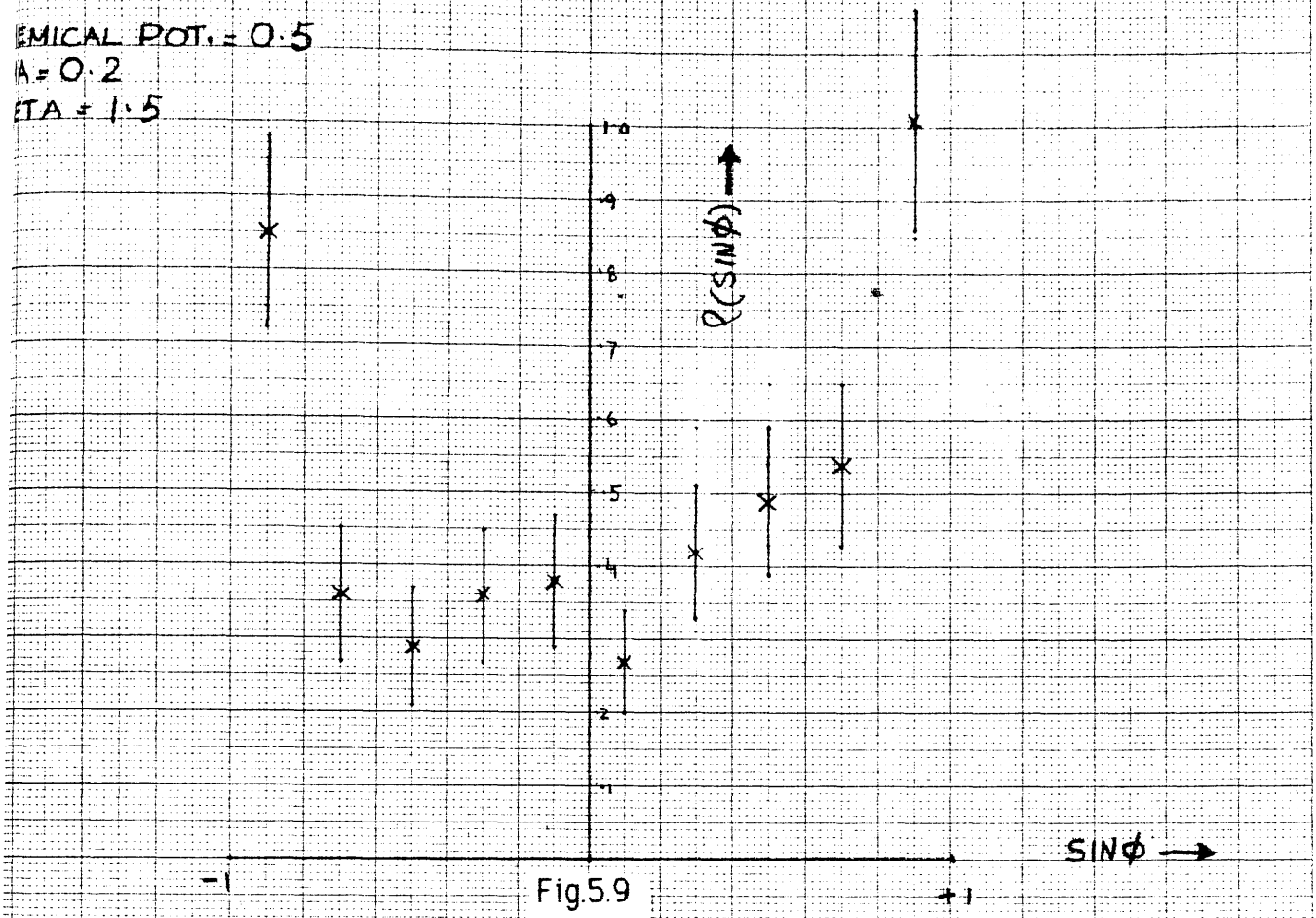

Fig.5.9

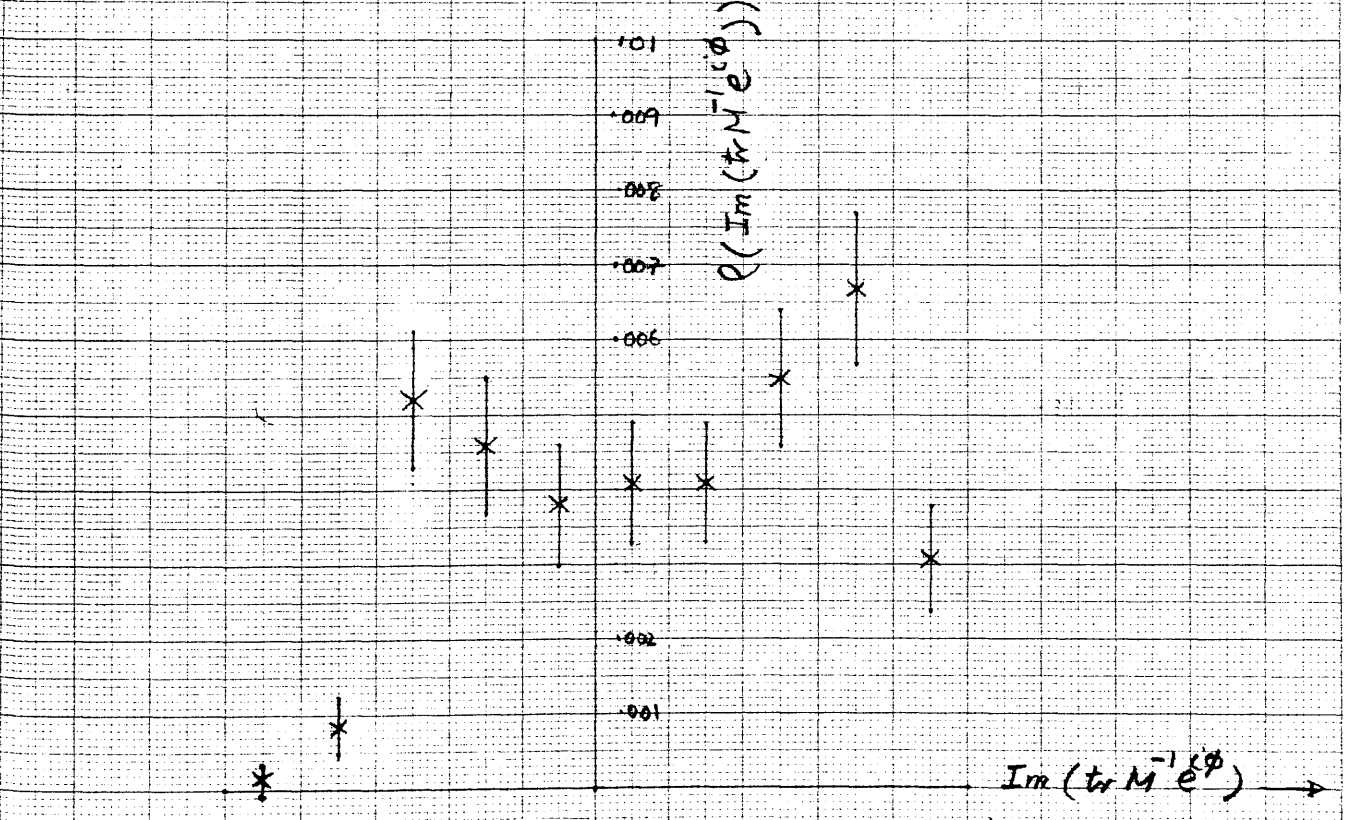

Fig.5.10

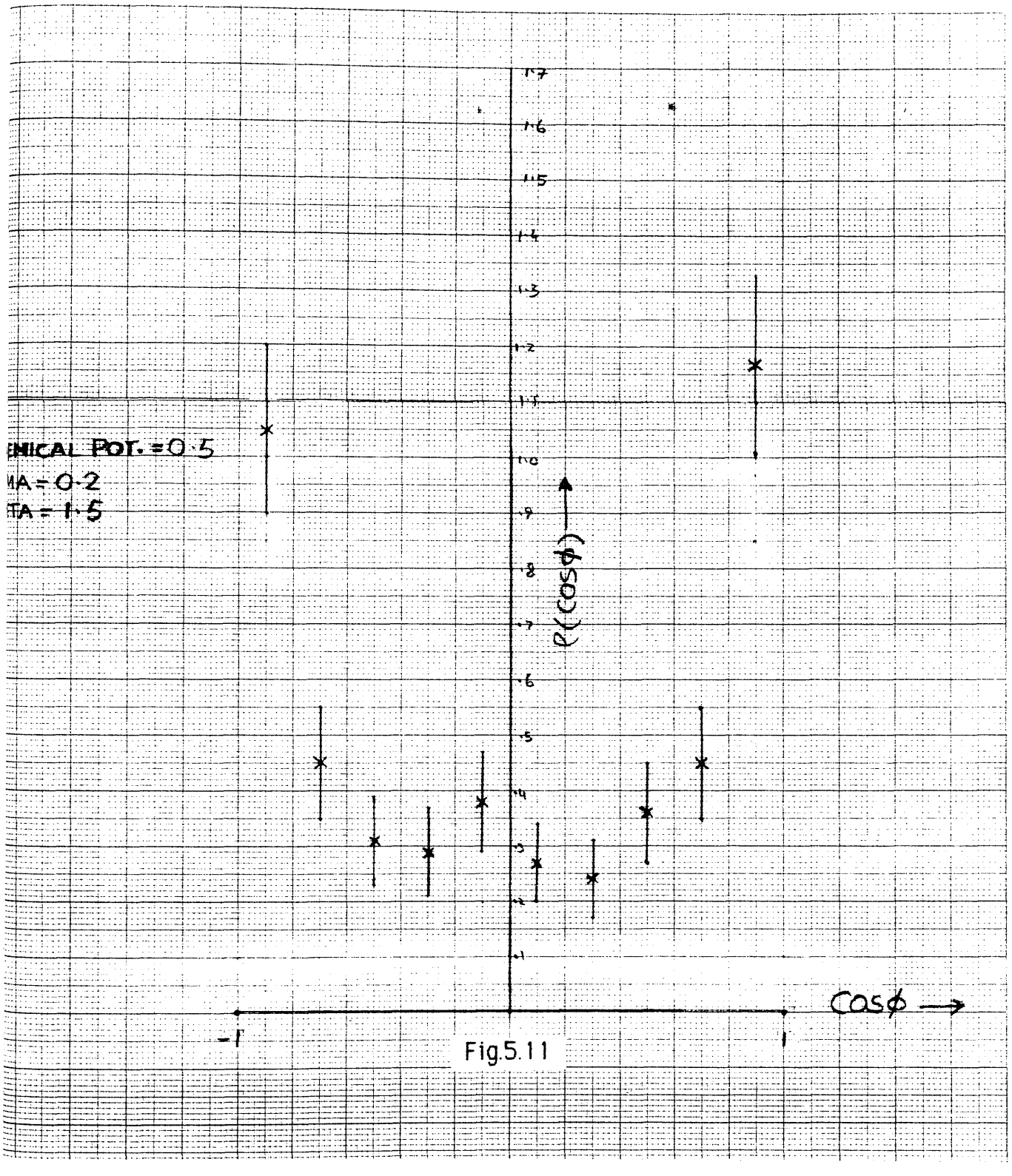
EMICAL POT. = 0·5
IA = 0·2
TA = 1·5
1·7
1·6
1·5
1·4
1·3
1·2
1·1
1·0
·9
·8
·7
·6
·5
·4
·3
·2
·1
P(cosϕ)
Cosϕ
-1
1

Fig.5.11

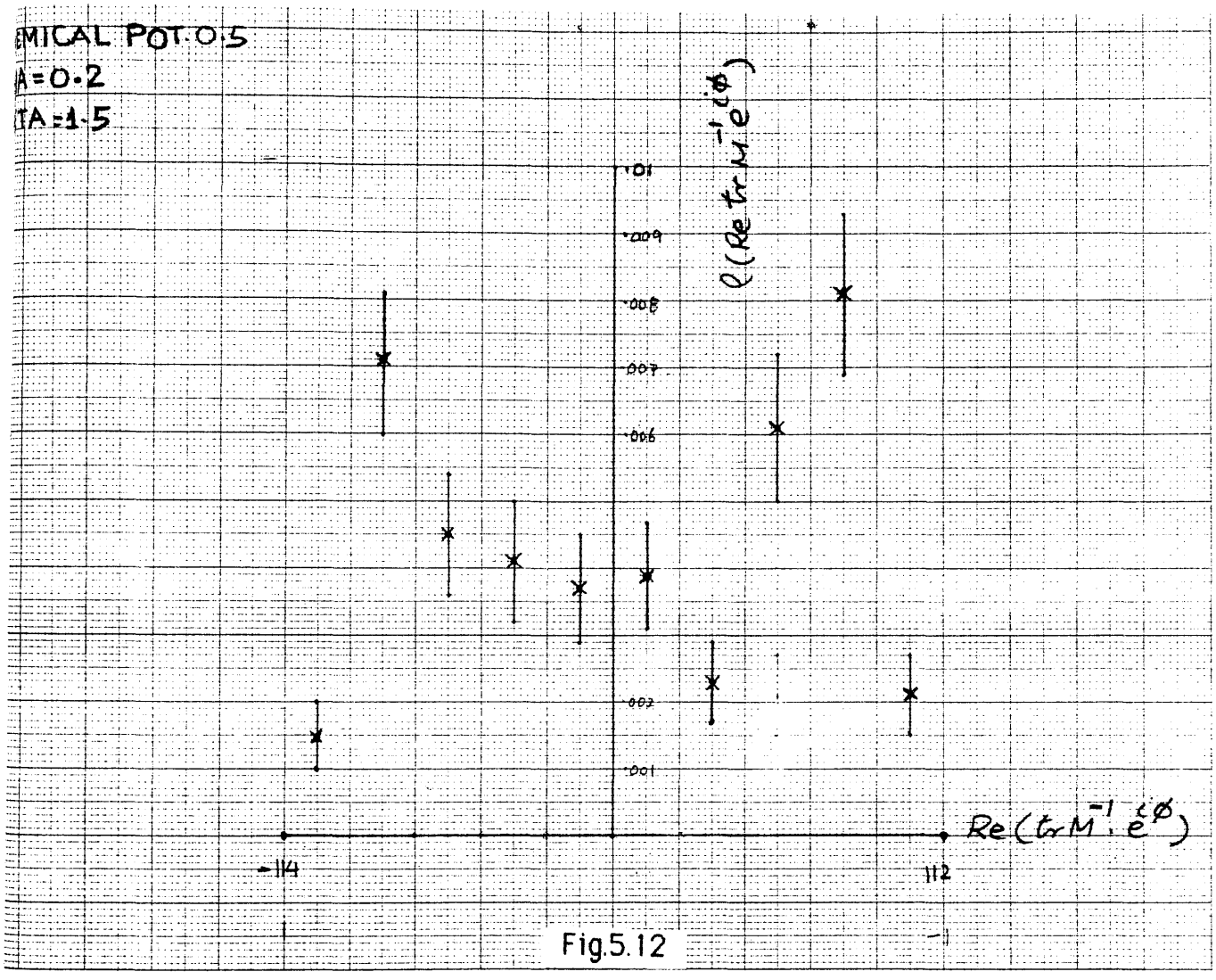
EMICAL POT 0.5
A=0.2
TA=1.5
·01
·009
·008
·007
·006
·002
·001
ρ((Re tr M⁻¹ e^{iφ}))
Re(tr M⁻¹ e^{iφ})
-1.14
1.12

Fig.5.12

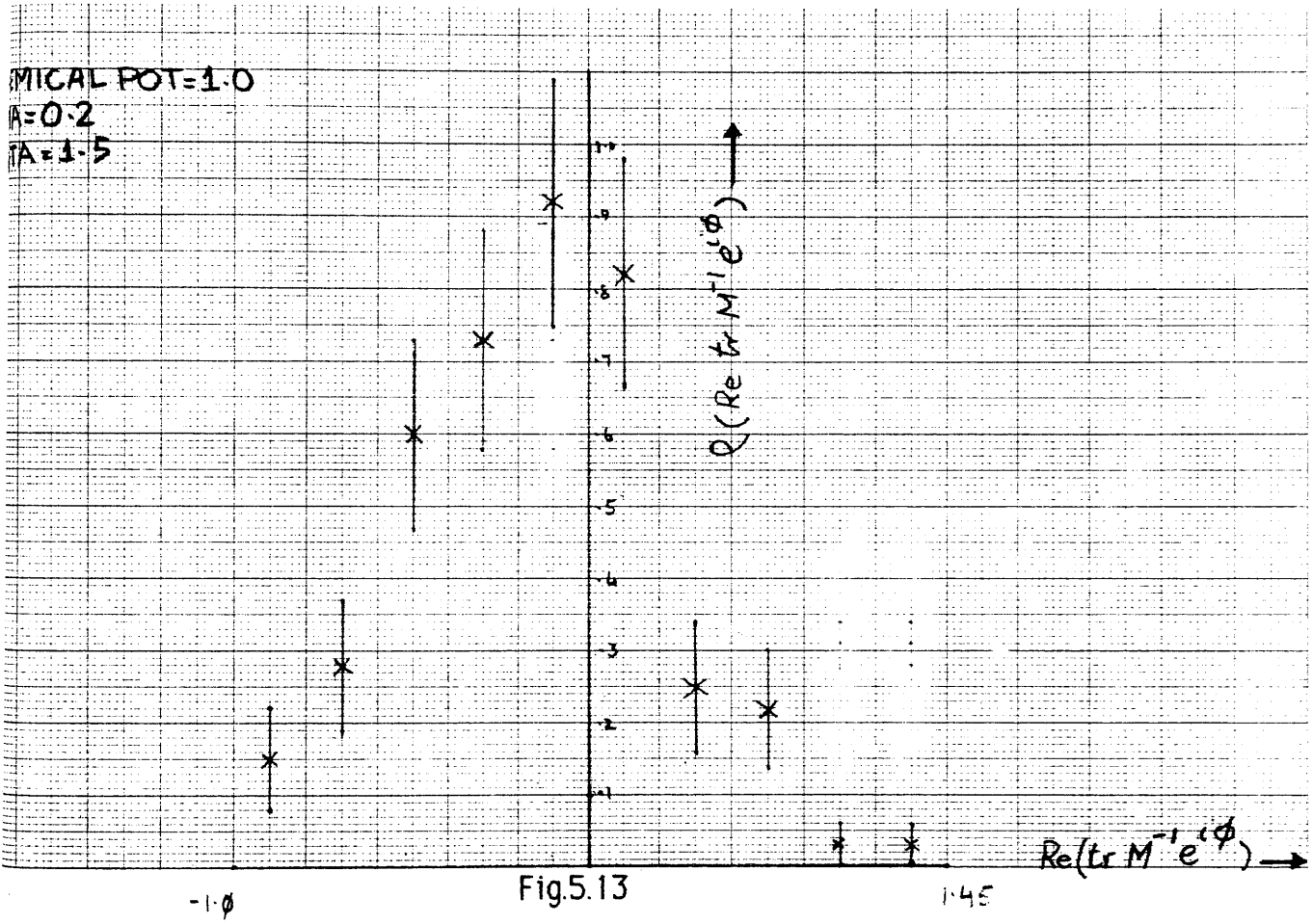

Fig.5.13

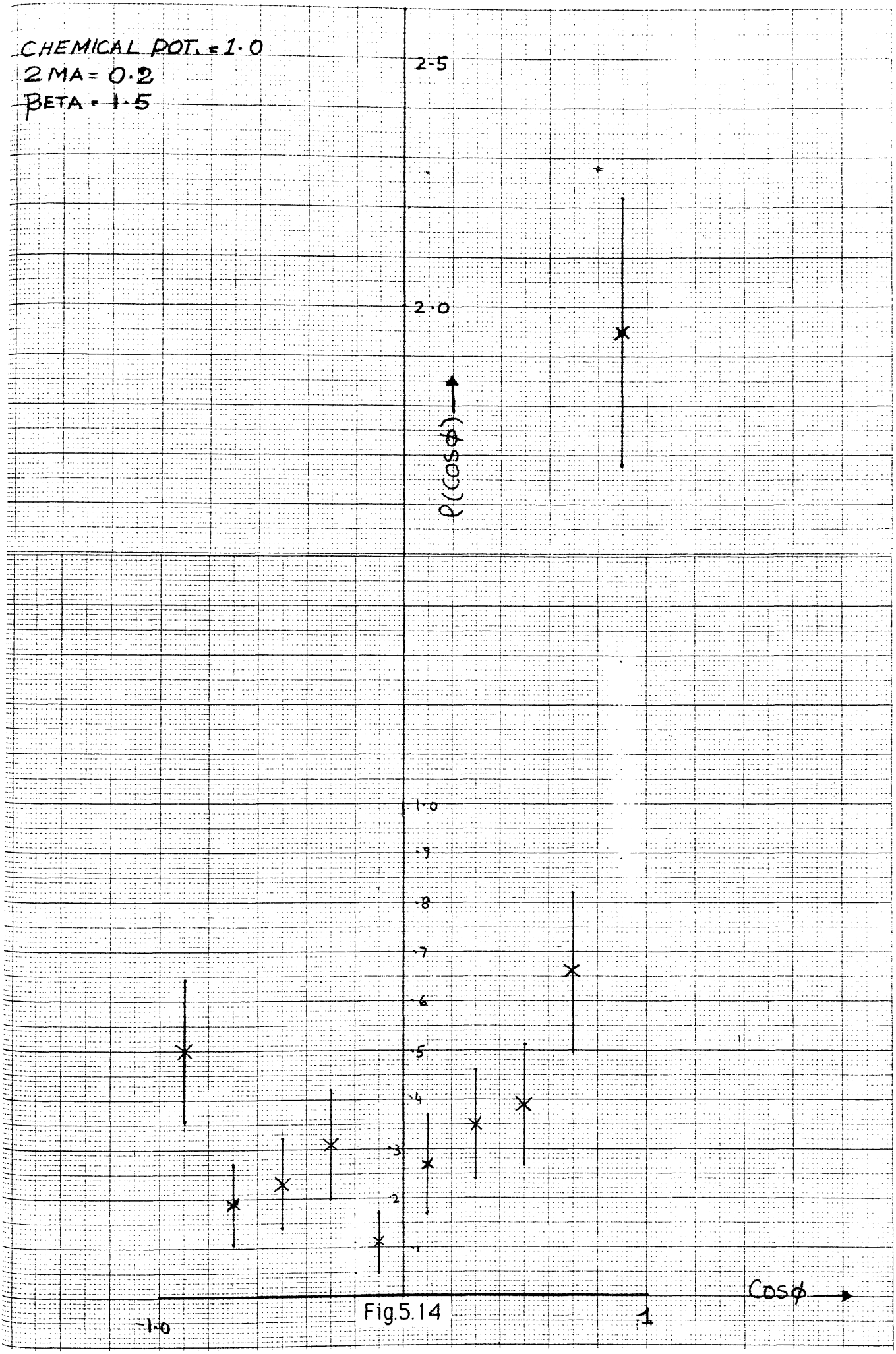
CHEMICAL POT. = 1·0
2 MA = 0·2
BETA = 1·5
2·5
2·0
ρ(Cosϕ)
1·0
·9
·8
·7
·6
·5
·4
·3
·2
·1
-1·0
1
Cosϕ

Fig.5.14

EMICAL POT. = 1.0
A = 0.2
TA = 1.5

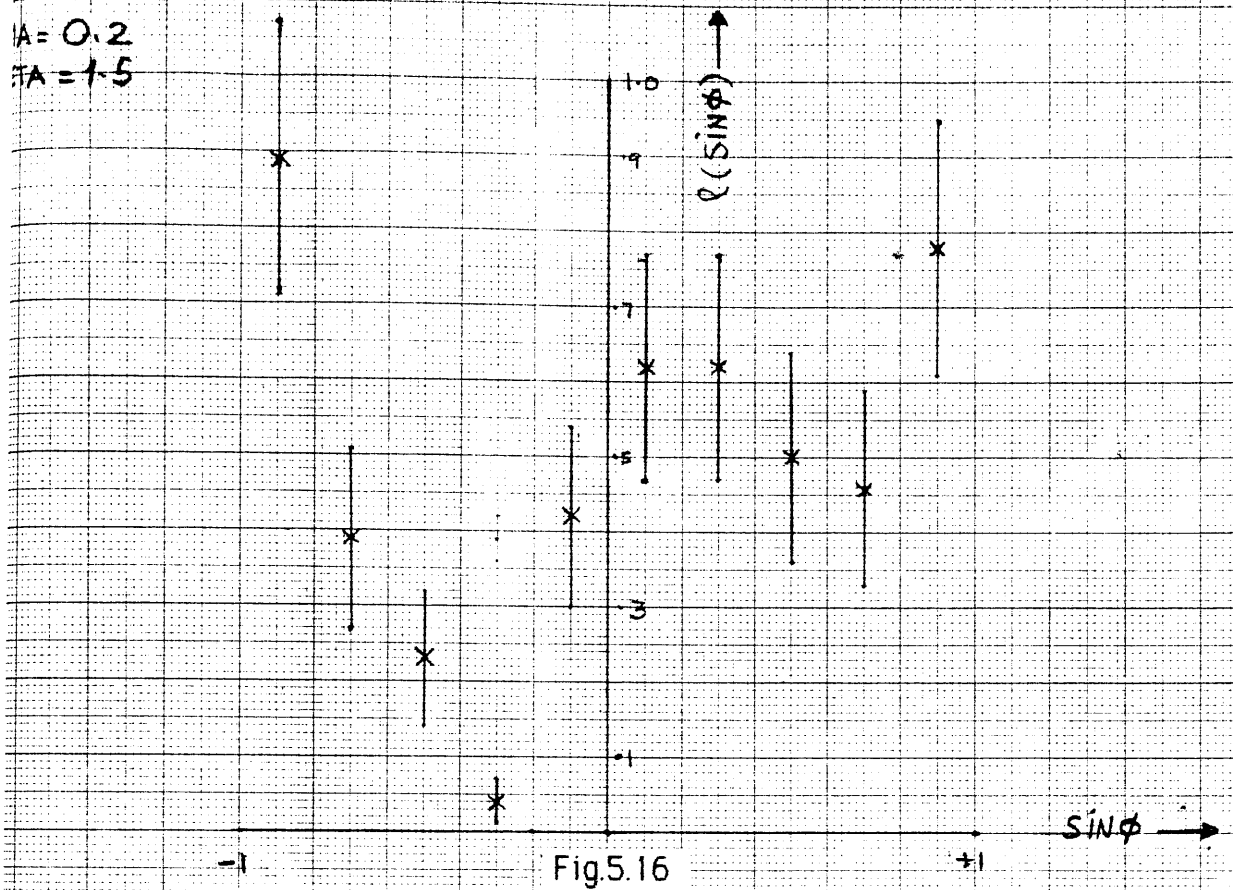

Fig.5.16

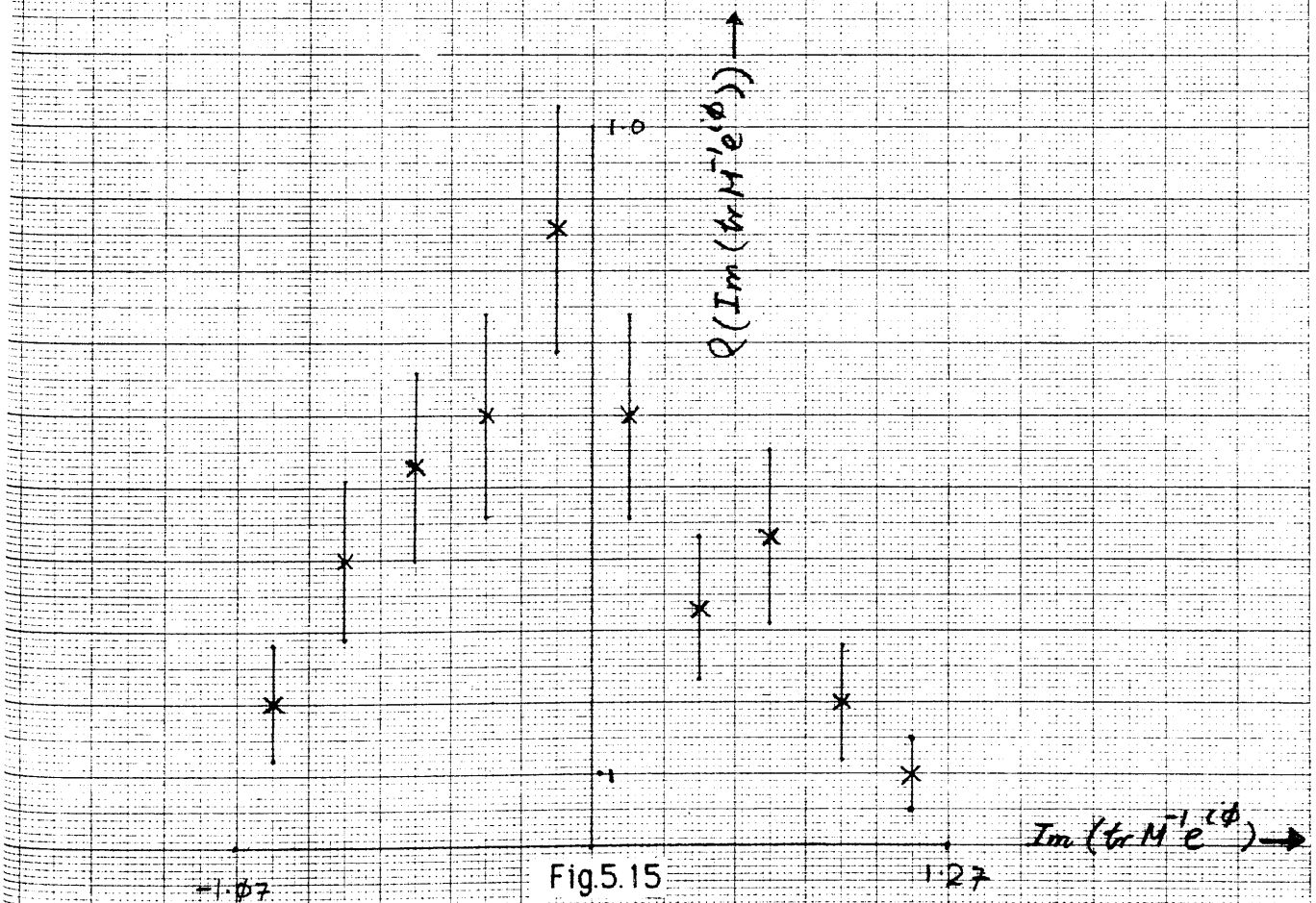

Fig.5.15

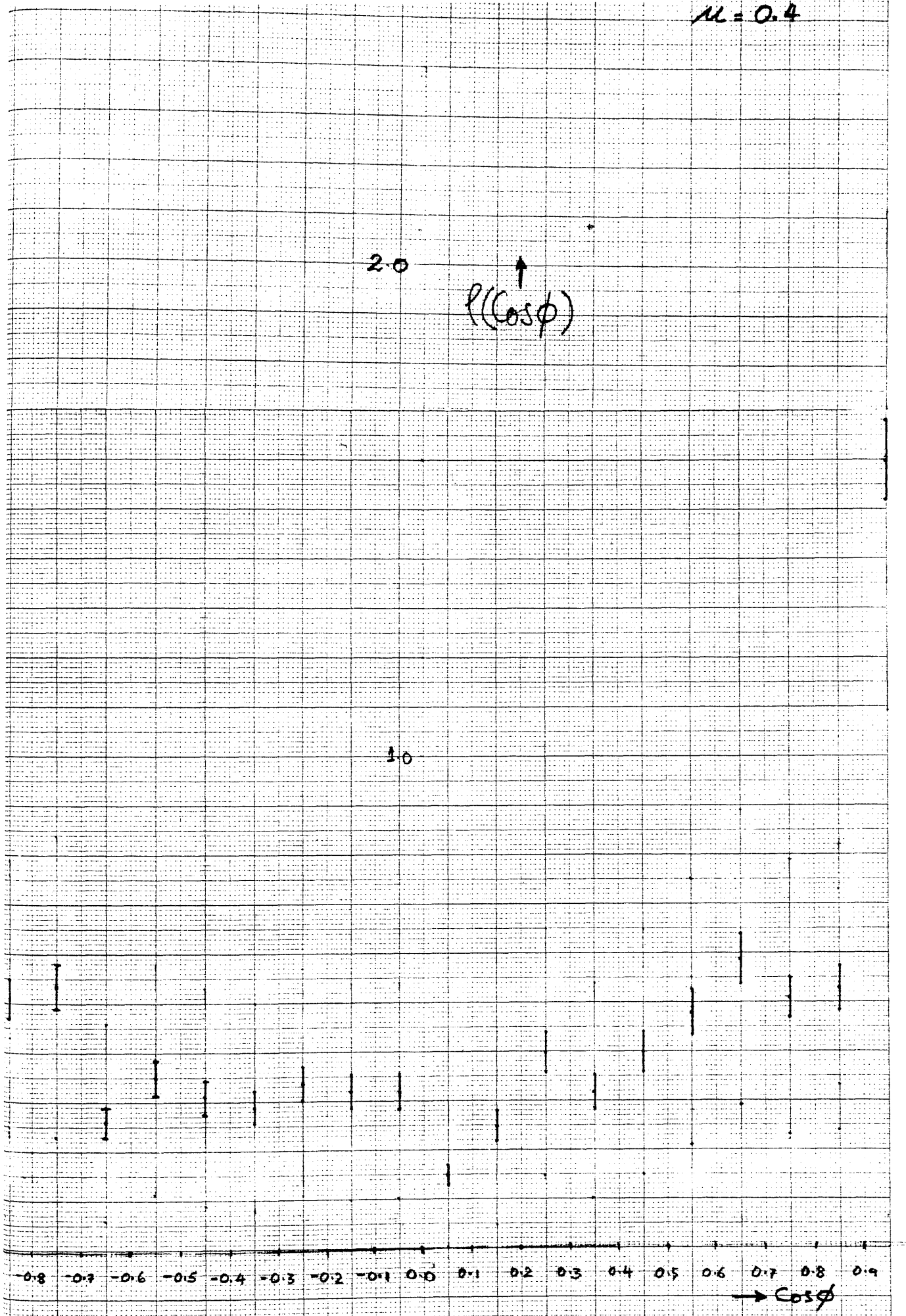
μ = 0.4
2·0
P((Cosφ)
1·0
-0·8 -0·7 -0·6 -0·5 -0·4 -0·3 -0·2 -0·1 0·0 0·1 0·2 0·3 0·4 0·5 0·6 0·7 0·8 0·9
Cosφ

Fig.5.17

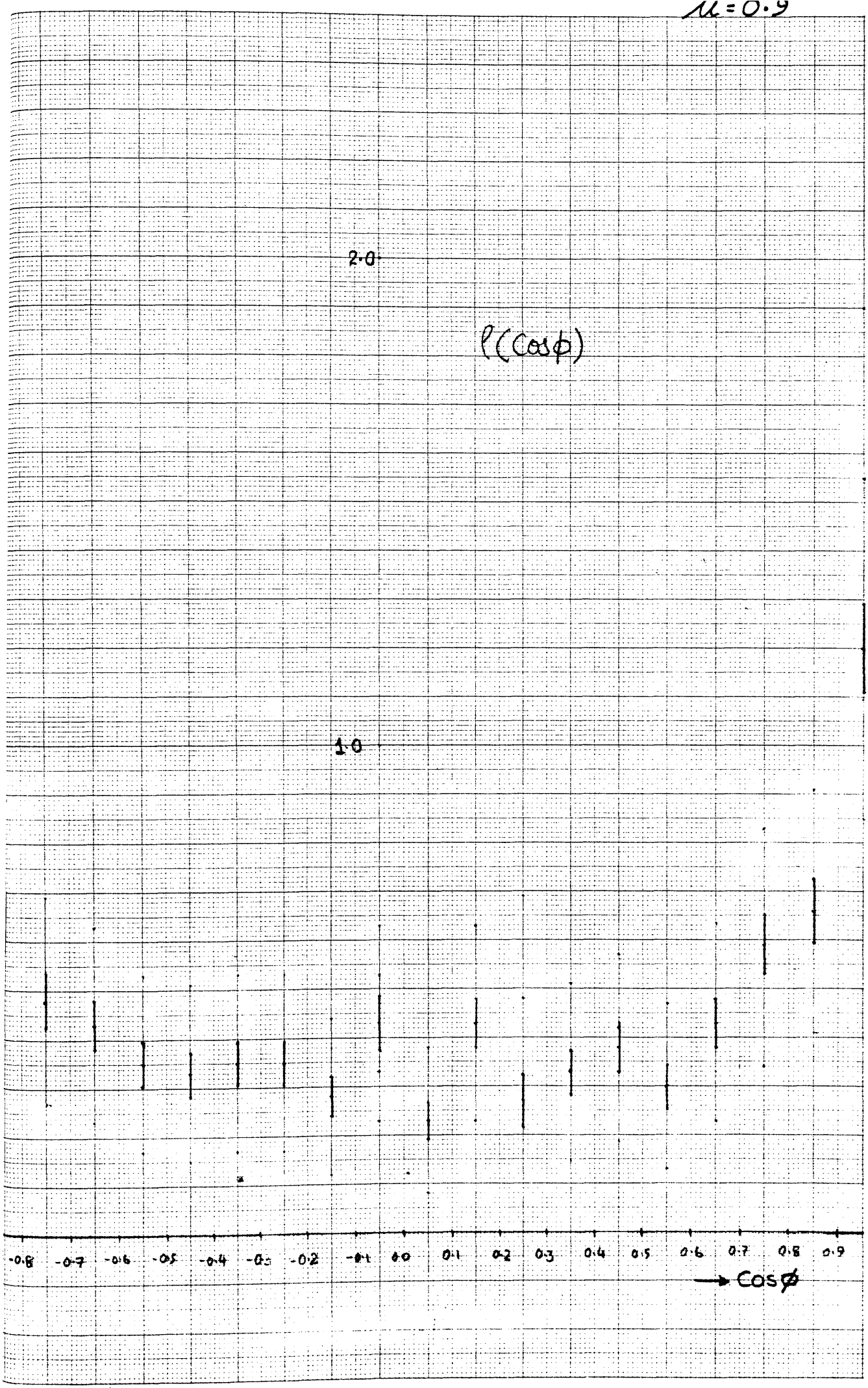
μ=0.9
2·0
P((Cosφ)
1·0
-0·8
-0·7
-0·6
-0·5
-0·4
-0·3
-0·2
-0·1
0·0
0·1
0·2
0·3
0·4
0·5
0·6
0·7
0·8
0·9
Cosφ

Fig.5.18

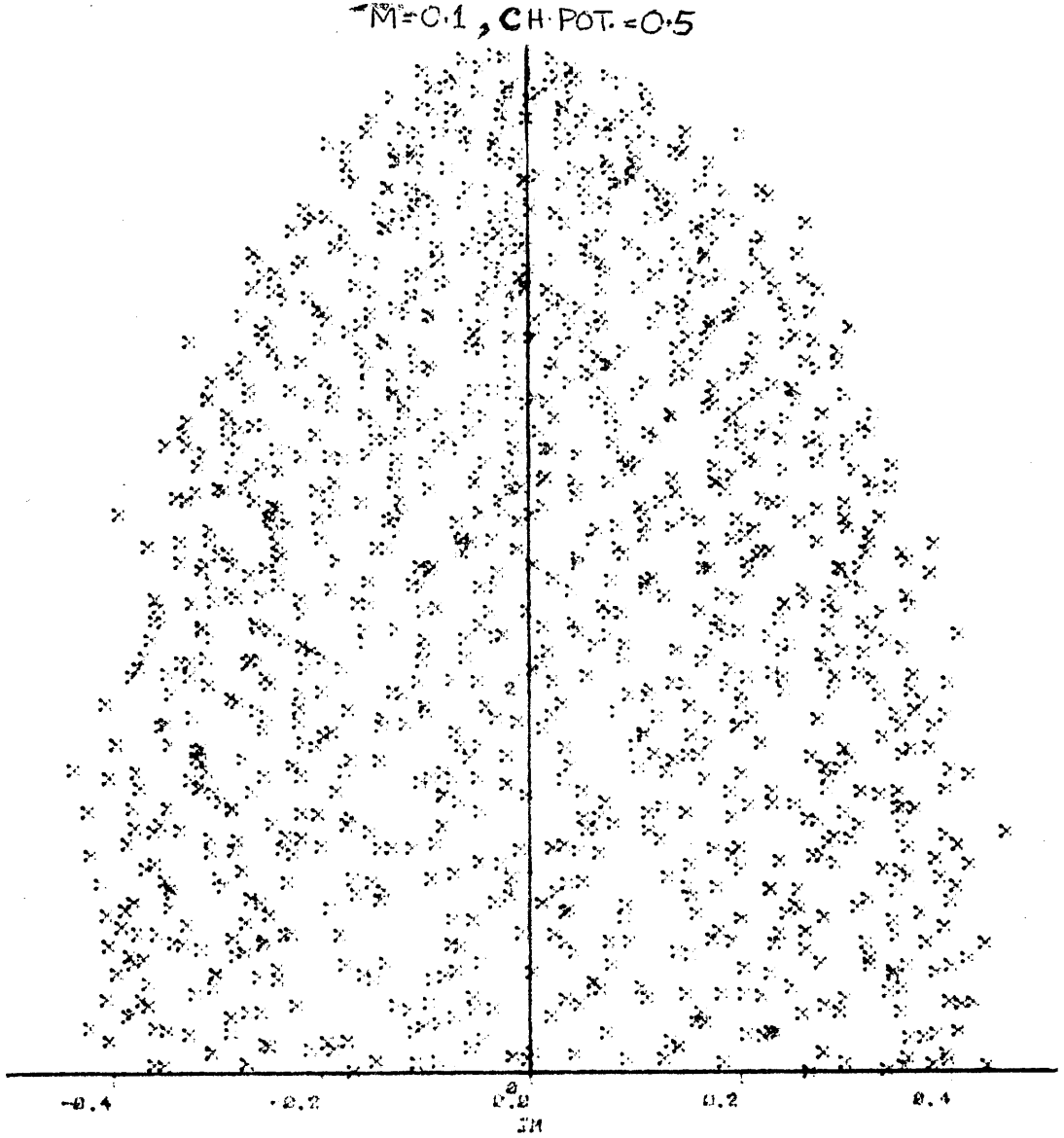

Fig.5.20

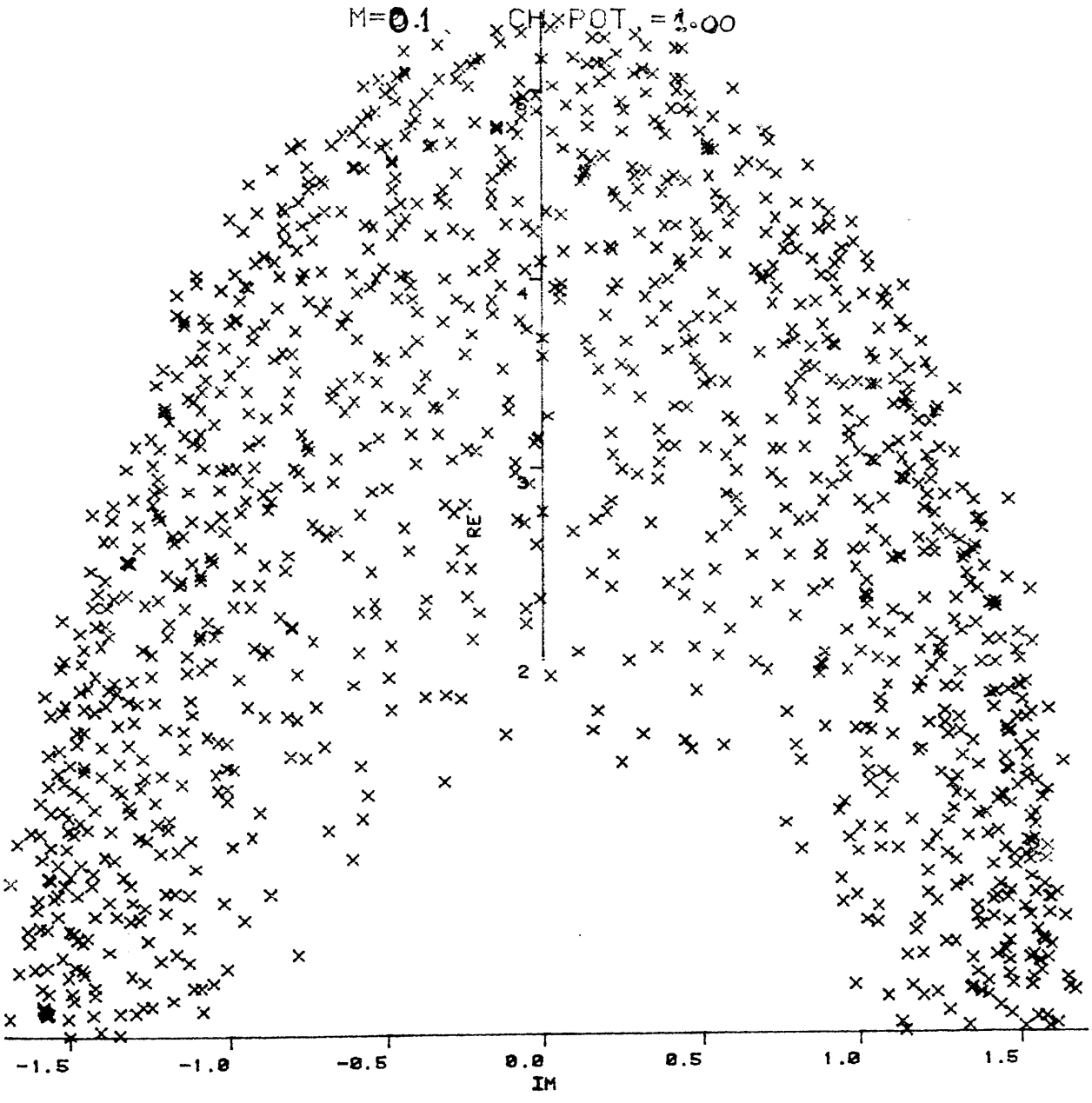

Fig.5.21

CONCLUSIONS:

Like the hermitian Lanczos method, the non-hermitian method has been found to be exact and is successful for calculating the eigenvalues of the fermion matrix and for inverting it. Since, with the introduction of the chemical potential, the fermion matrix becomes non-hermitian, the non-hermitian Lanczos method becomes essential.It has shown excellent convergence and accuracy for calculations with small quark masses. We simulated the finite density by including a chemical potential μ on a 4^4 lattice by multiplying the gauge links in the positive imaginary time direction by e^{μ} and links in the opposite direction by $e^{-\mu}$. The results from the finite density calculations for lattice QCD using the SU(2) gauge group, with the effect of internal fermion loops taken into account by calculating the fermion determinant, are very similar to those previously done with quenched QCD(which ignores the internal fermion loops) for the SU(2) and SU(3) gauge groups. As the fundamental representation of SU(2) is pseudoreal and the fermion determinant is real, this behaviour was expected. We confirmed our results from two representations of the chiral condensate for SU(2). For this group, indeed, the chiral symmetry is restored at half the pion mass and as the quark mass goes to zero, the critical chemical potential which restores the chiral symmetry also goes to zero. It means that, the critical chemical potential for restoring the chiral symmetry at zero mass quark is, again, found to be half the pion mass.However this is not a disaster for SU(2) which does not differentiate between the pion and baryons.

The inclusion of the internal fermion loops in the finite density calculations, using the SU(3) gauge group, causes the fermion determinant to be complex and we have a problem in simulating it via the Monte Carlo method. Since the complex conjugate configurations have a similar contribution, we can take only the real parts of the numerator and denominator in the expression of $<\bar{\psi}\psi>$. The effect of the complex phase of the determinant has been taken into account. The plots showing the behaviour of $<\bar{\psi}\psi>$ as a naive ratio of sums are not reliable as the results can be changed by altering the sampling criterion or order. We have interpreted our results using the normalized distributed function and have presented initial results. We used quark mass, m_q=0.1, coupling constant, β=1.5 for our analysis. Short runs at μ=0.3, show that the chiral condensate, $<\bar{\psi}\psi>$, is non-zero, i.e., chiral symmetry is broken. We analysed the chiral condensate, via the normalised distribution function, at μ=0.5 and

inferred with the help of results at μ=0.4 and 0.9, that the form of the chiral condensate in this range is not well determined. At μ=1.0, $<\psi\psi>$, is found to be zero and hence chiral symmetry is restored, which implies that the phase transition lies between μ=0.3 and 1.0. Also we have obtained eigenvalue distributions at μ=0.5 and 1.0. At μ=0.5, there is a slight decrease in density around the origin with an elliptical shape. At μ=1.0, there is a clear shift around the mass. Though, this analysis is valid only for zero chemical potential at finite temperature we make a conjecture that a similar kind of mechanism may signal a chiral phase and that the slight decrease in density at μ=0.5, signals that $\mu_c \cong 0.5$.

REFERENCES

(1)- Wilson K.G., Phy.Rev. D10 2445 (1974)

(2)- Feynmann R.P., Hibbs A.R., Quantum Mechanics and path integrals.

(3)- Elitzur S., Phy.Rev. D12 3978 (1975)

(4)- Kogut J.B., Review of Modern physics, vol.55, No.3,1983.

(5)- Balian R., Drouffe J.M., Itzykson C., Phy.Rev. D11 2104(1975)

(6)- Wilson K.G., Phys. Reports, 23, 331 (1975)

(7)- Metropolis N., Rosenbulth A.W., Rosenbluth M.N., Teller A.H., Teller E., J. Chem.Phys., 21, 1087, 1953.

(8)- Hasenfratz A., Hasenfratz P., Lattice gauge theories, Florida University preprint FSU-SCRI-85-2

(9)- Barbour I.M., Burden C.J., Phys.Lett. 161 B(1985) 357

(10)- Kuti J., Polonyi J., & Szlachanyi K., Phys. Lett. 101 B(1981), 199.
Mclarren L.D., Svetitsky B., Phys.Lett. 98B (1981) 85
Engels J., Karsh F., Montvay I., & Satz H., Phys.Lett.101B (1981),199

(11)- Hasenfratz A., Hasenfratz P., Phys.Lett.B93(1980) 165

(12)- Hasenfratz P., Karsch F., Phys. Lett. 125B (1983) 308
Kogut J., et al, Nucl.Phys.B 225(1983) 93

(13)- Barbour I.M., Behilil N.E., Gibbs P.E., Shierholz H.,Teper M., in The Recursion method and Its Application (Spring series in solid state sciences), ed. Pettifor D.G., Weire D.L., (Springer, Berlin, 1985), p.149

(14)- Barbour I.M., Behilil N.E., Gibbs P.E., Rafiq M., Moriarty K., Shierholz G. J. Comp. Phy. 68 (1987) 227

(15)- Gibbs P.E., Ph.D Thesis 1985

(16)- Nielsen H.B., Ninomiya M., Nucl.Phys.B193 (1981), 173

(17)- Satz H., Nucl.Phys.A418 (1984) 447(c)

(18)- Satz H., Ann.Rev.Nucl.Particle Science, 1985,35; 245

(19)- Mclerran L.D., Svetitsky B., Phy.Rev. D24(1981) 450

(20)- Creutz M., Phys.Rev. D21 (1980) 2308

(21)- Barbour I., Behilil N.E., Dagotto E., Karsch F., Moreo A., Stone M., Wyld H., Nucl. Phys. B275(1986) 161

(22)- Dagatto E., Moreo A., Wolff U., Illionoise Preprint ILL-337-86-12(1986)

(23)- Gibbs P.E., Phys. Lett.B 182 (1987) 369
Gibbs P.E., Glasgow University preprint.1986

(24)- Behilil N.E., Ph.D thesis, 1986

(25)- Creutz M., ' Quarks, Gluons and lattices, Cambridge University Press 1983.

(26)- Berg B., Engels J.,Kehl H., Waltl B., Satz H., Bielefeld preprint BI-TP 86/05

(27)- C.Baillie, K.C. Bowler, P.E.Bibbs, I.M.Barbour,M. Rafiq. Edinburgh University Preprint 87/400.